Study of Urethane Double-Coated Nylon Membranes for Fluid-Storage Applications

Author:

Micah Howell

A Master's Thesis

Submitted to the Faculty of Liberty University

In Partial Fulfillment of the Requirements for the degree of

Master of Science, Mechanical Engineering

School of Engineering

Lynchburg, Virginia

August 12, 2022

THE LIBERTY UNIVERSITY GRADUATE SCHOOL
STATEMENT OF COMMITTEE APPROVAL

By: Micah Howell

Dr. Hector Medina, Ph.D.

Major Professor

Professor of Mechanical Eng.

Liberty University School of Engineering

Approved By: Dr. Hector Medina

Dr. Thomas Eldredge, Ph.D., P.E.

Committee Member

Associate Professor of Mechanical Eng.

Liberty University School of Engineering

Dr. Carl Pettiford, Ph.D.

Approval of Director of Engineering

Graduate Program:

Liberty University School of Engineering

Dr. Marcos Lugo, Ph.D.

Committee Member

Assistant Professor of Mechanical Eng.

Liberty University School of Engineering

Dr. Mark Horstemeyer, Ph.D.

Approval of Dean of School of Engineering:

Liberty University School of Engineering

Name: Micah Howell

Date of Degree: August 19th, 2022

Institution: Liberty University

Major Field: Mechanical Engineering

Major Professor: Dr. Hector Medina

Title of Study: Study of Urethane Double-Coated Nylon Membranes for Fluid-Storage Applications

Pages in Study: 84

Candidate for Degree in Master of Science

Abstract

Polymer-coated fabrics are used for many fuel and water storage applications, such as in U.S. military field operations. Urethane-double-coated nylon (UDCN) is one such material used in collapsible fluid storage tanks. Research into the mechanical properties of UDCN membranes under different environmental conditions is necessary for substantiating its current operations as well as developing new technologies. Novel modular, closed-loop and scalable pumped-storage hydropower (PSH) systems are one technology that could use UDCN membrane tanks in order to mitigate large costs, risks, environmental impacts, and time-for-deployment associated with PSH system construction due to their modular, closed-loop technology. This study focuses on the mechanical testing of UDCN membranes and similar polymer-coated fabrics to observe their hyperelastic behavior and the effects of UV irradiation and hydrolysis on the membranes. Additional testing included creep testing of UDCN membranes to characterize the longevity and viscoelasticity of the material. A UDCN membrane tank was also used in a lab-scale PSH loop system to verify UDCN membrane material performance. The numerical solution for a mathematical model for membrane tanks was then developed in Python and calibrated using experimental data from the PSH loop system. Results from this study indicate that UDCN membranes are viable for use in developing PSH technologies due to the low stresses seen by UDCN membrane tanks during use as well as the durability of UDCN membranes under UV and hydrolytic degradation conditions.

Acknowledgements

I would first like to thank my advisor, Dr. Hector Medina, for his guidance and training throughout my graduate study. He has provided a plethora of wisdom and knowledge in many areas of engineering study, in addition to devoting his time to developing future engineers and innovators. I would like to thank both Dr. Medina and Dr. Thomas Eldredge for their patented PSH technology and their assistance in developing and constructing the lab-scale PSH loop used in this study. I would also like to thank Carson Farmer for his assistance with the PSH loop and data acquisition system, as well as his insight into hyperelastic modeling. I would like to thank the TRACER Lab, specifically Dr. Medina and Carson Farmer, for access to their hyperelasticity library. I would also like to thank Isabelle Perdew for her assistance with hydrolysis testing.

In addition to those directly involved in this study, I would also like to thank David Fazzina, Stephen Horstemeyer, Daniel Kenney and Jared Darius for their assistance with equipment training and support at CERE. I would also like to thank the faculty and staff at the Liberty University School of Engineering for cultivating an enriching learning environment throughout my undergraduate and graduate studies.

I would like to thank my family for their continued support throughout my time at Liberty. Their prayers and encouragement have helped me to persevere through the more difficult and demanding periods of study. I would also like to thank my friends and my church family for supporting me and helping to develop my character in the midst of my graduate studies.

I would also like to acknowledge that this study was partially funded by the DoE FAST award and GoVA funds, and would like to thank those organizations for their support.

Contents

List of Figures

List of Tables

List of Abbreviations & Units

PSH	**P**umped **S**torage **H**ydropower
UDCN	**U**rethane-**D**ouble-**C**oated **N**ylon
UV	**U**ltra**v**iolet
RT	**R**oom **T**emperature
DAQ	**D**ata **Acq**uistiion
PU	**P**oly**u**rethane
ASTM	**A**merican **S**ociety for **T**esting and **M**aterials
SR	**S**train **R**ate
MR	**M**ooney-**R**ivlin
SEM	**S**canning **E**lectron **M**icroscope
ISO	**I**nternational **O**rganization for **S**tandardization
h-mcs-PSH	**h**ybrid-**m**odular **c**losed-**l**oop **P**umped **S**torage **H**ydropower
PPE	**P**oly**p**ropyl**e**ne
LVDT	**L**inear **V**ariable **D**isplacement **T**ransducers
PVC	**P**oly**v**inyl **C**hloride
GUI	**G**raphical **U**ser **I**nterface
2D	**2**-**D**imensional
3D	**3**-**D**imensional

m	Meters
mm	Millimeters
μ**m**	Micrometers
min	Minutes
yr.	Year
wk.	Week
MPa	Megapascals
W	Watts
kW	Kilowatts
MW	Megawatts
in.	Inches
MJ	Megajoules
$^\circ$	Degrees
$^\circ$**C**	Degrees Celsius

Chapter 1

Introduction

Polymer-coated fabrics have been used in water and fuel storage for decades, with constant advancements being made to create lighter and more durable materials. Collapsible tanks made with polymer-coated fabrics have become the primary fuel storage vessels for field use by the U.S. military, while also being utilized for storing water [1]. In addition, collapsible tanks are being researched for use in novel modular pumped-storage hydropower (PSH) systems. A large percentage of the costs of PSH systems are associated with reservoir construction [2]. Thus, a modular system of collapsible tanks would mitigate much of the high costs currently associated with PSH systems. Due to the significant usage of collapsible fabric tanks in military applications, as well as the development of new technologies using such tanks, the materials used must be thoroughly tested.

Urethane-double-coated nylon (UDCN) is one material used in collapsible tanks. In order to understand the durability of UDCN membranes in industrial and military applications, significant testing must be performed. Mechanical testing provides insight into the longevity of the membrane during use and subsequently into the costs associated with installation and replacement of the tanks. As UDCN membrane tanks are already being used by the Army for fuel storage [1], research into their properties under different conditions will evaluate the efficiency of using UDCN membranes in current operations. This research also helps develop future technologies, such as the aforementioned modular PSH system. Research on UDCN membranes is largely unpublished, leaving a vacancy in the field of coated-fabrics and polymer science.

To characterize the mechanical properties of UDCN membranes, a comprehensive study was performed using four uniaxial test methods based on ASTM and ISO standards[3, 4, 5, 6, 7]: (1) Monotonic tensile tests at varied strain rates (2.5, 5 and 10 mm/min.); (2) Monotonic tensile tests conducted after accelerated ultraviolet (UV) exposure (1-5 yrs.); (3) Monotonic tensile tests conducted after hydrolysis (1, 2, 3, 4, 5, 6, 8, and 12 wks. of hydrolysis); and, (4) Creep testing at two temperatures (RT and 50°C). The study of UDCN membranes under conditions of UV irradiation, hyrolysis and creep are useful specifically for PSH applications but broadly for material characterization. Additional uniaxial tensile tests were performed on Seaman XR-5 8138 and 8142 geomembranes for further insight into coated-fabrics in regards to PSH applications.

An experimental verification of UDCN membrane material performance was also performed via implementation in a lab-scale PSH loop system. This lab-scale PSH loop was constructed and tested using a 100-gallon UDCN tank as the upper reservoir. Data was collected via a specialized DAQ setup with LabVIEW software, in order to observe the deformations seen by the material during operation. In addition, a numerical/analytical model of the flexible UDCN tank was created to approximate the stresses seen by the tank during use in the PSH loop. The purpose of the model is to provide baseline insight into the behavior of the tank as well as the safety of using UDCN for PSH applications.

Chapter 2

Urethane Double-Coated Nylon Membrane Mechanical Testing

2.1 Urethane Double-Coated Nylon

2.1.1 Material Classification and Properties

Urethane double-coated nylon (UDCN) is classified primarily as a coated-fabric comprised of polymers. UDCN is often used for fluid-storage applications ranging from water reservoir liners to fuel containment [8]. UDCN fabrics are specially engineered with a polyurethane (PU) coating for high abrasion and corrosion resistance [8]. Polyurethanes are highly durable due to their hyperelasticity and high mechanical strength [9]. Polyurethanes are copolymers comprised of soft-hard segments, which allow for localized strength or elasticity [1, 10, 11, 12]. This structure can be seen in Fig. 2.1. In addition, PU's can be cross-linked using different methods to increase mechanical strength [10, 13, 14]. While nylon-fibers do not exhibit the same level of elasticity as polyurethane, they serve to enhance the overall strength of the UDCN membrane.

The material used for study is a Seaman-engineered UDCN fabric. The nylon-fiber matrix is comprised of primary nylon-fiber bundles and secondary nylon-fiber bundles orthogonal to the primary bundles. The primary bundles contain significantly more nylon-fibers than the secondary bundles, which are weaved along the parallel primary bundles as represented in Fig. 2.2. This study will refer to specimens oriented

FIGURE 2.1: Schematic of urethane morphology with (a) soft segment, (b) hard segment, (c) structure reorientation after stress [1]

longitudinally, with applied loading parallel to the primary fibers, and transversely, with applied loading orthogonal to the primary fibers. For any specimens oriented at a defined angle, the angle is with respect to the transverse axis.

Seaman XR-5 geomembranes are also used in this study for comparison purposes. The XR-5 geomembranes contain polyester fibers rather than nylon fibers. In addition, the difference in the quantity of fibers between the primary and secondary directions is much less significant than for UDCN, though the distinction is present. For this reason, it is expected that the XR-5 geomembranes are less dependent on direction than UDCN.

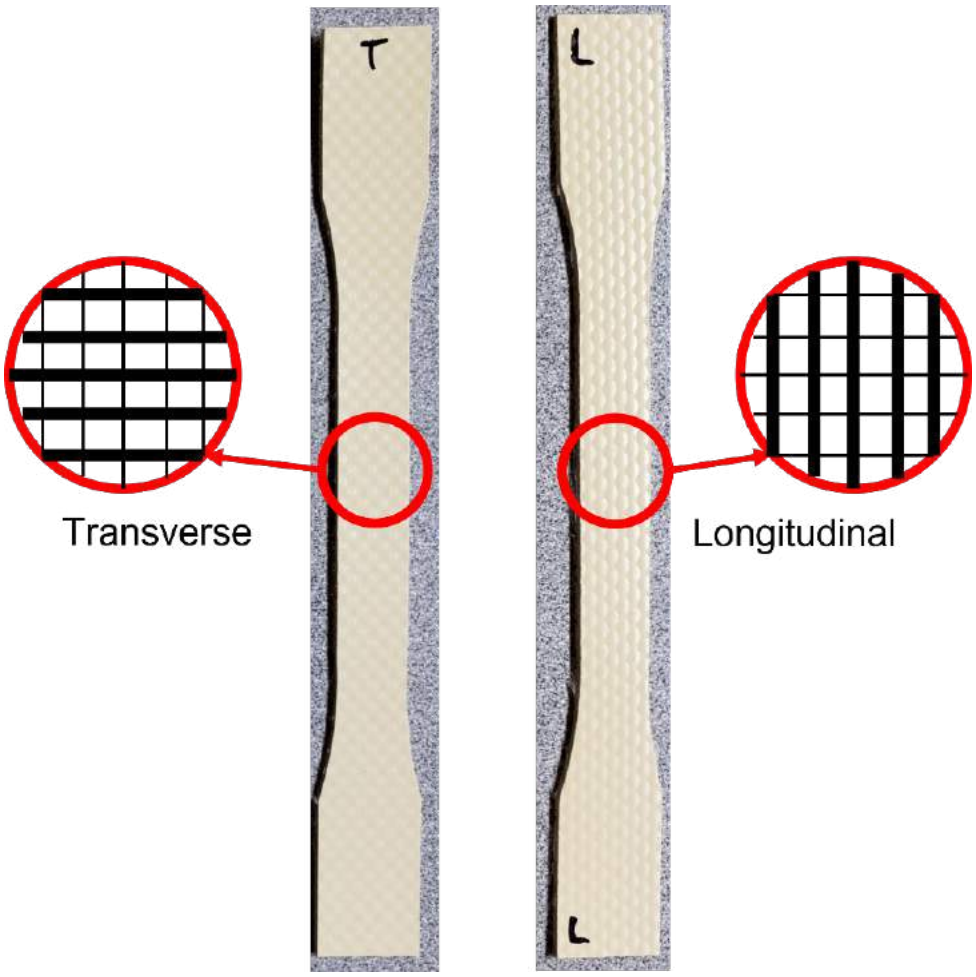

FIGURE 2.2: UDCN Type I Specimens with Nylon Fiber Orientations. Size of nylon fiber bundles is not to scale.

2.2 Monotonic Tensile Testing

2.2.1 Uniaxial Tensile Test Method

The material used for study was a UDCN fabric. As the uniformity of the nylon fibers varied depending on the orientation of the material, specimens were denoted with longitudinal and transverse orientations. For the longitudinal specimens, an applied tensile loading was parallel to the primary nylon fibers, while tensile loading for the transversely oriented specimens was applied perpendicular to the primary nylon fibers. Tensile tests were performed based on the ASTM D638 standard [3]. This standard was used in combination with ASTM D751 [4] to prevent stress concentrations at the grips from affecting the mode of failure. Specimens of each orientation were machined using an OMAX MicroMAX abrasive waterjet machine to the Type I dogbone specimen standard, which is specified for use by ASTM D638. The

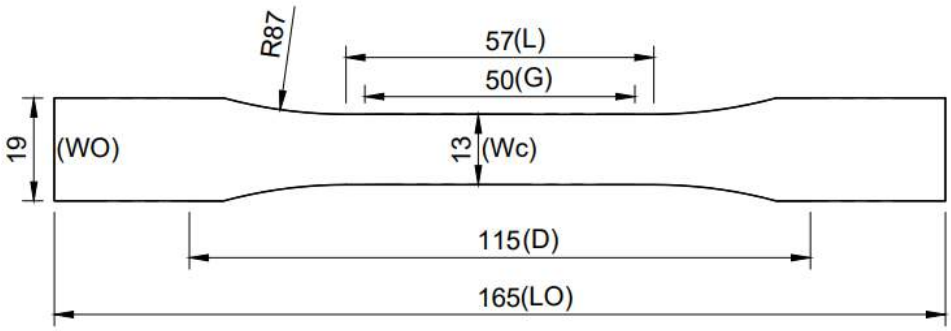

FIGURE 2.3: ASTM D638 Type I specimen. Dimensions are in mm, with WO=overall width, Wc=width of narrow section, LO=overall length, G=gage length, L=length of narrow section, D=distance between grips, and R=radius of fillet.

specimen dimensions and specimens can be seen in Fig. 2.3 and 2.4c, respectively. Five specimens of each orientation were loaded on an Instron 5982 universal testing system at strain rates of 2.5, 5, and 10 mm/min until failure (Fig. 2.4d). All mechanical testing for this study was performed using same Instron 5982 universal testing system, with all specimens machined on the same MicroMAX waterjet to the ASTM D638 Type I standard. For comparison purposes, the tests performed at room temperature at the 5 mm/min strain rate will be considered the control for monotonic testing.

Additional monotonic tensile testing was performed at 5 mm/min on UDCN specimens with varied orientations and on Seaman XR-5 geomembranes similar to UDCN. Ten total angled UDCN specimens were oriented with their primary nylon fibers at 30° and 60° from the transverse axis (perpendicular to loading). The five angled specimens of each orientation were then loaded at 5 mm/min until failure. Five transverse and five longitudinal specimens of Seaman XR-5 8138 (Fig. 2.4a) and 8142 (Fig. 2.4b) geomembranes were also loaded at 5 mm/min until failure. The XR-5 geomembranes have a thinner ethylene copolymer coating and contain polyester fibers rather than nylon.

2.2.2 Monotonic Uniaxial Tensile Experimental Results

The transverse UDCN specimens failed at stresses ranging from 38-41 MPa at 5 mm/min, with the strain at failure approximately 0.27. The 2.5 and 10 mm/min strain rates both saw an increase in tensile strength to 45 MPa and a decrease in strain at failure to 0.26. The transverse UDCN specimens have an angled fracture surface (Fig. 2.5a), indicating that the stress propagated at one edge and caused a diagonal tear

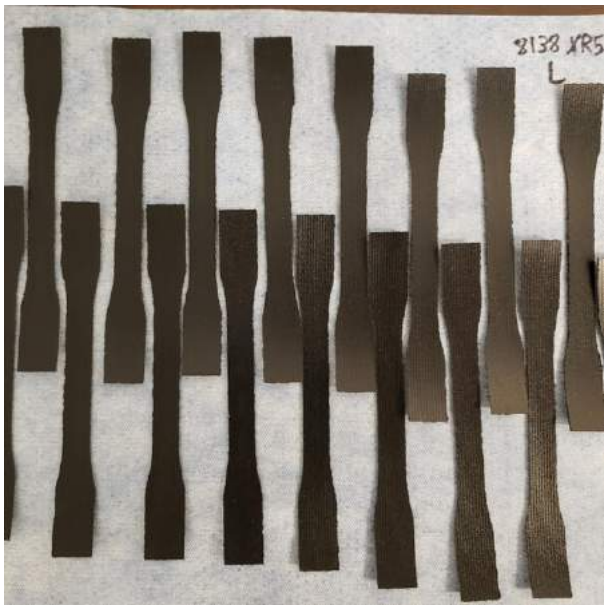

(A) Longitudinal XR-5 8138 Specimens

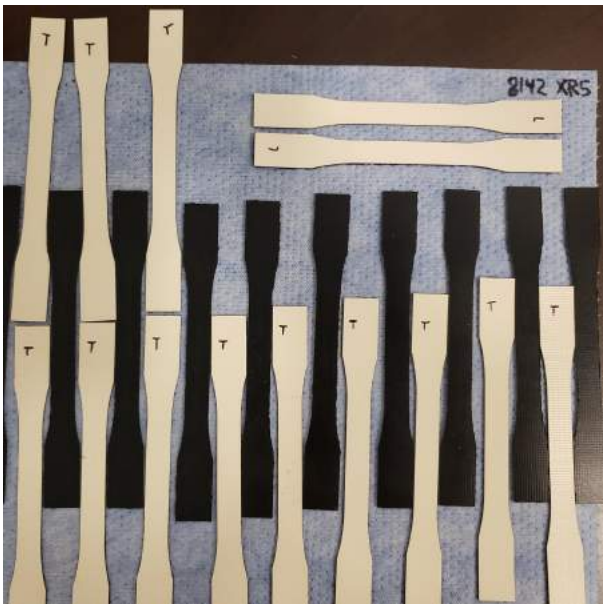

(B) XR-5 8142 Specimens

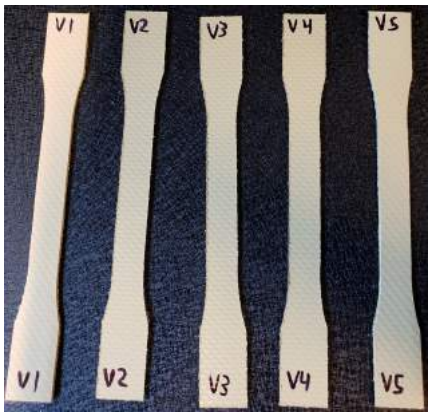

(C) Transverse UDCN Specimens

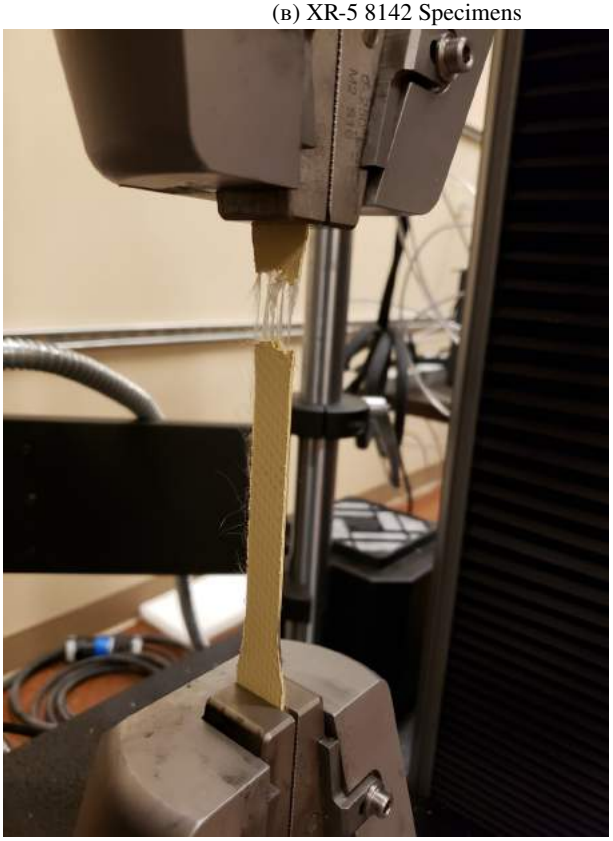

(D) Longitudinal UDCN Specimen Fracture

FIGURE 2.4: Type I coated-fabric specimens

through the material until failure. The tears occur at angles of 35°-50° in most cases, though the angles are reduced at the highest strain rate. This indicates a shearing failure of the polyurethane coating in the transverse specimens. The longitudinal specimens are more consistent across all strain rates, with the tensile strength ranging from 64-69 MPa and the strain at failure ranging from 0.16-0.17. Most longitudinal specimens fractured orthogonal to the loading (Fig. 2.5b), with a more symmetric stress concentration in the transverse direction. However, some of the longitudinal specimens failed at an angle, with the nylon fibers failing completely while the center of the urethane coating remaining attached (Fig. 2.6).

The angled UDCN specimens failed at similar stresses to the transverse specimens, ranging from 38-43 MPa. However, the strain at failure is much greater for the angled specimens, ranging from 0.52-0.54. The 60° and longitudinal specimens both have relatively smooth fracture surfaces that are perpendicular to the primary fibers (Fig. 2.5d,2.5b). Meanwhile, the fracture surface of the 30° specimens is jagged and uneven, yet parallel to the primary fibers (Fig. 2.5c). This indicates a tearing stress fracture of the polyurethane coating after an initial failure of the secondary nylon fibers. Average stress-strain data can be seen in Fig. 2.7-2.9 for the UDCN specimens.

The XR-5 geomembrane specimens failed at stresses ranging from 52-60 MPa, regardless of the direction. However, the strain at failure depended heavily on the direction. XR-5 8138 specimens failed at a strain of 0.2 in the transverse direction and 0.16 in the longitudinal direction. The difference in failure strains was the most significant for the XR-5 8142 specimens, failing at a strain of 0.24 in the transverse direction and 0.12 in the longitudinal direction. However, the mode of failure appears the same for all XR-5 specimens as shown by the even fracture surfaces orthogonal to the loading (Fig. 2.10). However, the fracture is asymmetric for all specimens in the direction perpendicular to the fabric. This behavior is shown by the curving of the specimens after failure, which is most extreme in the transverse 8138 specimens (Fig. 2.10a). The curving of the specimens implies that one side of the polymer coating experienced more microscopic stress fractures during loading, resulting in an asymmetrical weakening of the fabric. Average data for the XR-5 specimens is shown in Fig. 2.11, with comparison plots for the

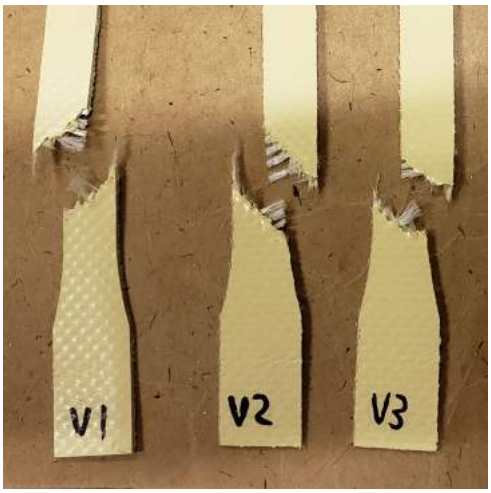

(A) Transverse UDCN Fractured Specimens

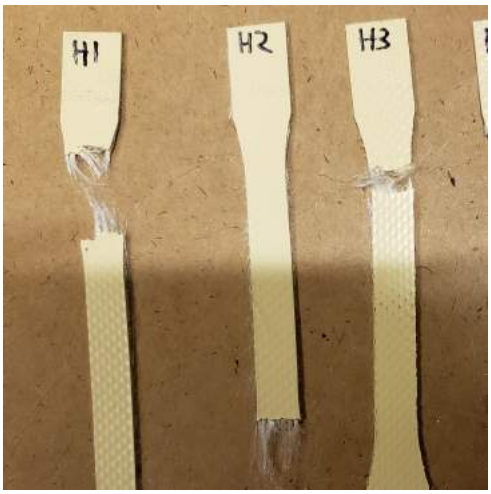

(B) Longitudinal UDCN Fractured Specimens

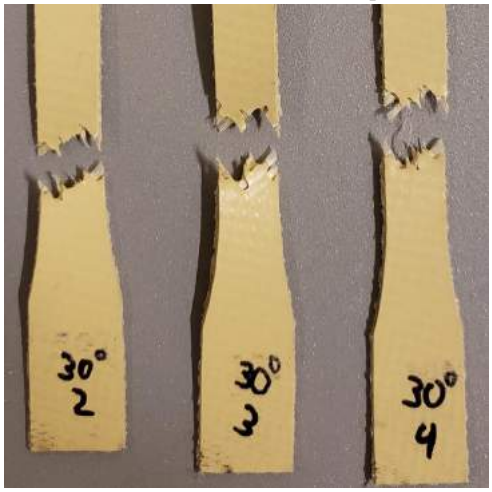

(C) 30° UDCN Fractured Specimens

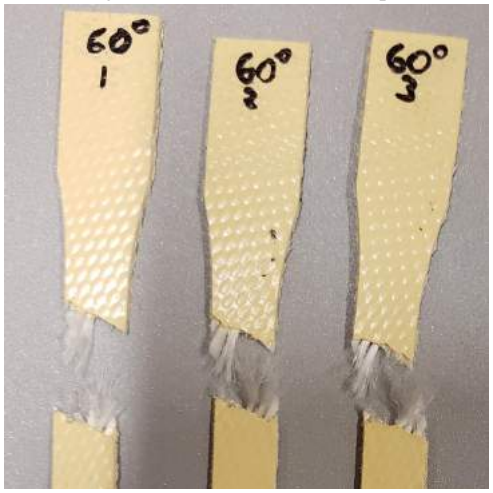

(D) 60° UDCN Fractured Specimens

FIGURE 2.5: UDCN fracture surfaces after 5 mm/min monotonic loading.

FIGURE 2.6: Longitudinal UDCN specimen fracture after 2.5 mm/min monotonic loading.

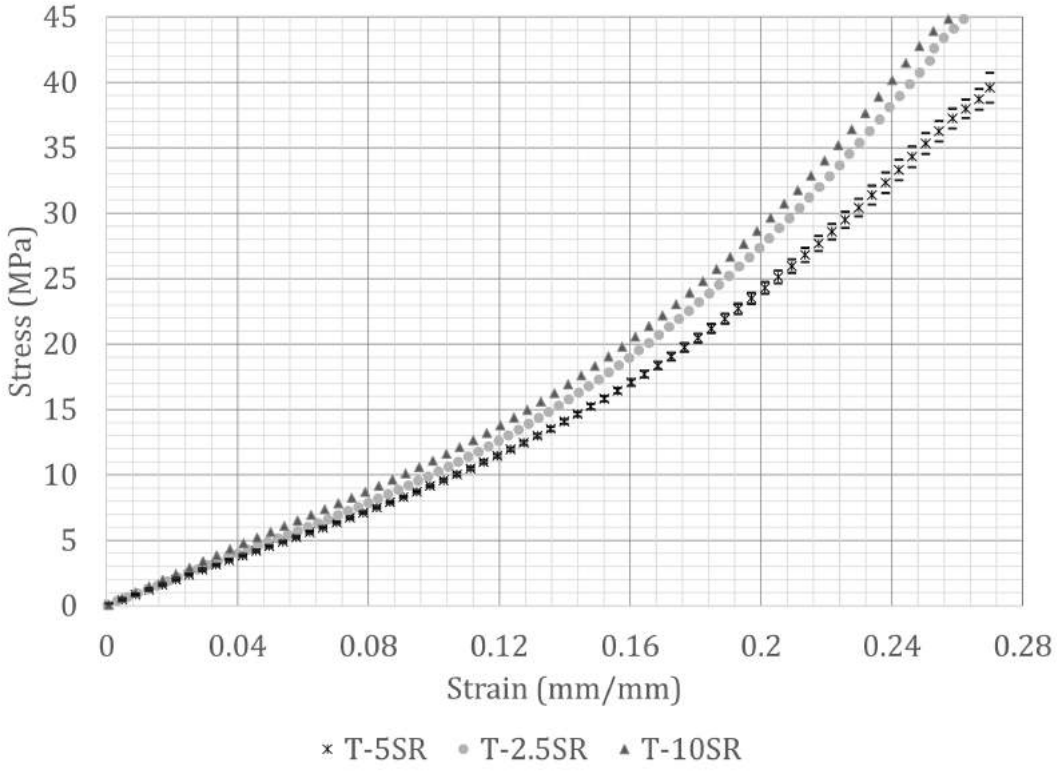

FIGURE 2.7: Transverse UDCN specimen strain-rate data. Each data set is the average of 5 specimens. There is a 95% confidence interval of ±2.82%, ±2.06% and ±0.38% for the 2.5, 5 and 10 mm/min strain-rates (SR), respectively.

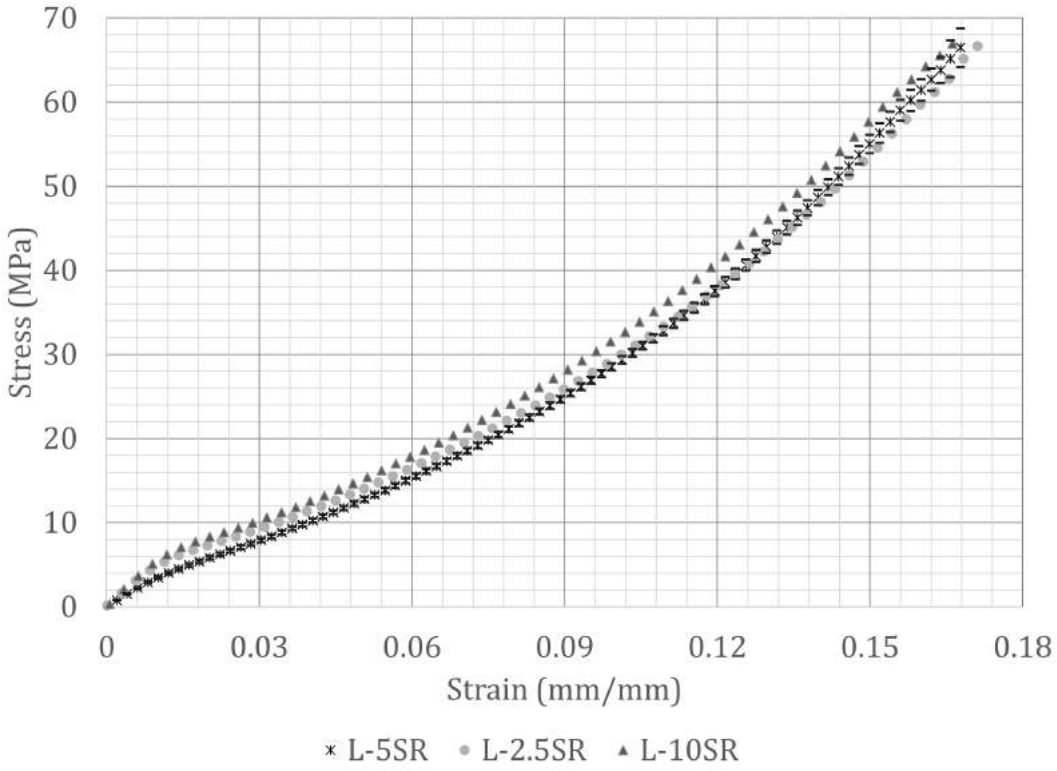

FIGURE 2.8: Longitudinal UDCN specimen strain-rate data. Each data set is the average of 5 specimens. There is a 95% confidence interval of ±2.69%, ±3.46% and ±1.56% for the 2.5, 5 and 10 mm/min strain-rates (SR), respectively.

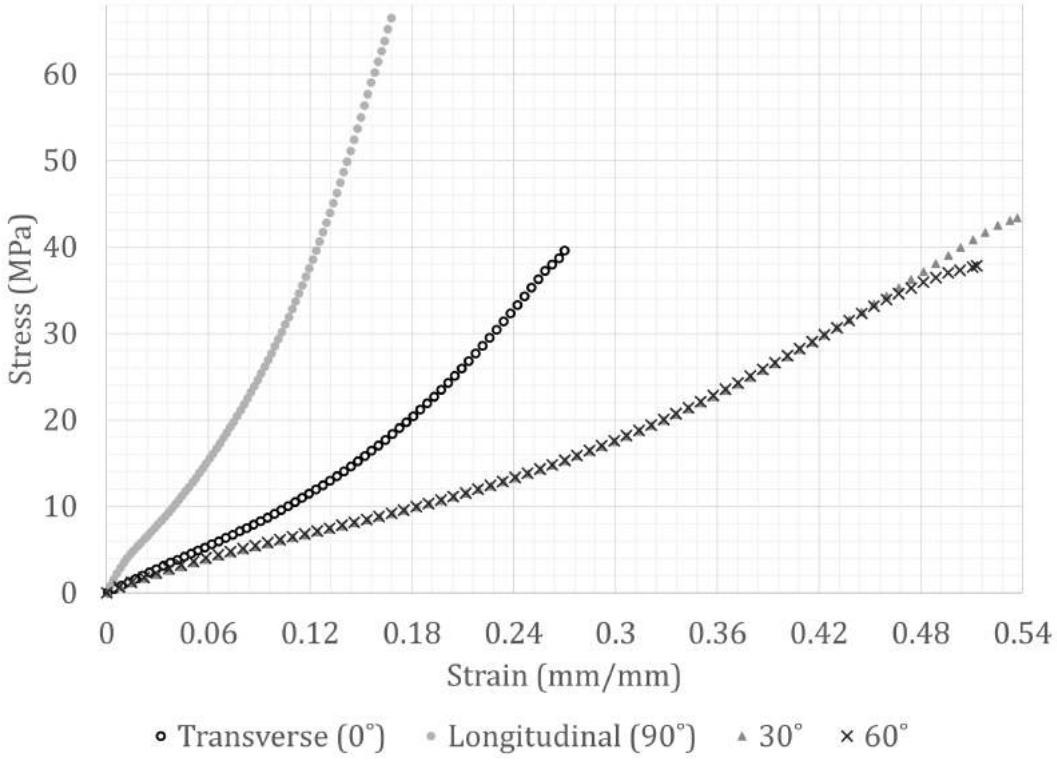

FIGURE 2.9: UDCN data at different orientations for 5 mm/min monotonic loading. Each data set is the average of 5 specimens. There is a 95% confidence interval of ±2.06%, ±3.46%, ±0.28% and ±1.35% for the transverse, longitudinal, 30° and 60° orientations, respectively.

UDCN and XR-5 specimens shown by Fig. 2.12 and 2.13.

2.2.3 UDCN Orientation and Viscoelasticity

There is a significant difference in the strength of UDCN between the transverse and longitudinal specimens (Fig. 2.9). The longitudinal specimens fail at a stress approximately 65% larger than the transverse specimens. This increase in strength is coupled with a decrease in deformation, with longitudinal specimens having a yield strain 37% smaller than the transverse specimens. This behavior is likely attributed to the interaction between the nylon-fiber matrix and the urethane coating. The strength of the longitudinal specimens corresponds with the strength of the primary nylon-fiber bundles. In the transverse direction, the strength of the specimens corresponds more with the strength of the urethane coating, with the secondary nylon-fiber bundles supporting the coating. This theory is supported by the reported breaking elongation of nylon, which ranges from 15-28% [15, 16]. The presence of longitudinal

(A) Transverse XR-5 8138

(B) Longitudinal XR-5 8138

(C) Transverse XR-5 8142

(D) Longitudinal XR-5 8142

FIGURE 2.10: XR-5 geomembrane specimen fracture after 5 mm/min monotonic loading.

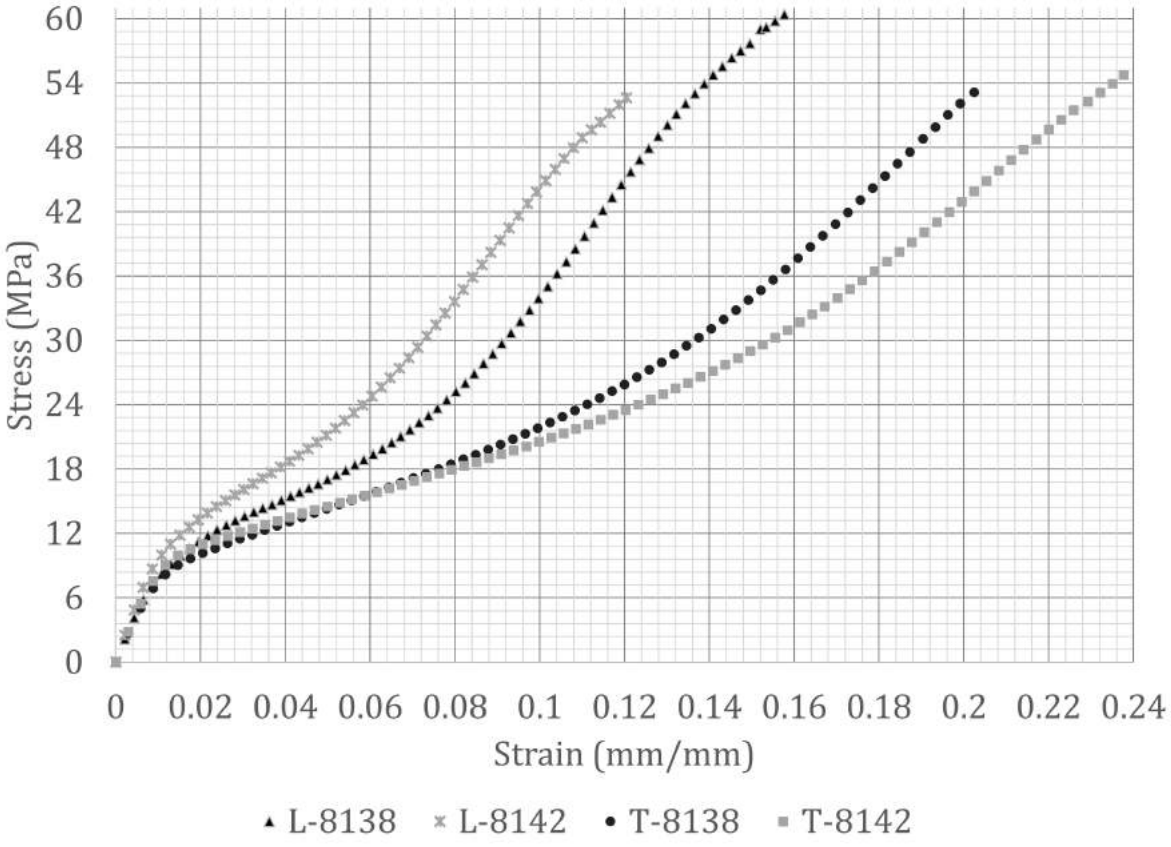

FIGURE 2.11: XR-5 geomembrane data after 5 mm/min monotonic loading. Each data set is the average of 5 specimens. There is a 95% confidence interval of ±0.42%, ±2.38%, ±1.2% and ±0.99% for the 8138 transverse, 8138 longitudinal, 8142 transverse and 8142 longitudinal orientations, respectively.

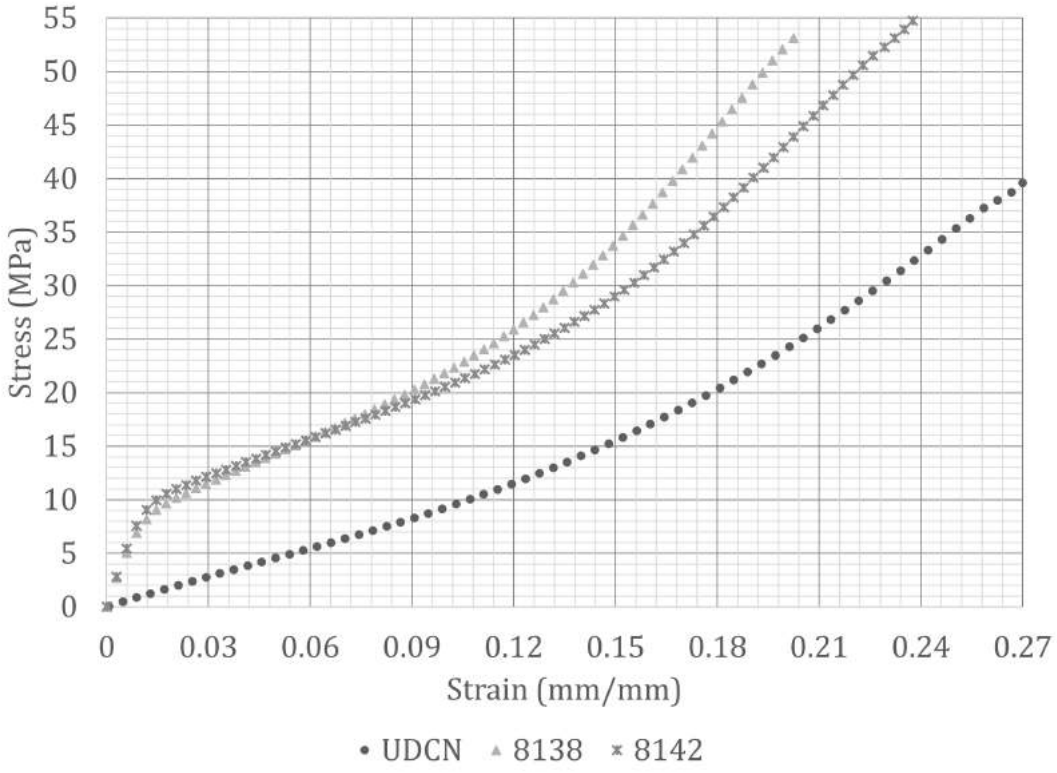

FIGURE 2.12: Transverse data for UDCN and XR-5 membranes monotonically loaded at 5 mm/min. Each data set is the average of 5 specimens. There is a 95% confidence interval of ±2.06%, ±0.42% and ±1.2% for the UDCN, 8138 and 8142 membrane specimens, respectively.

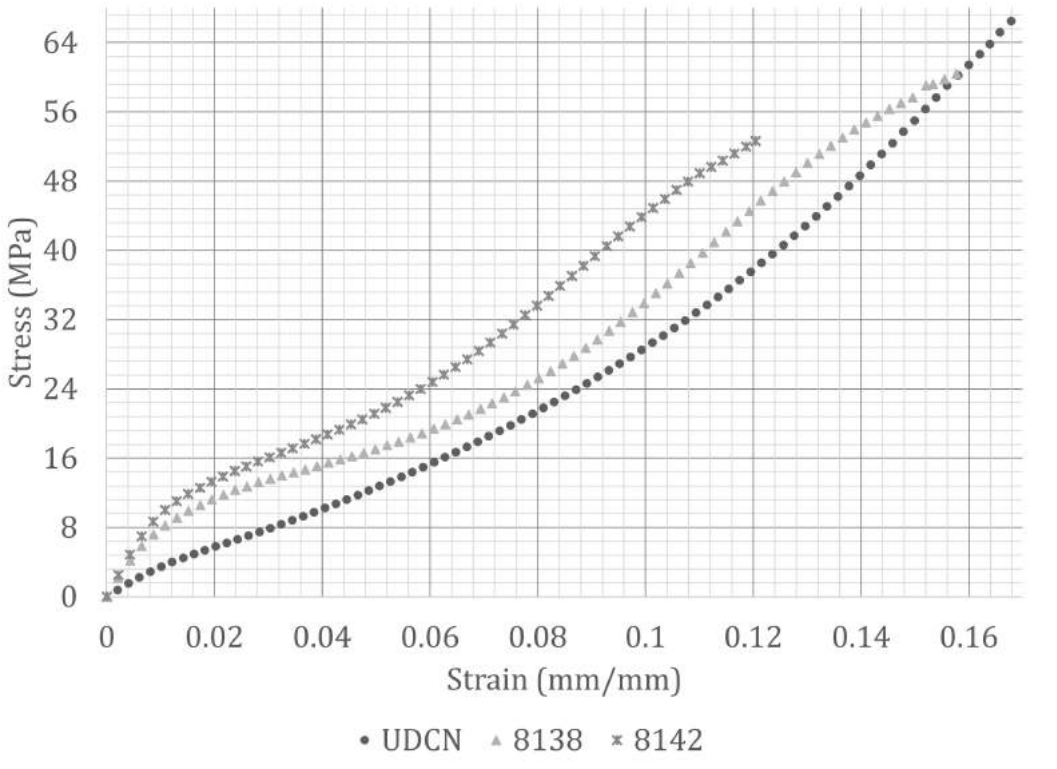

FIGURE 2.13: Longitudinal data for UDCN and XR-5 membranes monotonically loaded at 5 mm/min. Each data set is the average of 5 specimens. There is a 95% confidence interval of ±3.46%, ±2.38% and ±0.99% for the UDCN, 8138 and 8142 membrane specimens, respectively.

TABLE 2.1: Average Tensile Strength of UDCN Control Specimens and Urethane Coating

Specimen	**Tensile Strength (MPa)**
Transverse (0°)	39.6
30°	43.4
60°	37.8
Longitudinal (90°)	66.48
Compounded Urethane Coating	35.5 [17]

specimens that failed with the urethane coating partially intact (Fig. 2.6) is more evidence that the primary nylon fibers are the dominant support in that direction. The failure of the primary nylon fibers results in a failure of the longitudinal specimens, even when the coating is mostly intact.

The UDCN specimens oriented at 30° and 60° exhibited significantly greater hyperelastic behavior than both the transverse and longitudinal specimens, as seen by the increase in strain. As the tensile strength is similar for the 30°, 60° and transverse specimens, the strength of the 30° and 60° specimens is primarily linked to the strength of the urethane coating. This correlation is consistent with the reported tensile strength of urethane coatings [17] as shown in Table 2.1. The tensile strength of urethane coating is lower than the tensile strength of the UDCN specimens since the specimens are reinforced by a nylon-fiber matrix.

While the transverse and inclined specimens had similar tensile strengths, the strain at break was significantly different. The 30° and 60° specimens strained 24-27% more than the transverse specimens. The transverse specimens have the secondary nylon-fiber bundles throughout the entire length of the specimen, which decreases the elongation allowed. In contrast, the fibers in the 30° and 60° specimens do not run throughout the entire length of the specimen, but rather in relatively short spans. This results in each nylon bundle acting locally on the specimen to increase the strength in its respective locale. Since the nylon bundles in the 30° and 60° specimens do not traverse the full length of the specimen, the elongation is not restricted by the properties of the nylon.

The transverse specimens show significant viscoelastic behavior, with the maximum stress increasing by 10.1% for both 2.5 and 10 mm/min strain rates. The longitudinal specimens exhibit less pronounced viscoelastic behavior. The viscoelastic region in the longitudinal specimens primarily occurs in the strain range 0.1-0.25, while in the transverse specimens the region begins at 0.4 and extends until failure. The

TABLE 2.2: Average Tensile Strength of XR-5 Geomembrane Specimens

Specimen	**Tensile Strength (MPa)**
Transverse XR-5 8138	53.1
Transverse XR-5 8142	54.7
Longitudinal XR-5 8138	60.4
Longitudinal XR-5 8142	52.6

difference between the tensile strengths at each strain rate lies within the error bounds for the 5 mm/min longitudinal specimens. In contrast, the stress data for the transverse specimens at 2.5 and 10 mm/min begins to diverge from the 5 mm/min data at the start of the viscoelastic region, and at failure this effect is magnified. This indicates that the urethane coating may be more sensitive to viscoelastic effects than the nylon fibers.

2.2.4 UDCN vs XR-5 Geomembrane Comparison

The XR-5 geomembranes exhibit the same orientation-dependent stress-strain behavior as the UDCN membranes, though to a smaller degree. The longitudinal specimens fail at a lower strain than the transverse specimens, but the tensile strength is similar in most cases. The most significant difference in tensile strengths is in the XR-5 8138 specimens, where the longitudinal tensile strength is 7.3 MPa larger than the transverse tensile strength, shown in Table 2.2. In contrast, the difference in tensile strengths for the XR-5 8142 specimens is just 2.1 MPa. This behavior indicates that, as with the UDCN membranes, the XR-5 geomembranes are more dependent on the polyester-fiber matrix in the longitudinal direction and conversely so in the transverse direction. However, this behavior is less pronounced for the XR-5 geomembranes since the fiber bundles are more comparable in both directions. In the UDCN membranes the fiber bundle sizes are significantly different in both directions. The behavior shown is also supported by reported values for breaking elongation of polyester, which ranges from 10-25% [15, 16]. As with the UDCN membranes, the breaking elongation in both the longitudinal and transverse directions lie within the reported range for polyester, so it is possible that the type of polyester is different for both directions.

Nylon fiber typically has a higher tenacity than polyester fiber, which correlates to a higher strength [18, 19]. However, nylon fibers typically have a lower density than their polyester counterparts, which

FIGURE 2.14: Stress-strain curves for different polyester and nylon cords [18]

results in polyester typically having a higher reported strength [15, 16]. The behavior shown by Fig. 2.12 and 2.13. show both of these cases. The longitudinal data shows a higher strength for the membranes with nylon fibers, meaning that the density of the fibers in the longitudinal direction is similar. As the converse is true for the strengths in the transverse direction, the densities of the polyester fibers are substantially larger than those of the nylon fibers in that direction. Comparing Fig. 2.11 and 2.14, the polyester fibers in the transverse direction behave more similarly to typical polyester fibers, while the polyester fibers in the longitudinal direction behave more like nylon fibers. This behavior is not new as researchers have aimed to develop polyester cords with elongations similar to nylon, as shown in Figure 2.14 [18]. The longitudinal polyester fiber stress-strain behavior is similar to the nylon-like polyester cord, while the same is true for the transverse polyester fibers and the standard polyester cord.

The tensile strength of the transverse UDCN membranes is strongly correlated with the urethane coating, which is not the case for the transverse XR-5 geomembranes. While the increase in strain from the longitudinal to transverse specimens implies that the tensile strength is dependent on a different factor in each direction, the similar magnitudes of the tensile strength in both direction can indicate either of two cases: (1) the tensile strength of the coating is similar to that of the polyester fibers; or (2) the polyester fibers are different in each direction. The latter seems to be supported by aforementioned research into

nylon-like polyester synthesis [18]. However, the scope of this study does not focus on the behavior of XR-5 geomembranes, and as such cannot conclude decisively one way or the other without further investigation.

2.2.5 Energy Analysis

Calculating the energy as the area beneath the stress-strain curve shows that the energy is consistent between the tranvserse and longitudinal UDCN specimens. The strain rate affects the energy, but only minimally. The total energy is also similar between the UDCN and XR-5 geomembrane specimens, in the transverse and longitudinal directions. However, in the 30° and 60° UDCN specimens there is a significant increase in energy. The energy in the 30° UDCN specimens is more than double the energy in both the longitudinal and transverse specimens. This is likely attributed to the difference in energy between the urethane coating and nylon fibers. The stress-strain behavior of UDCN, and subsequently the strain energy at failure, in the transverse and longitudinal directions is primarily dependent on the behavior of the nylon fibers. In contrast, the stress-strain behavior of UDCN in the 30° and 60° orientations is primarily dependent on the behavior of the urethane coating.

2.2.6 Hyperelastic Modeling

A computational library prepared by Dr. Medina's lab at Liberty University was utilized to fit hyperelastic models to the monotonic test data. Approximately 75 hyperelastic models were considered in this library, with approximately 40 models explicitly tested with the experimental data. Neo-Hookean and a 2nd-order Mooney-Rivlin models were tested as they are common, but they did not provide a good fit. The lowest order model that fit the UDCN test data relatively well was the Gent model. While the Gent model has a mean-squared error of less than 1 for each test case, the model does begin to diverge near the break point. In addition, the initial viscoelastic region at the start of the longitudinal data sets is not modelled well using the Gent model (Fig. 2.15). The Yeoh and Exponential-Logarithmic models fit more closely with most of the data sets, especially the transverse specimens (Fig. 2.16), but again did not adhere to the

initial regions for the longitudinal UDCN test data.

The Biderman, James-Green-Simpson, and Haines-Wilson models were also fit to the longitudinal, 30°, and 60° UDCN test data, yielding minimal mean-squared error (Fig. 2.18 and 2.17). This is because the Biderman, James-Green-Simpson, and Haines-Wilson models are 4th, 5th and 6th-order Mooney-Rivlin models, respectively, which allows for a significant amount of control due to the number of parameters. The XR-5 geomembranes showed significant hyperelastic and viscoelastic behavior, and due to this were not modeled well by most of the tested models. The Biderman, James-Green-Simpson, and Haines-Wilson models did provide good fits per the same reasoning mentioned previously. The XR-5 hyperelastic models are shown in Appendix A.

Based on the previous conclusions about the dominance of urethane or nylon in different directions of UDCN, hyperelastic models may fit one or the other composing material better. For example, the Gent, Yeoh and Exponential Logarithmic models fit the transverse, 30° and 60° specimens well, indicating a good correlation to the urethane material (Fig. 2.17). In contrast, the nylon-dominated longitudinal behavior is not fit well by the same models (Fig. 2.15), instead being fit by derivatives of the Mooney-Rivlin model (Fig. 2.18). As higher order Mooney-Rivlin models can fit most hyperelastic materials, it is not significant that they also fit the transverse UDCN data well.

2.3 UV Degradation

2.3.1 UV Effects on Urethane and Nylon

Urethane and nylon have different behaviors when exposed to ultraviolet (UV) radiation, resulting in a complex behavior for UV irradiated UDCN. UV effects on urethanes occur via photooxidative degradation, more commonly referred to as photodegradation [20, 21]. Photodegradation of urethanes specifically occurs via photo-Fries and Norrish reactions and entails both chain scission and cross-linking [20, 21]. While both chain scission and cross-linking are forms of photodegradation, chain scission has a weakening effect while cross-linking has a strengthening effect. Since both reactions occur simultaneously in

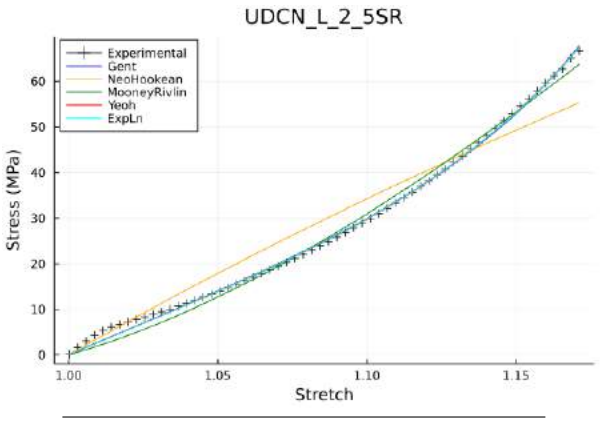

(A) 2.5 mm/min

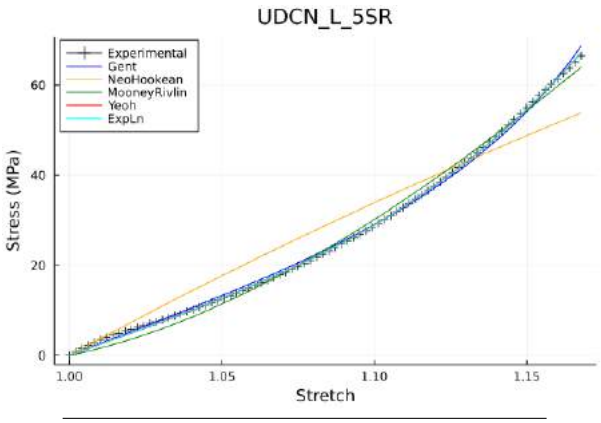

(B) 5 mm/min

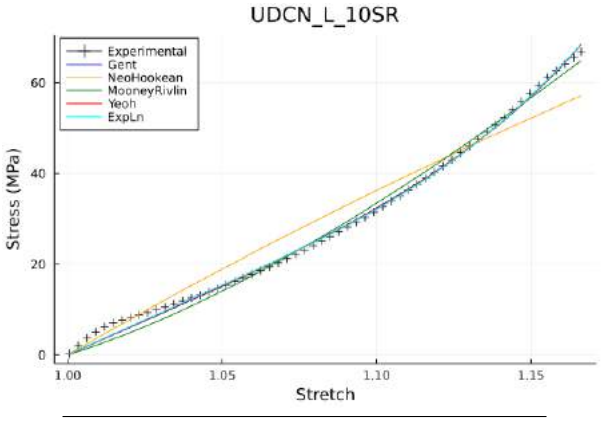

(C) 10 mm/min

FIGURE 2.15: Hyperelastic models for longitudinal UDCN specimens at various strain-rates.

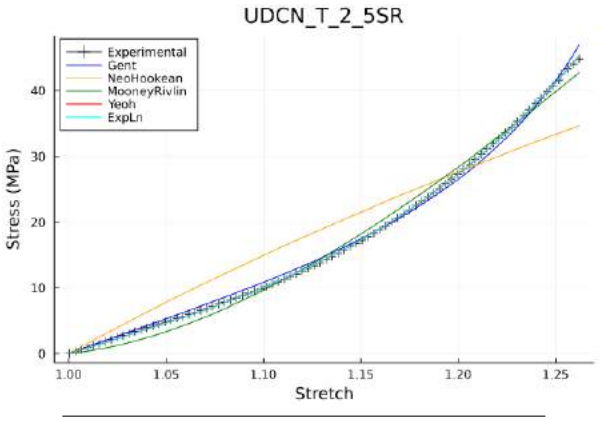

(A) 2.5 mm/min

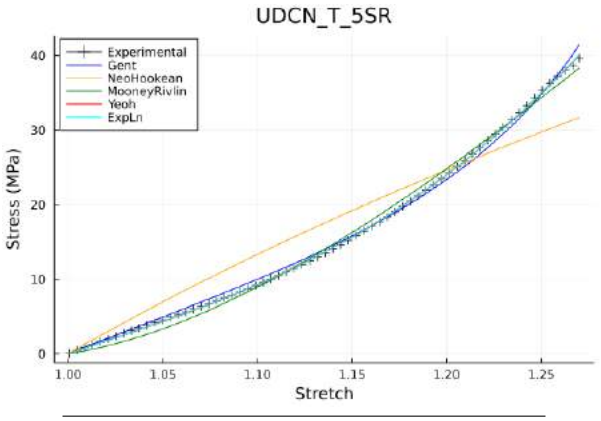

(B) 5 mm/min

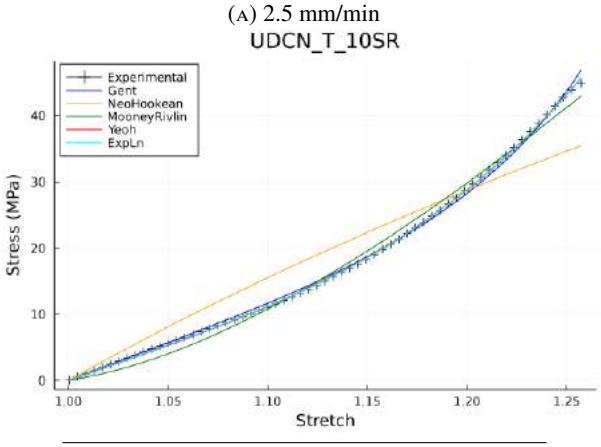

(C) 10 mm/minc

FIGURE 2.16: Hyperelastic models for transverse UDCN specimens at different strain-rates.

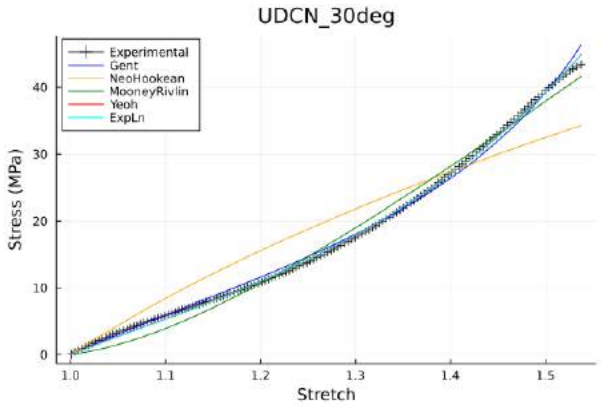

(A) Low-Order Models (30°)

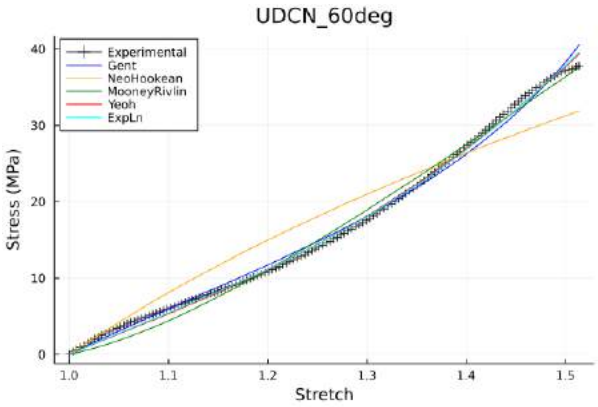

(B) Low-Order Models (60°)

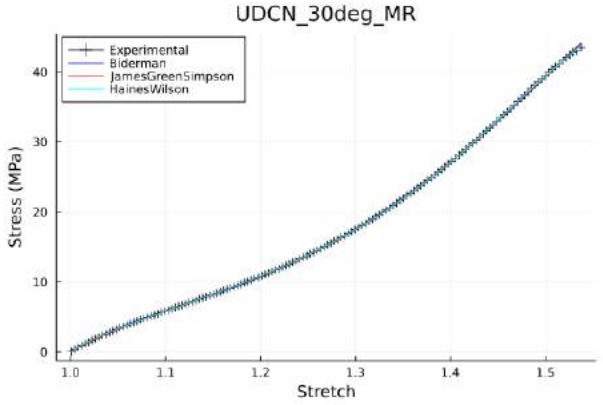

(C) Mooney-Rivlin Models (30°)

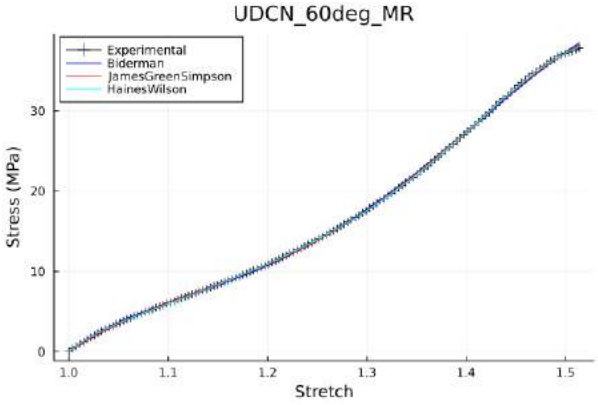

(D) Mooney-Rivlin Models (60°)

FIGURE 2.17: Hyperelastic models for angled UDCN specimens.

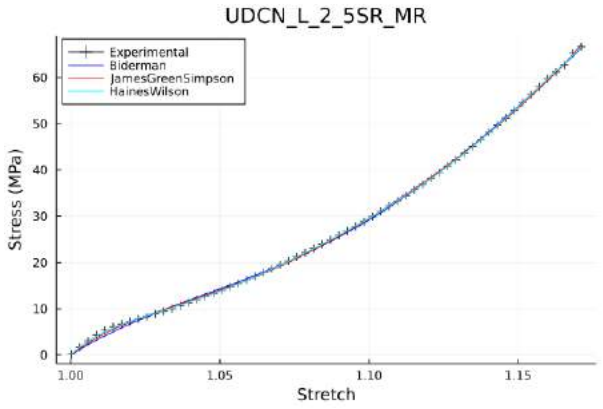

(A) 2.5 mm/min

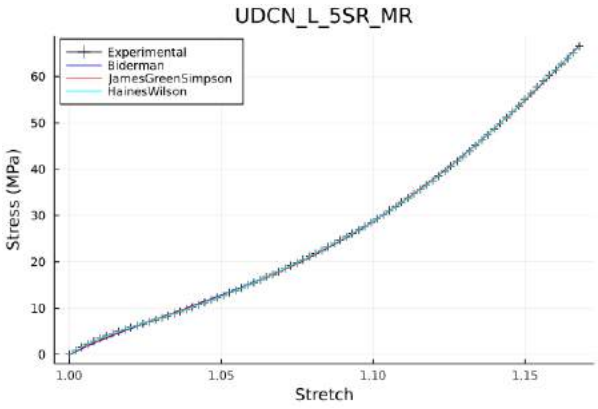

(B) 5 mm/min

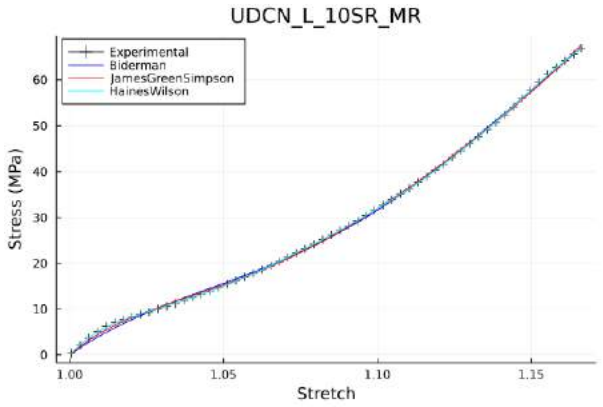

(C) 10 mm/min

FIGURE 2.18: Mooney-Rivlin hyperelastic models for longitudinal UDCN specimens at different strain-rates.

urethanes, different urethane structures may exhibit strengthening or weakening under UV irradiation, depending on which reaction is dominant for that structure. UV and gamma radiation are both used for cross-linking polyurethanes, which is desirable for strengthening the material and increasing heat resistance [13, 20].

Studies on the UV degradation of fibers often finds nylon to have significant deterioration after prolonged UV exposure [22, 23, 24]. Photodegradation of nylon fibers results in a significant decrease in both strength and elasticity [22, 23, 24]. Thus, the use of nylon in UDCN membranes could prove to decrease the strength of the material, provided that cross-linking in the coating does not dominate the material strength. One study showed nylon 66 fibers having a 97.5% decrease in toughness after 28 hours of accelerated UV exposure, while polyester fibers only saw a 66% decrease in toughness [22]. The UV resistance of polyester fibers compared to nylon fibers [16, 22] is not important for this study, but could prove beneficial for future work in fluid-storage applications due to the use of polyester fibers in the XR-5 geomembranes tested in this study.

2.3.2 Accelerated UV Exposure Test Method

UDCN specimens of each orientation were subjected to accelerated UV exposure via a Maxima ML-3500S UV-A lamp. Two specimens of each orientation were placed 4.75 in. from the UV lamp (Fig. 2.19a) housed within an environmental chamber, resulting in an irradiance of 5014 W/m^2. The window in the environmental chamber was covered with aluminum foil to prevent light from entering the chamber during testing. The specimens were exposed for 14 days (Fig. 2.19b), resulting in a total irradiance equivalent to the annual irradiance in Central Virginia [25]. Following the UV exposure period, the specimens were subjected to monotonic tensile loading at 5 mm/min until failure. Two and five years equivalent of accelerate UV exposure were achieved using the same method, with the distance between the specimens and the lamp decreased to 3 in. This increased the irradiance to 12,500 W/m^2, requiring $\approx$11 days of exposure for two years irradiation equivalence, and $\approx$27 days of exposure for five years irradiation

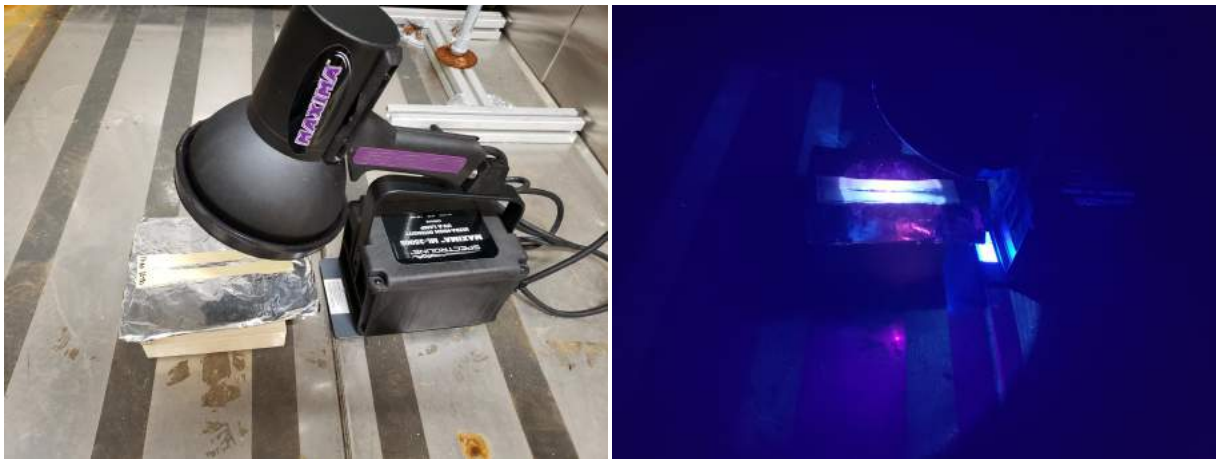

(A) UV irradiation experiment setup. (B) UV Experiment

FIGURE 2.19: UV irradiation experiment setup and testing on UDCN specimens.

equivalence. Following the exposure period, the specimens were subjected to monotonic tensile loading at 5 mm/min until failure.

2.3.3 UV Irradiation Experimental Results

Data from the UV experiments is shown in Fig. 2.20 and 2.21, as well as Table 2.3. The UV irradiated specimens exhibited no distinguishable change in coloration from the base UDCN material. The transverse specimens showed a significant increase in strain energy after UV irradiation. The same effect is seen in the longitudinal specimens, though to a lesser degree.

TABLE 2.3: Strain Energy and Tensile Strength for UV Irradiated UDCN Specimens

UDCN Specimen	**Strain Energy (MJ/m^3)**	**Tensile Strength (MPa)**
Transverse (No UV Irrad.)	4.264	39.6
Transverse (1 yr. UV Irrad.)	6.522	61.0
Transverse (2 yr. UV Irrad.)	7.350	65.8
Transverse (5 yr. UV Irrad.)	8.132	71.6
Longitudinal (No UV Irrad.)	4.468	66.5
Longitudinal (1 yr. UV Irrad.)	5.745	74.2
Longitudinal (2 yr. UV Irrad.)	7.538	87.7
Longitudinal (5 yr. UV Irrad.)	5.215	68.0

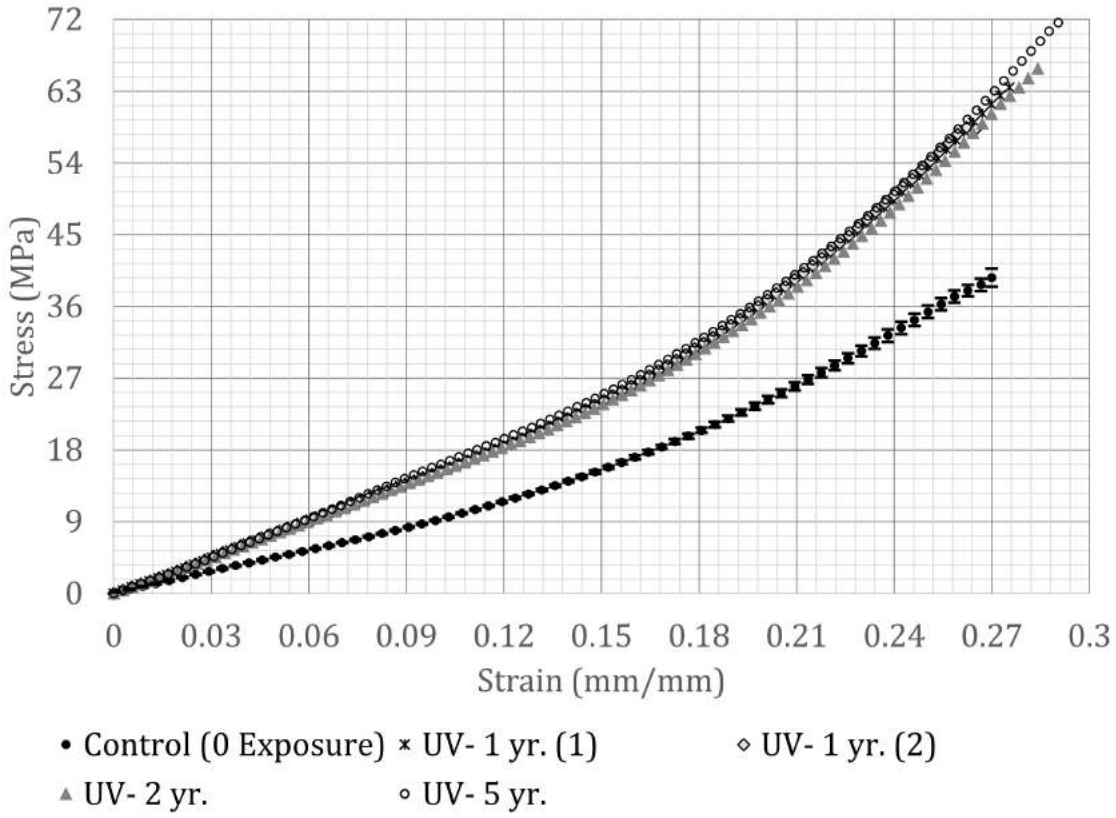

FIGURE 2.20: Transverse UDCN UV Experiment Data. Control is the average of 5 UDCN specimens tested at 5 mm/min at room temperature.

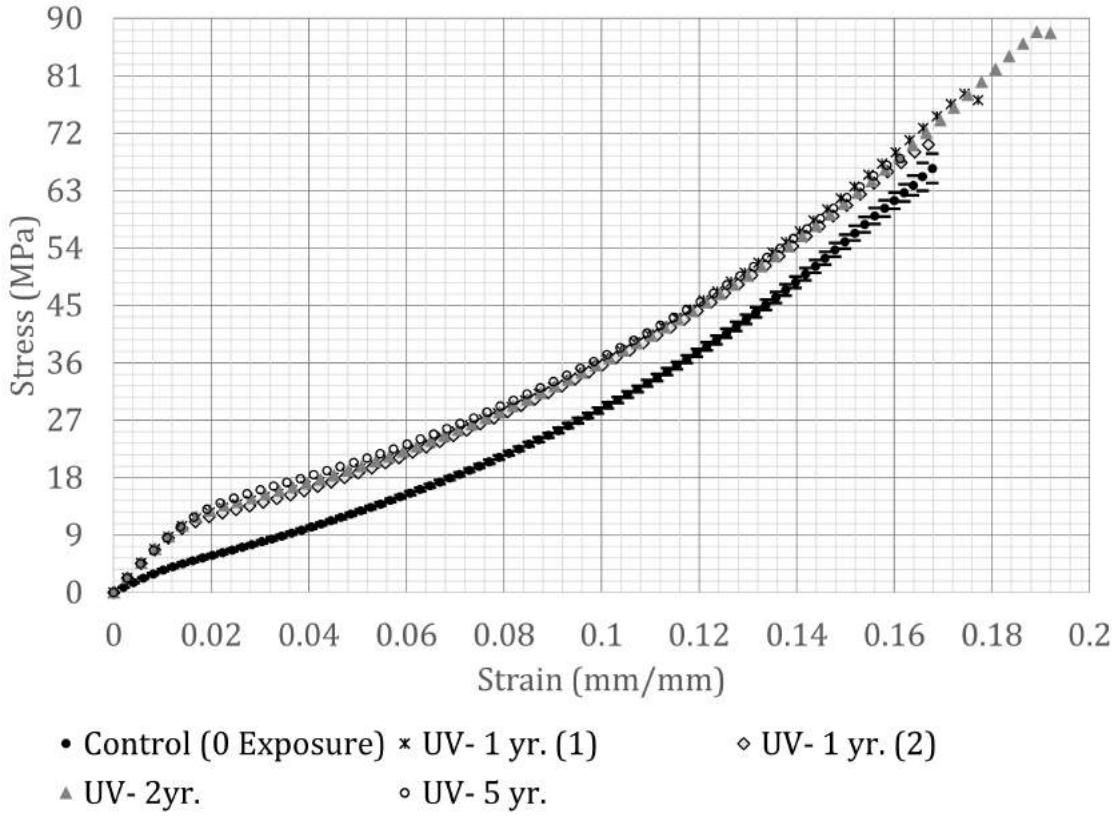

FIGURE 2.21: Longitudinal UDCN UV Experiment Data. Control is the average of 5 UDCN specimens tested at 5 mm/min at room temperature.

2.3.4 Comparison and Analysis

With the behavior between the four irradiated specimens of each orientation being so similar, there are several possible effects of UV irradiation on UDCN, as well as on the directional behavior of UDCN. Based on the consistency of the test data and the increase of strain energy and tensile strength, along with published research, it can be deduced that UV irradiation increases the strength of urethane, and subsequently UDCN.

There is a significant increase in strain energy in the UV irradiated UDCN specimens, as shown by Table 2.3, Fig. 2.20 and Fig. 2.21. The small sample size results in inconsistencies with the trend, but there is an increase in strain energy in all UV irradiated specimens. This behavior is most prominent in the transverse specimens, and less so in the longitudinal specimens. There is also a significant increase in tensile strength in the UV irradiated transverse specimens (Table 2.3). This behavior is present in the longitudinal specimens as well, but to a much smaller degree. The strain energy and tensile strength changes after UV irradiation are explained by the structure of UDCN as determined through the control UDCN specimen data.

The stress-strain behavior of UDCN specimens in the longitudinal direction is dominated by the nylon fibers. As nylon degrades when exposed to UV irradiation [22], the longitudinal specimens will theoretically have a decrease in both tensile strength and strain energy after prolonged UV exposure. However, the opposite is true due to the cross-linking of the urethane coating. The cross-linking in urethane strengthens the UDCN at a greater degree than the nylon degrades, resulting in an increase of strain energy. As the nylon fibers in the longitudinal direction are still the primary mode of failure, the urethane cross-linking only strengthens the material to a limit determined by the nylon, as seen by the minimal increase in tensile strength. This interaction between the cross-linking of urethane and UV degradation of nylon is seen more clearly in the transverse direction.

The UV irradiated transverse UDCN specimens experience a significant increase in both strain energy and tensile strength due to the transverse failure dependence on the urethane coating. Cross-linking

that occurs in the urethane drastically increases the strength of UDCN in the transverse direction as the secondary nylon fibers are not the primary structural component. As the UV irradiation simultaneously degrades the nylon fibers and cross-links the urethane coating, the urethane becomes stronger than the nylon fibers and dominates the material behavior. While cross-linking and chain scission both occur in the urethane coating, the increase in strength indicates a cross-linking dominance. This dominance could also be a result of thermal degradation as a result of prolonged heat exposure from the UV lamp. Thermal aging exhibits cross-linking dominance in polyurethanes at smaller time spans, while longer time spans sees a chain scission dominance [20]. In addition, the change in temperature directly affects the viscoelastic response of UDCN, and further testing would prove fruitful in distinguishing between the effects of cross-linking versus viscoelasticity.

Since a small number UDCN specimens were tested using the UV irradiation procedure (eight specimens in total), any conclusions drawn are considered preliminary. However, the stress-strain behavior of the tested specimens is very similar for the respective orientations, which indicates a degree of accuracy with these tests. Future testing is expected to verify the results of these preliminary tests.

2.3.5 Hyperelastic Modeling

Hyperelastic fits were performed on the UV irradiated specimen data. The Gent, Yeoh and Exponential Logarithmic models fit well with the transverse specimen data (Fig. 2.22a-2.22c), but not with the longitudinal data. The viscoelastic region in the longitudinal UDCN specimens is more pronounced after UV irradiation, and as such the error is large for the Gent, Yeoh and Exponential Logarithmic models. The Biderman, James-Green-Simpson, and Haines-Wilson models were again used to develop strong hyperelastic fits for the longitudinal UV test data (Fig. 2.22d-2.22f).

2.3.6 SEM Characterization

UDCN membranes under prolonged UV exposure indicate an increase in strain energy due to cross-linking. While this is not fully verified with the small sample size for tensile testing, SEM characterization

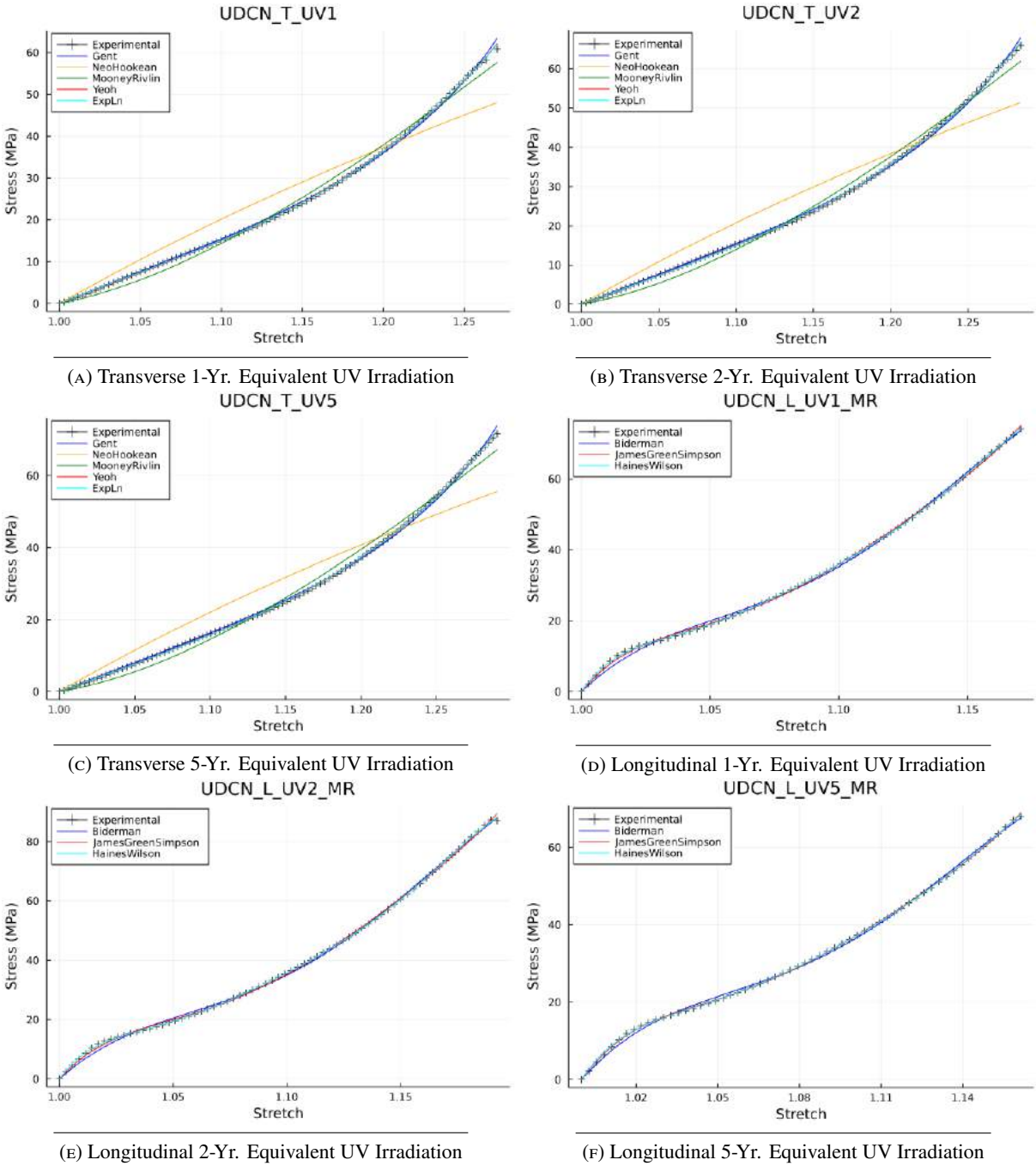

(A) Transverse 1-Yr. Equivalent UV Irradiation

(B) Transverse 2-Yr. Equivalent UV Irradiation

(C) Transverse 5-Yr. Equivalent UV Irradiation

(D) Longitudinal 1-Yr. Equivalent UV Irradiation

(E) Longitudinal 2-Yr. Equivalent UV Irradiation

(F) Longitudinal 5-Yr. Equivalent UV Irradiation

FIGURE 2.22: Hyperelastic models for transverse and longitudinal UDCN specimens after accelerated UV-A irradiation.

of the material supports this theory. Samples from the fractured UV irradiated specimens as well as a sample from a non-irradiated specimen were electroplated with gold for conductivity. The specimens were then observed using both a Jeoh JSM-IT100 and a Zeiss Sigma 500 VP SEM. Polyurethanes typically display high porosity without cross-linking, and higher degrees of cross-linking decrease the porosity [13, 26, 27]. Fig. 2.23 shows increased cross-linking on the cross-section of the samples subjected to UV irradiation, indicated by the comparatively low amount of porosity in the irradiated specimens. Inspection of the surface of UV irradiated specimens (Fig. 2.24) also shows remarkable similarities to photo-cross-linked polyurethanes [28]. The structures formed on the UDCN membrane surface after UV irradiation (Fig. 2.25) also exhibit similar smooth-rigid properties seen in chemically cross-linked polyurethanes [29].

2.4 Hydrolysis

2.4.1 Hydrolytic Behavior of Urethane Coated Fabrics

Understanding the effects of hydrolysis on UDCN membranes requires a knowledge of how urethanes and nylon fibers react with water. Nylon fibers exhibit greater degrees of degradation in both humid environments and when wet [15, 23]. In addition, photodegradation in nylon increases in humid climates, which is especially significant for uses in outdoor fluid-storage applications. Urethanes can exhibit high resistance to hydrolysis if they are polyether urethanes [1, 17, 20]. Polyester urethanes are very susceptible to hydrolysis, which are more commonly used in coated fabrics [1, 17, 20, 30]. Due to these effects, polyester urethane coated fabrics are well suited for fuel storage, while polyether urethane coated fabrics are more suited for water storage [1, 17]. Hydrolysis can be limited in polyester urethanes by adding certain stabilizers during synthesis [17, 20].

UDCN fabrics are highly dependent on their urethane coating to resist or succumb to hydrolysis. US Army researchers found a wide array of behaviors when studying hydrolysis effects on different UDCN fabrics [1, 17]. While practically all tested UDCN fabrics exhibited a decrease in tensile strength over

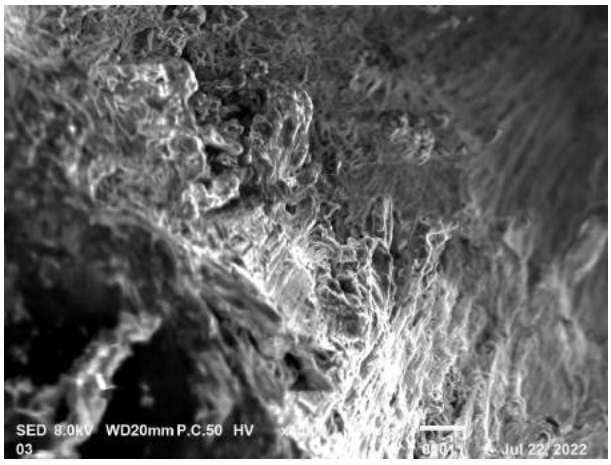

(A) 0 UV Irradiation

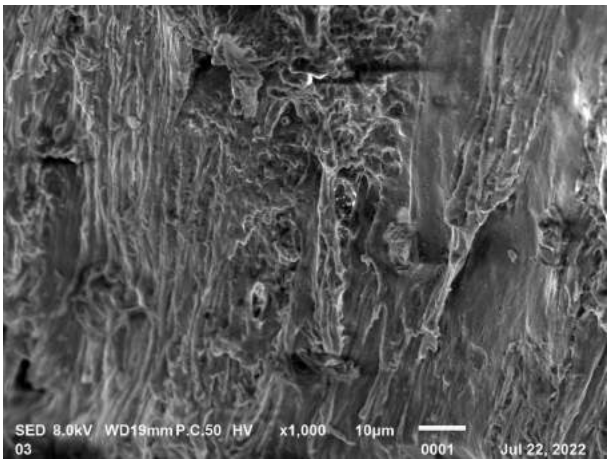

(B) 5-Year Equivalent UV Irradiation

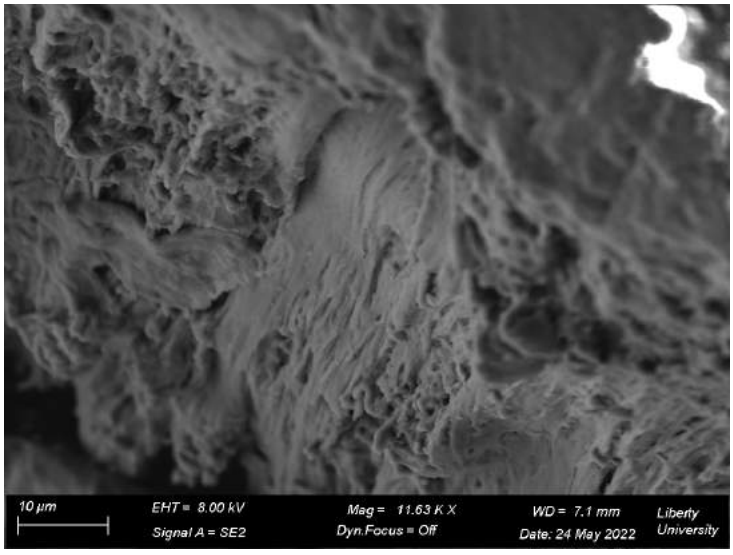

(C) 1-Year Equivalent UV Irradiation

FIGURE 2.23: SEM images of UDCN membrane cross-sections after UV irradiation. All images are at the 10 μm scale.

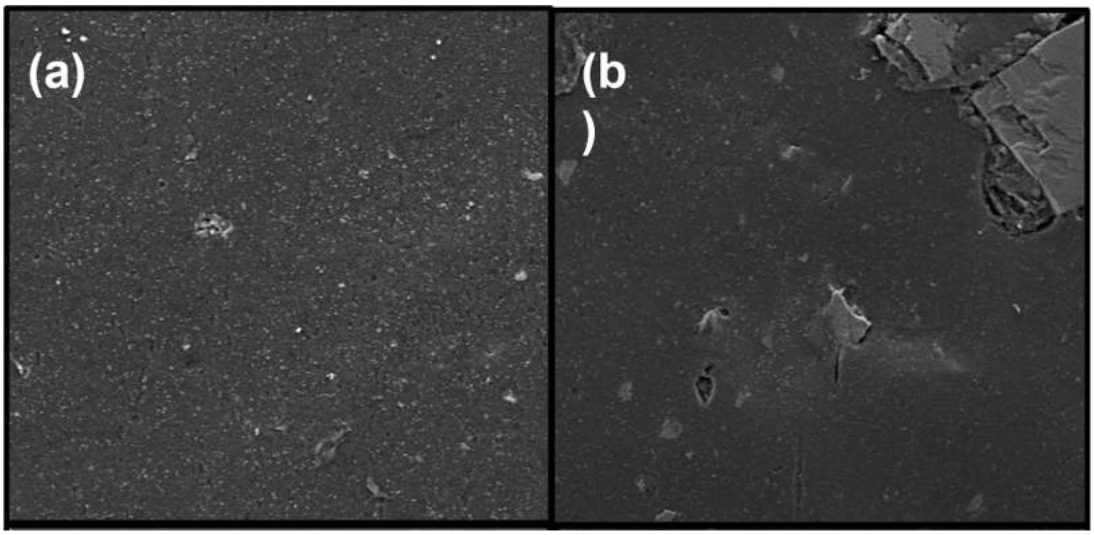

Removed to comply with copyright

https://doi.org/10.1007/s10924-017-1058-6 [28]

FIGURE 2.24: SEM imaging of: (a) UDCN membrane prior to UV irradiation, (b) UDCN membrane after 1-yr. equivalent UV-A irradiation, (c) Polyurethane prior to UV exposure [28], (d) Polyurethane after 40 days accelerated UV-B exposure [28]. All imaging is at the same 20 μm scale.

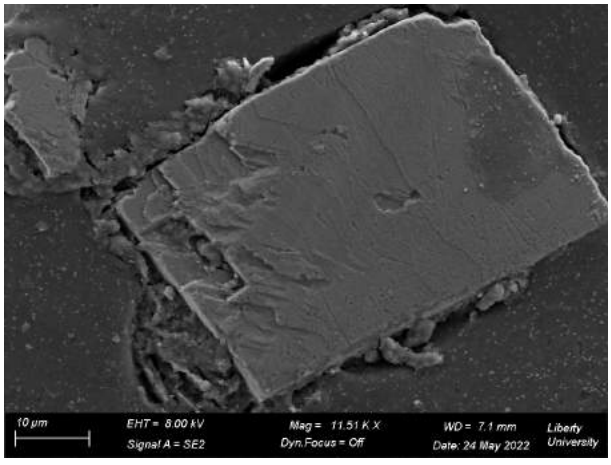

(A) Location 1, 10 μm scale

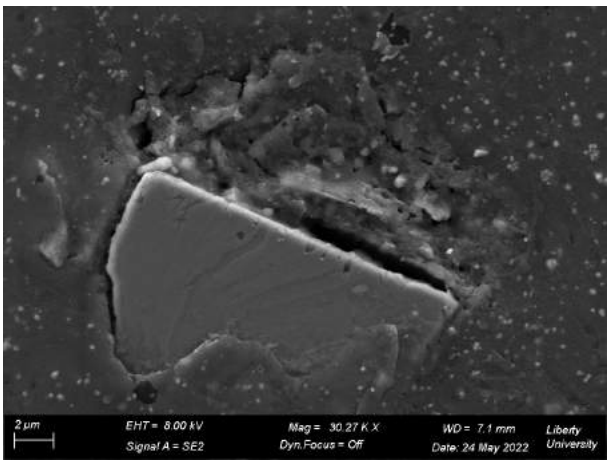

(B) Location 2, 2 μm scale

FIGURE 2.25: SEM images of UDCN membrane surface after 1-year equivalent UV irradiation.

(A) Water Immersed UDCN Specimens

(B) Sealed Hydrolysis Testing Container

FIGURE 2.26: UDCN specimens immersed in water for hydrolysis testing.

longer periods of water immersion, some of the fabrics showed significant resistance to hydrolysis, including those manufactured by Seaman [1]. Research into the behavior of the polyurethane coatings in combination with different additives showed that short periods of water immersion could increase both the tensile strength and ultimate elongation [17]. The Seaman engineered UDCN membrane used in this study is expected to behave similarly to the Seaman UDCN fabrics tested by US Army researchers.

2.4.2 Hydrolysis Test Method

A total of 24 of each transverse and longitudinal UDCN specimens were submerged in water in a sealed plastic container (Fig. 2.26). After one week of exposure, three specimens for each orientation were removed from the container and subjected to monotonic tensile loading at 5 mm/min until failure. This process was repeated to obtain hydrolytic monotonic tensile data for 2, 3, 4, 5, 6, 8 and 12 weeks of water submersion. Additionally, the process was repeated using 4 and 8 weeks of water exposure for UDCN specimens at 30° and 60° orientations, and for transverse and longitudinal XR-5 8138 and 8142 geomembrane specimens. There were three specimens tested for each orientation and quantity of weeks of water immersion.

2.4.3 Hydrolysis Experimental Results

Fractured hydrolysis specimens are shown in Appendix B, with no significant differences in the fracture surfaces between the water-immersed and dry-tested specimens. Most of the monotonic tensile test results on the water-immersed specimens showed a significant decrease in tensile strength (Fig. 2.27-2.30). The

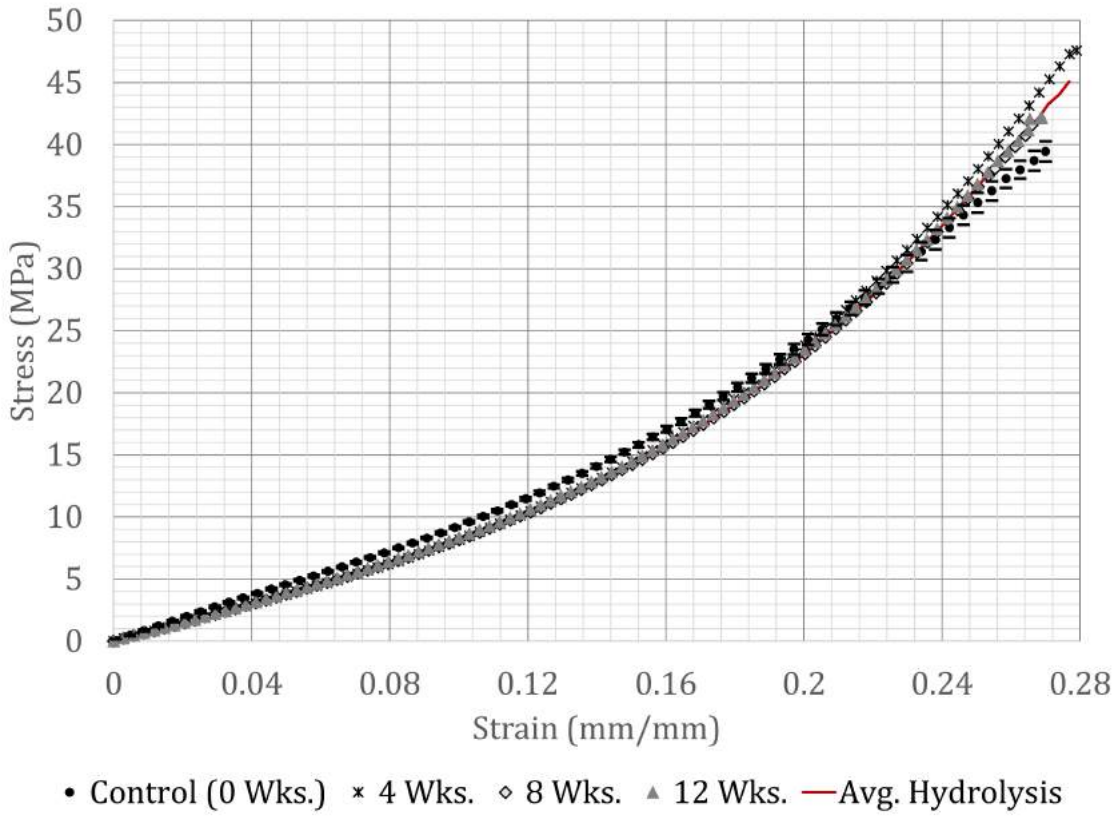

FIGURE 2.27: Stress-strain data for transverse UDCN specimens after water-immersion. Each data set is the average of 3 specimens tested at 5 mm/min. There is a 95% confidence interval of ±2.06%, ±1.92%, ±4.36% and ±2.28% for 0, 4, 8 and 12 weeks of water-immersion, respectively.

data for the UDCN specimens was nearly identical across all of the immersed test specimens, so only the most relevant data sets are shown. The transverse UDCN data did not see the same decrease in tensile strength as the other UDCN specimens (Fig. 2.27). In fact, the tensile strength increased in all cases for the transverse specimens, in addition to an increase in fracture strain in most cases. The water-immersed transverse specimens also saw lower stresses at small strains than the control specimens.

The tensile strength of the XR-5 specimens decreased with increasing water-immersion time (Fig. 2.31). The decrease in strength is a gradual reduction for the XR-5 geomembranes, as opposed to a sharp decrease for the majority of UDCN membrane specimens. In addition, the UDCN membranes appear to reach a lower limit for the strength and energy, while the XR-5 membranes do not reach that limit. However, the behavior of the XR-5 membranes at lower strains is indistinguishable between the different weeks of water-immersion, as is the case in the UDCN membranes.

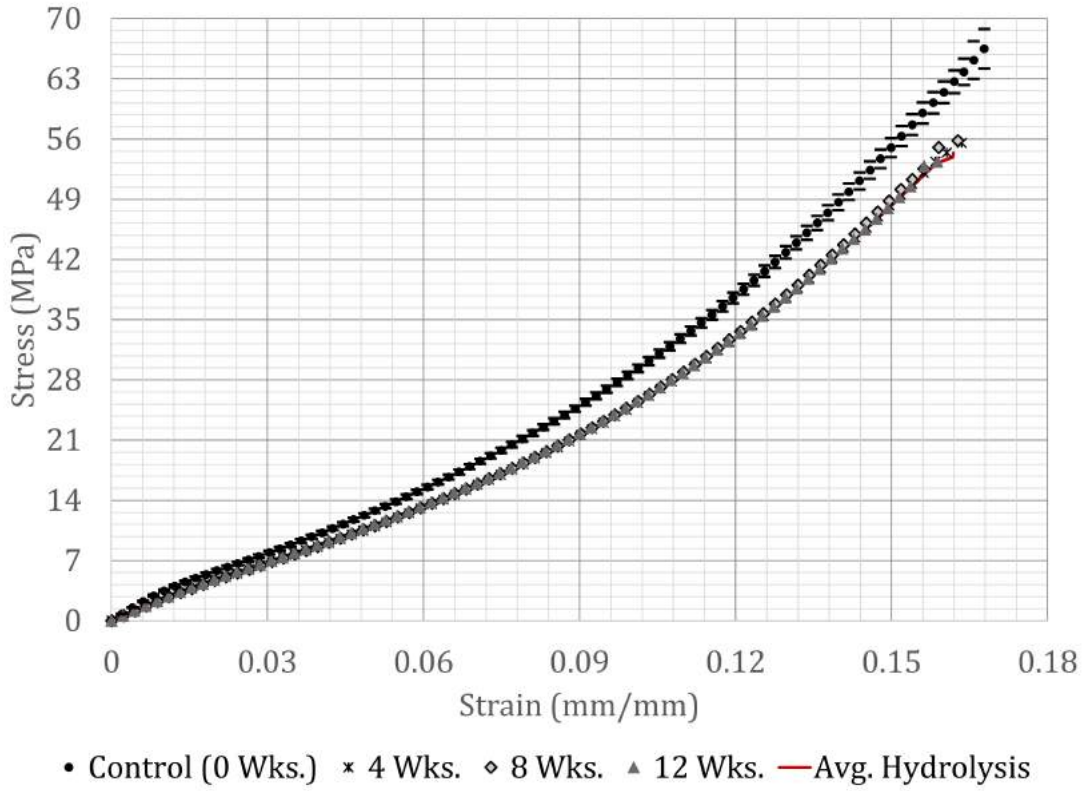

FIGURE 2.28: Stress-strain data for longitudinal UDCN specimens after water-immersion. Each data set is the average of 3 specimens tested at 5 mm/min. There is a 95% confidence interval of ±3.46%, ±2.66%, ±2.31% and ±8.37% for 0, 4, 8 and 12 weeks of water-immersion, respectively.

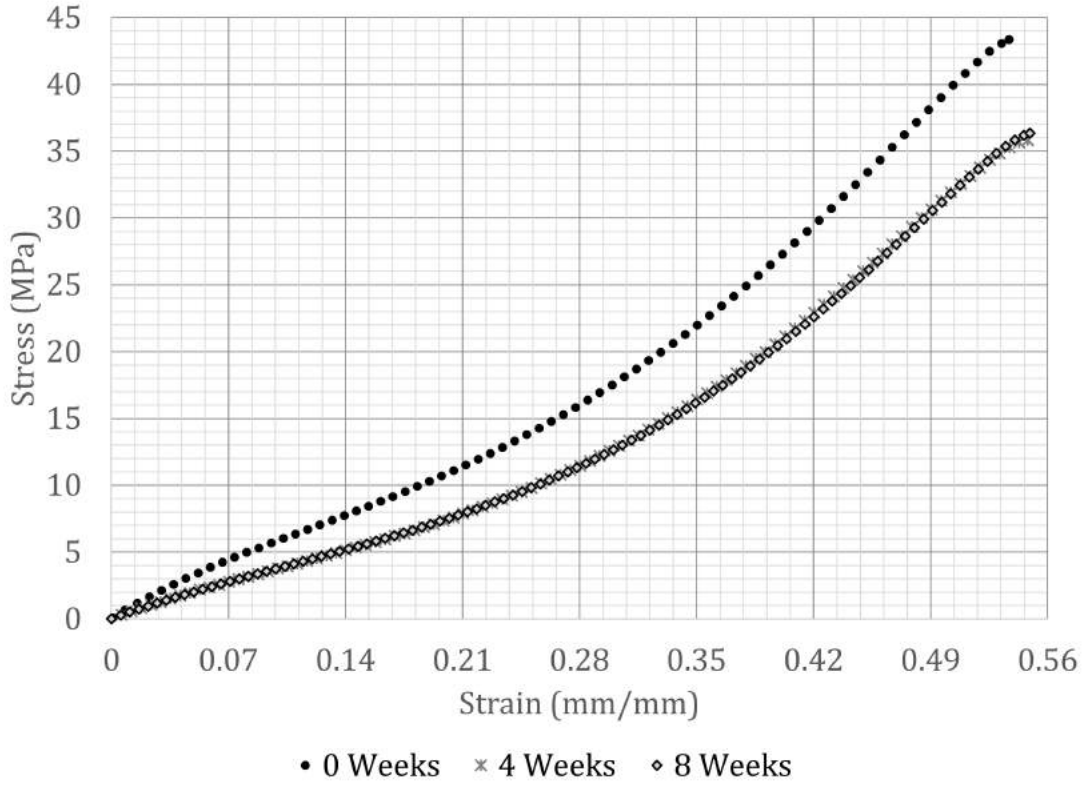

FIGURE 2.29: Stress-strain data for 30° UDCN specimens after water-immersion. Each data set is the average of 3 specimens tested at 5 mm/min. There is a 95% confidence interval of ±0.28%, ±0.75% and ±2.18% for 0, 4 and 8 weeks of water-immersion, respectively.

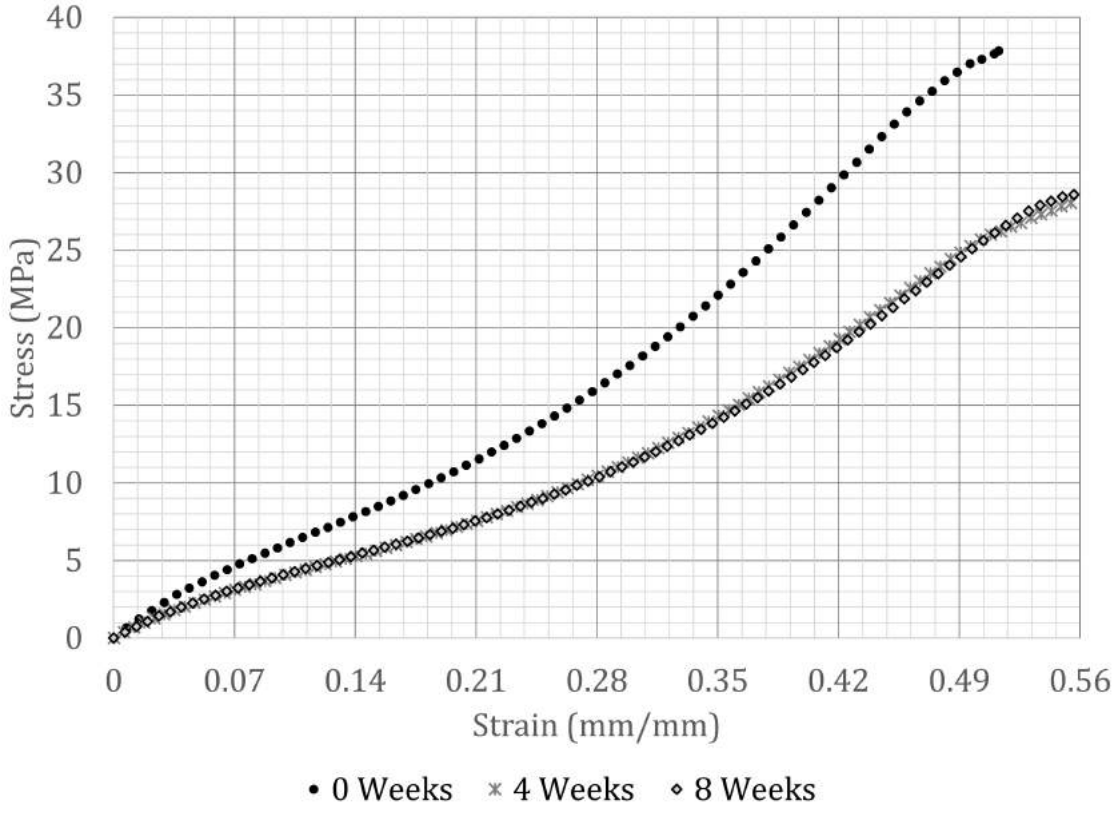

FIGURE 2.30: Stress-strain data for 60° UDCN specimens after water-immersion. Each data set is the average of 3 specimens tested at 5 mm/min. There is a 95% confidence interval of ±1.35%, ±3.17% and ±2.02% for 0, 4 and 8 weeks of water-immersion, respectively.

2.4.4 Analysis and Comparison

The transverse UDCN specimens displayed little to no hydrolysis effects, with the tensile strength actually increasing slightly after water exposure. The total strain energy remained similar, decreasing by less than 4% after water exposure (Table 2.4). As the data is closely grouped for the transverse UDCN specimens- both before and after water exposure- no strong conclusions can be made based on that data alone. The longitudinal and angled UDCN specimens provided much more insight in regards to hydrolysis.

As with the transverse hydrolysis specimens, the data after each week of water exposure for the longitudinal specimens remained very similar. However, water did have a significant effect on the UDCN membrane as evidenced by Figure 2.28. The longitudinal specimens saw a decrease in both tensile strength and strain energy after just one week of water exposure. This hydrolysis effect remained constant throughout the twelve weeks of testing despite the increased time of water exposure. Due to the longitudinal specimen's primary dependence on the primary nylon fibers, the data implies an initial weakening of nylon fibers

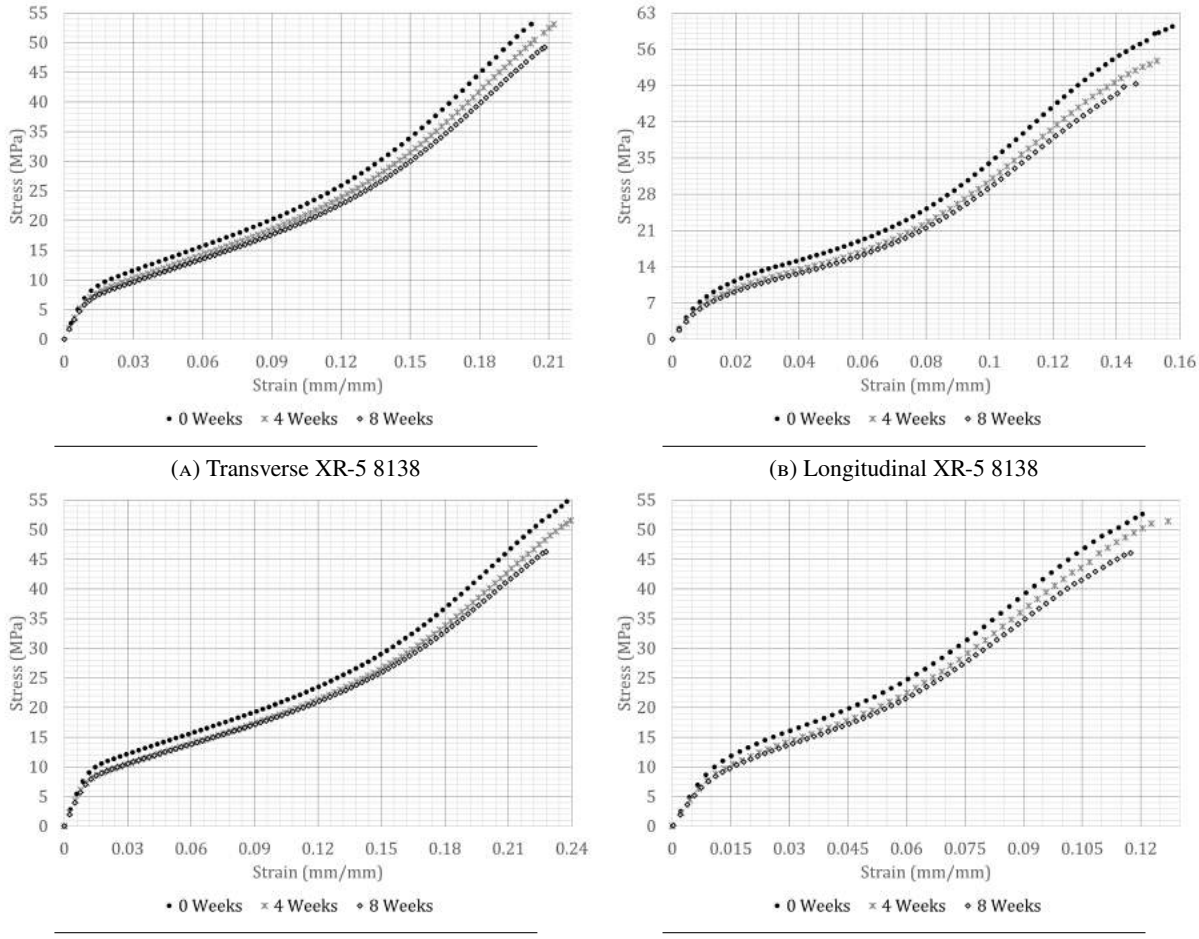

(A) Transverse XR-5 8138

(B) Longitudinal XR-5 8138

(C) Transverse XR-5 8142

(D) Longitudinal XR-5 8142

FIGURE 2.31: Average stress-strain data for XR-5 geomembrane specimens after water-immersion. Each data set is the average of 3 specimens tested at 5 mm/min. The 8138 transverse specimens have a 95% confidence interval of ±0.42%, ±0.91% and ±0.34% for 0, 4 and 8 weeks of water-immersion, respectively. The 8138 longitudinal specimens have a 95% confidence interval of ±2.38%, ±2.0% and ±0.87% for 0, 4 and 8 weeks of water-immersion, respectively. The 8142 transverse specimens have a 95% confidence interval of ±1.2%, ±3.3% and ±1.77% for 0, 4 and 8 weeks of water-immersion, respectively. The 8142 longitudinal specimens have a 95% confidence interval of ±0.99%, ±0.46% and ±0.56% for 0, 4 and 8 weeks of water-immersion, respectively.

due to hydrolysis. This conclusion is supported by reported tenacity values for dry and wet nylon 6 fibers [15]. However, similar decreases in strain energy and tensile strength occur in the urethane-dominated angled specimens.

Since the angled UDCN specimens behave primarily like their urethane constituent, Table 2.4 implies that urethane is weakened due to hydrolysis. This behavior mimics that seen in the nylon fibers in the longitudinal specimens. However, urethanes have been reported to degrade to varying degrees due to hydrolysis [20, 31]. This degradation is often due to voids created through water absorption in urethane [20]. The hydrolytic degradation of both urethane and nylon is supported by the longitudinal and angled

TABLE 2.4: Strain Energy and Tensile Strength of Water-Immersed UDCN Specimens

UDCN Specimen & Weeks of Water Submersion	**Strain Energy (MJ/m^3)**	**Tensile Strength (MPa)**
Transverse (0, control)	4.264	39.6
Transverse (4)	4.633	47.6
Transverse (8)	3.948	41.6
Transverse Average Change	**-3.91%**	**12.63%**
Longitudinal (0, control)	4.468	66.5
Longitudinal (4)	3.619	55.5
Longitudinal (8)	3.627	55.8
Longitudinal Average Change	**-18.91%**	**-16.32%**
30° (0, control)	9.612	43.4
30° (4)	7.64	35.8
30° (8)	7.655	36.2
30° Average Change	**-20.44%**	**-17.05%**
60° (0, control)	8.563	37.8
60° (4)	7.263	28.1
60° (8)	7.09	28.6
60° Average Change	**-16.19%**	**-25%**

data, which brings into question the transverse UDCN data.

The lack of hydrolytic degradation in the transverse UDCN specimens seemingly contradicts reports on urethane and nylon fibers [1, 15, 17, 20, 23, 30]. However, the fracture surfaces may be useful in analyzing this phenomenon. The fracture surfaces for transverse UDCN specimens without water exposure were all significantly angled, with the failures generally occurring at angles of 35°-50°. In the transverse specimens tested after hydrolysis, the fracture is either fully orthogonal to the loading or has a small angle. The orthogonal mode of failure is present in the longitudinal specimens and indicates a failure of the urethane coating simultaneous with the failure of the nylon fibers. This is significant because the transverse specimens without hydrolysis showed an asymmetrical stress concentration along an edge that propagated across the material until failure. The UDCN membranes immersed in water exhibit a decrease in tensile strength simultaneous with an increase in fracture strain in the urethane coating, evidenced by the behavior of the angled specimens. The increase in elasticity of the urethane coating results in the failure of the transverse specimens becoming nylon-fiber dominant as it cannot withstand higher strains. The reason for the increase in tensile strength in the transverse UDCN specimens is then a combination of nylon-fiber dominance with the lack of an asymmetrical stress concentration.

The XR-5 geomembrane specimens displayed hydrolytic deterioriation in all test cases. While the

TABLE 2.5: Strain Energy and Tensile Strength of Water-Immersed XR-5 Specimens

XR-5 Specimen & Weeks of Water Submersion	**Strain Energy (MJ/m^3)**	**Tensile Strength (MPa)**
Transverse 8138 (0, control)	5.042	53.1
Transverse 8138 (4)	5.151	53.0
Transverse 8138 (8)	4.715	49.0
Longitudinal 8138 (0, control)	4.748	60.4
Longitudinal 8138 (4)	3.859	53.7
Longitudinal 8138 (8)	3.343	49.3
Transverse 8142 (0, control)	6.204	54.7
Transverse 8142 (4)	5.793	51.5
Transverse 8142 (8)	5.071	46.2
Longitudinal 8142 (0, control)	3.269	52.6
Longitudinal 8142 (4)	3.356	51.4
Longitudinal 8142 (8)	2.741	46.1

UDCN specimen data remained consistent for all weeks of water exposure, the XR-5 specimens gradually weakened with additional weeks of submersion. Table 2.5 showcases this effect. Both the strain energy and tensile strength of XR-5 specimens in both orientations decreased with increased water exposure, with a couple slight exceptions for the strain energy. While the XR-5 8142 specimens saw similar changes in strain energy between the longitudinal and transverse specimens, the decrease in strain energy for the XR-5 8138 specimens was significantly larger in the longitudinal direction than in the transverse direction.

2.4.5 Hyperelastic Modeling

Hyperelastic modeling was performed for the hydrolysis data using the same methods previously mentioned for the control and UV irradiated specimens. Similar trends were seen, with the Gent, Yeoh and Exponential Logarithmic models fitting the UDCN data well. While these models did not fit the longitudinal UV specimens well under the control and UV irradiation conditions, they did fit the post-hydrolysis data very well (Fig. 2.32). While the angled hydrolysis specimens had low mean-squared errors with the Gent, Yeoh and Exponential Logarithmic models, the models did not fit the initial or yielding regions well. For this reason, the previously mentioned higher-order Mooney-Rivlin models were also tested for the angled specimens.

Based on the hyperelastic models used, the longitudinal UDCN specimens became less hyperelastic as

they degraded from hydrolysis. This effect is attributed to the nylon fibers losing both strength and elasticity from hydrolytic deterioration. The angled UDCN specimens also saw a decreased hyperelasticity due to hydrolysis. The decrease in strain energy reflects a hydrolytic deterioration in the angled UDCN specimens. This behavior is shown by the lowered mean-squared errors in the Gent, Yeoh and Exponential Logarithmic models. As with the control XR-5 data, Biderman, James-Green-Simpson, and Haines-Wilson models for the hydrolyzed XR-5 membranes are shown in Appendix A.

2.5 Creep

2.5.1 Creep and Viscoelasticity

The monotonic tensile testing of UDCN showed a strain-rate sensitivity for the material. This viscoelastic behavior, and specifically non-linear viscoelasticity, is common among polymers, especially in urethanes [32, 33, 34]. Creep testing, as well as temperature-dependent creep testing, is often used to further explore the viscoelastic response of materials. Viscoelasticity in UDCN is pertinent for fluid-storage applications due to both temperature changes as a result of weather and the small strain-rate resulting from filling or emptying the storage tanks.

This study investigates the creep response of UDCN membranes for the purpose of modeling and predicting the behavior of UDCN under varied thermal and loading conditions. A creep model is especially useful for predicting stresses seen by and longevity of UDCN membrane tanks in fluid-storage applications. The results of the performed creep testing, and subsequently the developed creep model, were implemented with results from a lab-scale PSH loop in order to develop an analytical model for flexible membrane tanks in PSH applications.

2.5.2 Creep Test Method

Creep testing was performed on Type I ASTM D638 UDCN specimens, using the ASTM D2990 [5] and ISO 899-1 [7] standards as references. Three stress values were selected at even increments at 3.833 MPa,

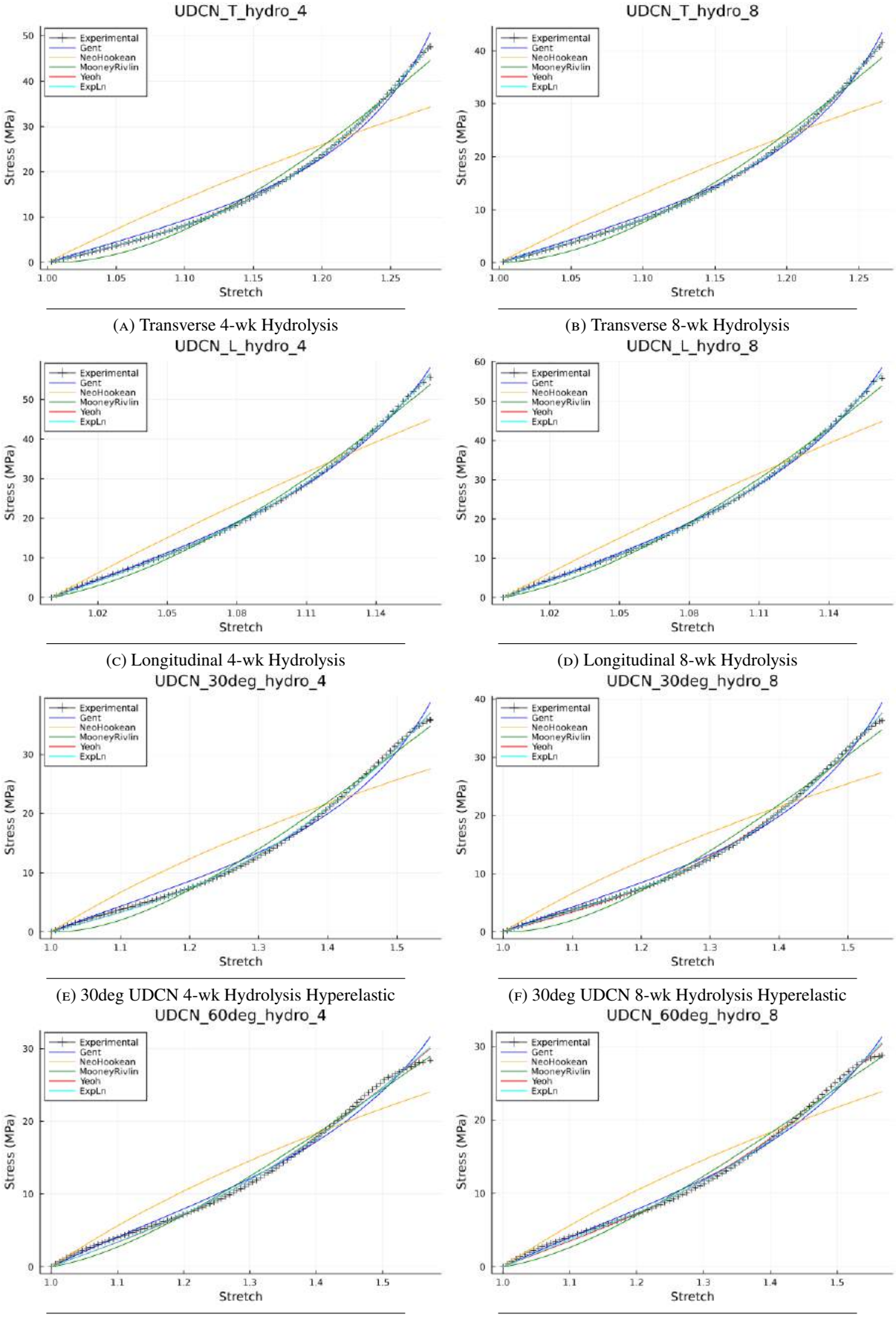

(A) Transverse 4-wk Hydrolysis

(B) Transverse 8-wk Hydrolysis

(C) Longitudinal 4-wk Hydrolysis

(D) Longitudinal 8-wk Hydrolysis

(E) 30deg UDCN 4-wk Hydrolysis Hyperelastic

(F) 30deg UDCN 8-wk Hydrolysis Hyperelastic

(G) 60deg UDCN 4-wk Hydrolysis Hyperelastic

(H) 60deg UDCN 8-wk Hydrolysis Hyperelastic

FIGURE 2.32: Hyperelastic models for UDCN membranes after water-immersion.

FIGURE 2.33: Modified 50° creep UDCN specimen with holes for pin grips.

7.667 MPa and 11.5 MPa, which corresponds to a range of 15-50% of the fracture strain for the transverse UDCN specimens under monotonic loading. This range was selected to provide an adequate range of testing for both longitudinal and transverse specimens while staying under the approximated 1000-hour creep-rupture limit of 12 MPa for the transverse specimens. Three UDCN specimens of both longitudinal and transverse orientations were tested at each stress level on an Instron 5982 universal testing system. The tensile load was ramped within 5 seconds to the load required for the stress level, and that loading was held constant for five hours. These room temperature creep tests were performed at 21°C.

The process was also repeated at 50°C using a Severn SF2291A split furnace with an Instron TCS3203 temperature controller. The UDCN specimens in the 50°C tests were altered to allow the use of the split furnace pin-grips (Fig. 2.33). To compensate for the holes, square grips were attached on either side of the specimen to bear the load from the pin. The grips were offset slightly so only the square grips received directly loading from the pin grips instead of the creep specimens themselves. While these modifications were made to distribute the loading throughout the grips of the specimens, there is still a stress concentration around the holes in the modified specimens. However, this stress concentration is assumed to have an insignificant affect on the gauge section of the specimens due to the small loading applied and the narrow width of the gauge section.

2.5.3 Creep Data and Analysis

All strain-time plots of the creep experimental data are located in Appendix C. The transverse specimens at room temperature show a direct correlation between the stress and strain. After 5 hours at 11.5 MPa, the transverse specimens reach a strain of 0.13, which is approximately 50% of the fracture strain as determined by monotonic testing. At 7.667 and 3.833 MPa, the strains after 5-hours decrease to approximately 68% and 33% of the strain at 11.5 MPa, respectively. This approximately linear

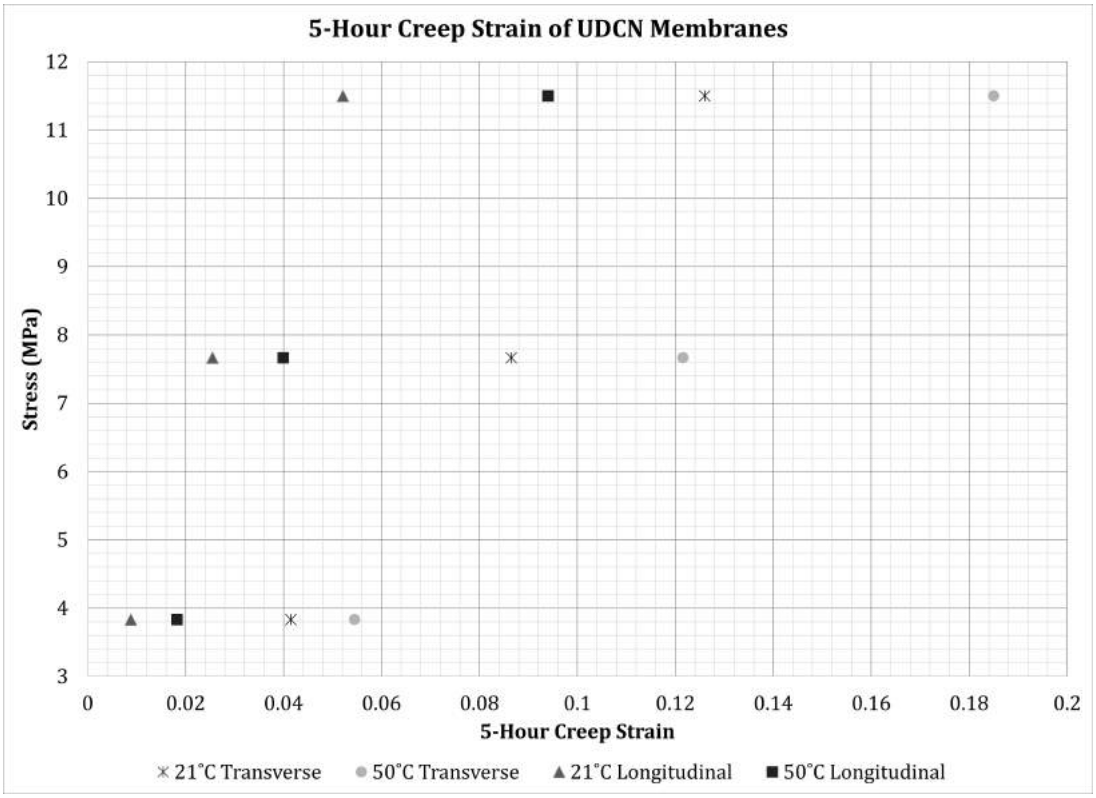

FIGURE 2.34: UDCN membrane creep strain after 5-hours. Each data point is an average of three specimens.

TABLE 2.6: Transverse Specimen Creep Strain at 5-hours

Stress (MPa)	Temperature (°C)	Average 5-hr. Strain
11.5	21	0.126
11.5	50	0.185
7.667	21	0.0865
7.667	50	0.1216
3.833	21	0.0415
3.833	50	0.0545

relationship between the constant stress and strain after creep is also present in the transverse specimens tested at 50°C. Fig. 2.34 indicates this linearity for the transverse specimens, while the longitudinal data indicates a logarithmic relationship between stress and creep strain. The 5-hour strain for longitudinal specimens at 3.833 MPa is 17-19% of the strain at 11.5 MPa, depending on the temperature. The 5-hour strain at 7.667 MPa is 42-49% of the strain at 11.5 MPa. The values used for these calculations are shown in Tables 2.6 and 2.7.

There are two main distinctions between the data from the room temperature and 50°C creep tests. The first of which is the significant increase in strain correlating to the increase in temperature. The

TABLE 2.7: Longitudinal Specimen Creep Strain at 5-hours

Stress (MPa)	**Temperature (°C)**	**Average 5-hr. Strain**
11.5	21	0.0521
11.5	50	0.094
7.667	21	0.0255
7.667	50	0.0399
3.833	21	0.0088
3.833	50	0.0182

increase in strain is expected as it is the typical behavior at increased temperatures [33, 35, 36]. The more interesting difference between the temperatures is the stabilization of strain at higher temperatures. The strain increases at a higher rate for the specimens at room temperature than the specimens at 50°C. Though the difference in the strain rates during creep is not considerable, its presence is atypical for polyurethanes [35, 36]. Further investigation is required to find the cause of this phenomenon.

Further creep tests are required to provide an in depth characterization of creep for UDCN membranes. The Instron used for testing has a 100 kN load cell while the loads applied during testing were all smaller than 1 kN. This developed fluctuations in the data that is most noticeable at smaller loadings and higher temperatures. To compensate for this issue in future tests, a machine with a smaller load cell should be used. This will also aid in providing larger ranges for both stress and temperature in order to better characterize creep in UDCN.

For most of the data sets, the strain is much more precise for two of the specimens than it is for the remaining specimen. However, there is no correlation between the order of specimen testing and the precision of the data. While the overall precision is good for most of the specimens, the transverse specimens tested at 50°C at 11.5 MPa exhibit a significant difference in strains from Specimen 10 to Specimens 11 and 12. The reason for this discrepancy is likely user error, with the assumption that the temperature in the furnace was not at steady-state prior to inserting Specimen 10. This theory is supported by data for Specimen 10 lying almost halfway between the data for Specimens 11 and 12 and Specimens 1-3. This issue can be solved in future testing by adding a heating period to the test procedure to ensure the furnace reaches the proper temperature.

2.5.4 Creep Modeling

Creep modeling of UDCN membranes requires a model that works well for non-linear viscoelastic materials. Research into different models found that the Nutting and Miller-Norton laws are well suited for UDCN characterization [35, 37, 38, 39, 40, 41]. The Nutting equation (Eqn. 2.1) is a power law equation for nonlinear viscoelastic materials often used to model the primary and secondary creep regions of polymers.

$$\varepsilon = \varepsilon_0 + A\sigma^n t^m \tag{2.1}$$

where ε_0 is the initial strain, σ is the constant stress, t is time, and A, n and m are material constants [37, 39]. The relations n>1 and m<1 are required in the Nutting equation, with the values for polymers typically in ranges of 1.4 < n < 3 and 0.15 < m < 0.3 [37, 42].

The Miller-Norton law (Eqn. 2.2) is another power law equation used in the same scenarios as the Nutting equation, except the Miller-Norton law is also temperature dependent [35, 40, 41].

$$\varepsilon_{cr} = \frac{A\sigma^n t^m}{m+1} exp\left(\frac{-Q}{RT}\right) \tag{2.2}$$

where $\varepsilon_c r$ is the creep strain, Q is the activation energy, T is the absolute temperature, R is the universal gas constant, t is time, σ is the constant stress, and A, n and m are material constants [35, 40, 41]. Upon further inspection, the Nutting and Miller-Norton laws are effectually equivalent and can be simplified into Eqn. 2.3, which is temperature and time dependent.

$$\varepsilon = \varepsilon_0 + \frac{A\sigma^n t^m exp\left(\frac{-Q}{RT}\right)}{m} \tag{2.3}$$

Nutting creep was found to effectively model creep based on the collected data, using $n = 1.95$ and $m = 0.15$ for all cases. The values of ε_0 and A were found to change depending on stress and temperature, so a relation could be derived once more data is collected. The implementation of the modified Miller-Norton law (Eqn. 2.3) is plausible, but currently inaccurate without a greater sample of test data.

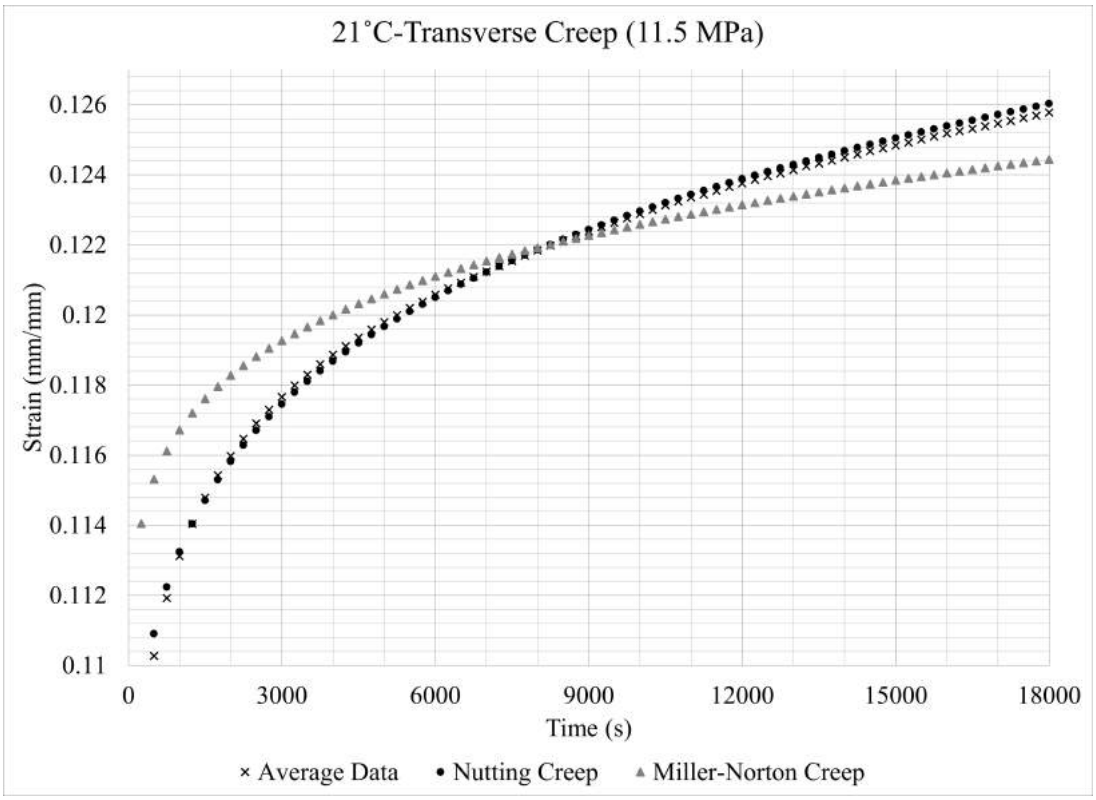

FIGURE 2.35: Creep models at 21°C.

Preliminary results found that the initial strain must be temperature dependent for any degree of accuracy with the temperature dependent model. The constant A should also be temperature dependent for better accuracy, but more data is necessary to accurately determine the temperature dependent relation for these variables. Fig. 2.35 and 2.36 show the results of preliminary testing, where the Nutting creep models were optimized for each temperature, while the constants for the Miller-Norton model were held constant between the temperatures except for ε_0.

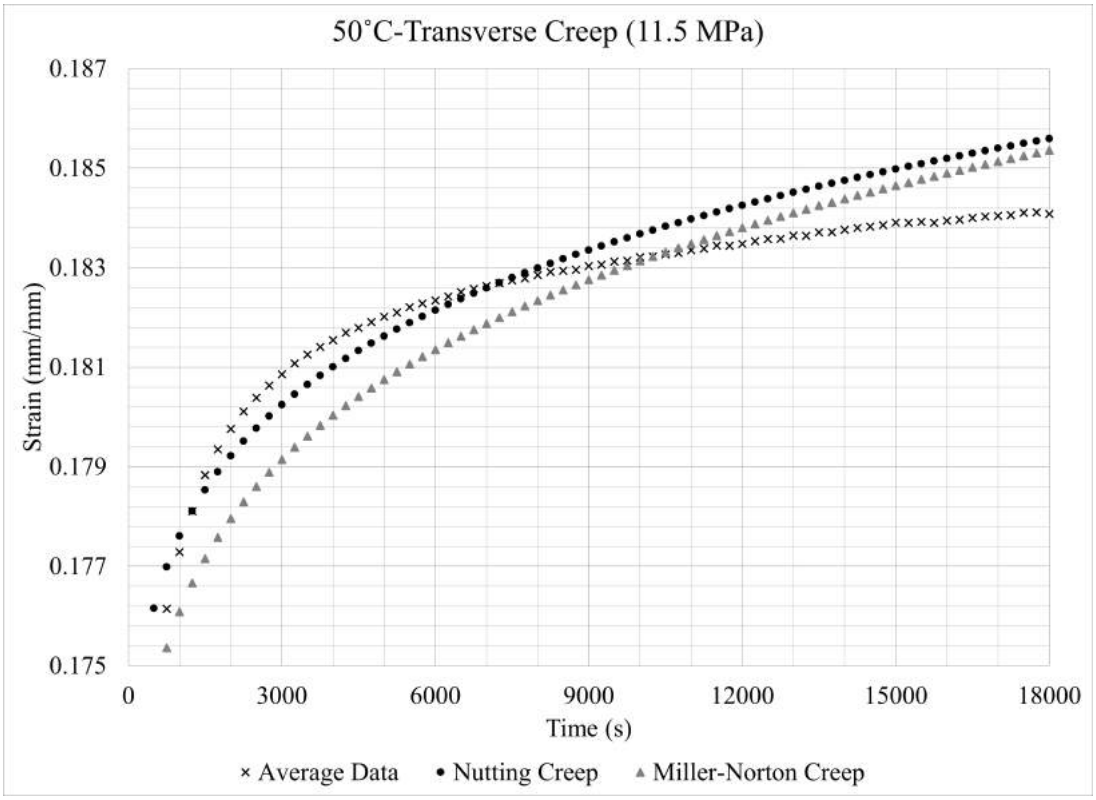

FIGURE 2.36: Creep models at 50°C.

Chapter 3

Pumped-Storage Hydropower Experiment

3.1 PSH Introduction

Pumped storage hydropower (PSH) is an energy storing method that utilizes the potential energy of water as it travels from an upper to lower reservoir [2, 43]. PSH technologies are constantly being researched and developed to provide more clean energy sources [43, 44]. One of the biggest issues with current PSH technologies is the high costs associated with reservoir construction [2, 45, 46, 47]. A hybrid modular closed-loop PSH system (h-mcs-PSH) has been proposed by Drs. Thomas Eldredge and Hector Medina which would use polymeric bladder tanks to reduce capital costs [43, 44]. Average PSH costs were $ 2638/kW as of 2018, with some technologies costing upwards of $ 3400/kW [45, 47]. The proposed h-mcs-PSH system could utilize UDCN membrane bladder tanks to decrease these costs to $ 2235/kW for a 10 MW plant [43, 44]. In addition, h-mcs-PSH systems have a much smaller footprint than typical PSH systems, allowing for more environmentally friendly and urban implementations [43, 44].

3.2 Lab-scale PSH Loop Construction

3.2.1 Design of PSH Loop

The lab-scale PSH loop uses a 100-gallon UDCN-membrane tank as the upper reservoir and a 100-gallon polypropylene (PPE) tank as the lower reservoir. Water flow is controlled via a system of four solenoid

FIGURE 3.1: PPE Tank and Hydraulic Mock Setup

valves connected around a Finish Thompson SP10 pump. Water flow into and out of the lower reservoir will also be controlled via a manual needle valve. A preliminary setup of the PPE tank and hydraulic system is shown in Fig. 3.1. The UDCN bladder tank used in the PSH loop is shown in Fig. 3.2. The design of the system allows the UDCN bladder tank to be filled while atop 30-foot scaffolding when the 1st and 3rd solenoid valves are open, and the 2nd and 4th valves are closed. When the 2nd and 4th solenoid valves are opened and the 1st and 3rd valves are closed, the UDCN bladder tank empties into the PPE tank. The solenoid valves are controlled via LabVIEW software, which also records data from all attached sensors.

Three types of sensors were utilized for data collection in the lab-scale PSH loop. A submersible pressure transducer (Fig. 3.3b was used inside the UDCN bladder tank to monitor the volume of water inside the tank. Strain gauges (Fig. 3.3a) were mounted in different locations on the surface of the UDCN tank to monitor displacements seen in the membrane during operation of the PSH loop. Since strain gauges are better suited for controlled environments than for outdoor use, linear variable displacement transducers (LVDTs) were also used to monitor displacement (Fig. 3.3c).

(A) 100-gallon UDCN Bladder Tank

(B) Filled UDCN Bladder Tank

FIGURE 3.2: UDCN membrane bladder tank used in the lab-scale PSH experiment.

(A) Omega Strain Gauges

(B) APG PT-510 Submersible Pressure Transducer

(C) Solartron LVDT

FIGURE 3.3: Sensors used for data collection in the lab-scale PSH loop.

3.2.2 Implementation of PSH Design

Implementation of the lab-scale PSH loop required a significant amount of time for design and construction in order to ensure safety and functionality. Wooden supports were designed and reinforced by steel plating to house the PPE tank. A support for the UDCN tank was fashioned using a wooden pallet and reinforced with plywood. These supports were necessary to prevent the tanks from sliding or tipping, as well as to provide access beneath for tubing and connections. A 30-foot scaffolding was constructed and secured to a tree for stability in order to house the upper reservoir, shown in Fig. 3.4. After the scaffolding was secured and the upper reservoir was mounted, the hydraulic and electrical connections were implemented. A PVC conduit was utilized at the base of the scaffolding (see Fig. 3.5)for the wires to pass safely inside the control room. The control room housed the power sources and DAQ controls for the system, seen in Fig. 3.6. The initial sensor placements are shown in Fig. 3.7.

3.2.3 Revision of System and Improvements

The initial PSH-loop design required regular maintenance and innovation due to effects from weather and nature. These issues would not be significant in a larger-scale PSH-loop, but for the lab-scale system they proved to be a severe hindrance. The PSH-loop construction was finished in the winter and testing began promptly. However, this resulted in the water freezing in both the vinyl tubing and the pump. To resolve this issue, 30-gallons of RV & Marine antifreeze were added to the system as seen in Fig. 3.8, resulting in a 76%-24% ratio of water to antifreeze.

The locale where the PSH-loop was constructed often experiences high wind gusts and storms, which resulted in the UDCN tank folding over when not in use, and even being blown over the side of the scaffolding. While ropes and the tubing secured the tank from fully separating from the system, the issue of wind was ever-present during the experimentation phase. The repeated folding of the tank in combination with rain and UV degradation rendered the mounted strain gauges unusable. The UDCN tank was further weighed down by fifty gallons of water and secured by bungee cords to prevent the tank

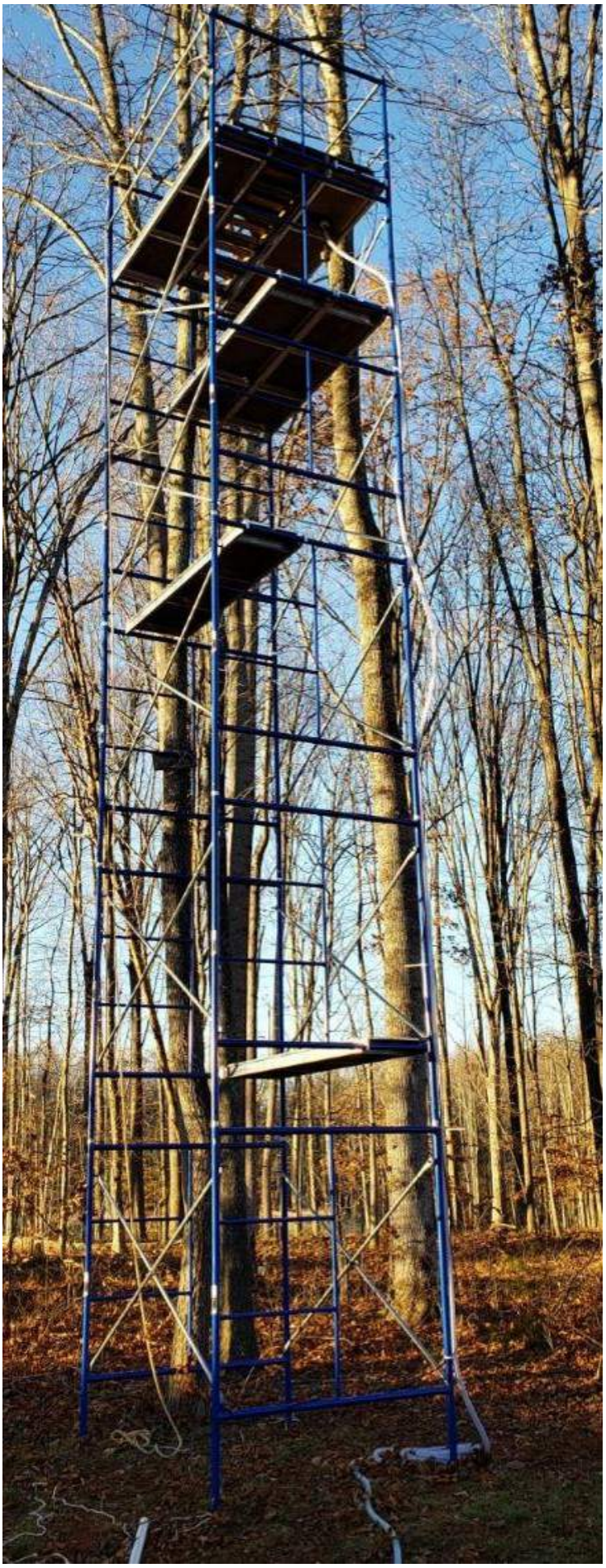

FIGURE 3.4: Scaffolding with UDCN Bladder Tank and Connections

FIGURE 3.5: Sensor Wiring, PVC Conduit and Hydraulic Tubing

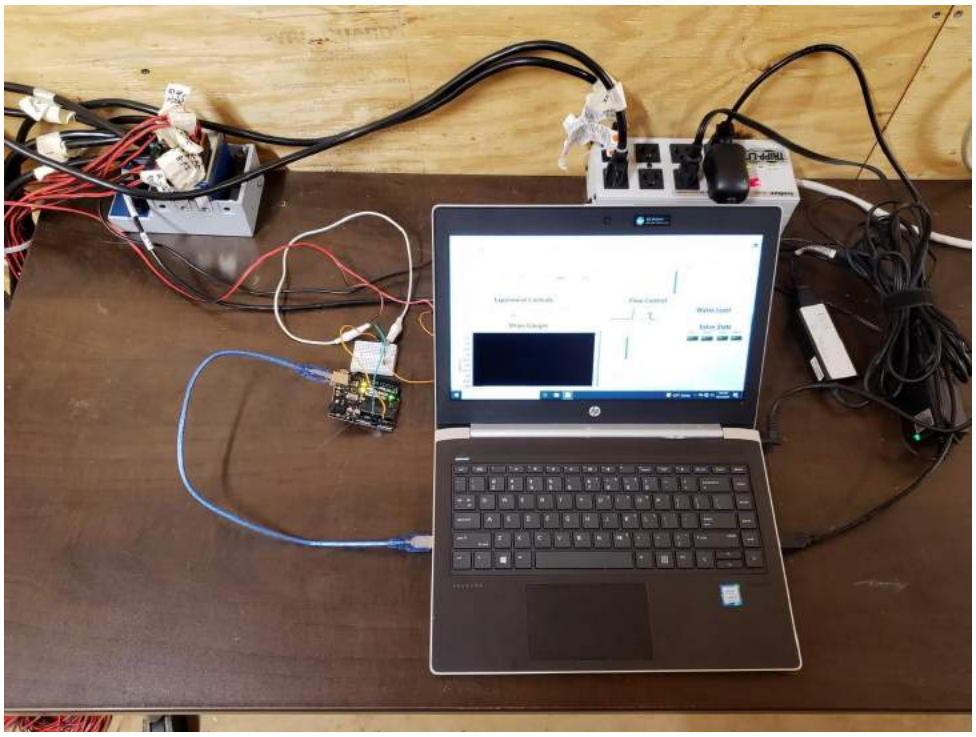

FIGURE 3.6: LabVIEW DAQ and Sensor Modules

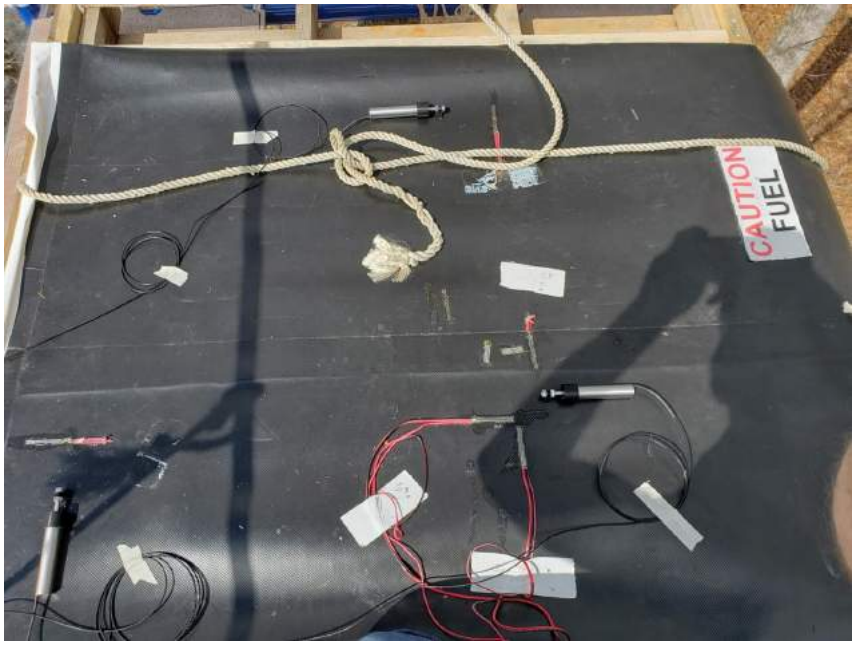

FIGURE 3.7: UDCN Membrane Tank with Sensors and Security Rope

FIGURE 3.8: PPE Tank Filled with Antifreeze-Water Solution

from lifting. However, one storm proved severe enough to ignore these precautions and required the UDCN tank to be grounded temporarily for safety reasons. The PSH-loop was run while the UDCN tank was mounted at ground level, as seen in Fig. 3.9. Results from these tests were considered valid since the 30-foot height difference is negligible for the behavior of the UDCN-membrane during use.

The last significant issue that arose during the PSH-loop experiment was squirrels. The pallet supporting the UCDN tank proved to be an ideal spot for a pregnant squirrel to nest. The pregnant squirrel ignored methods for repelling rodents, but the nest was removed before any damage was done. The area was doused with a solution of hot peppers and water in order to deter any squirrels from nesting there in the future. However, upon investigation of discrepancies in the data from the LVDT sensors, it was found that squirrels had destroyed the wiring of three of the four sensors (Fig. 3.10a). Within weeks the squirrels had created another nest, which was subsequently removed before the area was again doused with rodent repellent. To prevent any damage to the remaining LVDT sensor, the wiring was secured

FIGURE 3.9: PSH loop testing with both tanks at ground level.

inside a reinforced vinyl tube retrofitted as a conduit as seen in Fig. 3.10b.

3.3 PSH Loop Data Collection and Analysis

3.3.1 Initial Results of PSH Experiment

After the PSH loop was fully implemented and the sensors calibrated, the loop was run for 2-3 hour intervals. The system had a total of 125-gallons of the water-antifreeze solution while in use to prevent the pump from running without water. The DAQ was calibrated to automatically switch from filling to emptying the UDCN tank when the pressure reading inside the bladder tank equated to 95 gallons of fluid. The opposite switch occurred when the UDCN tank was emptied to 30-gallons to prevent overfilling the PPE tank. The LVDT sensors were placed in the locations shown in Fig. 3.11a. As the inlet and outlet of the UDCN tank were vertically aligned, the UDCN tank was also flipped to collect displacement data along the seam of the tank, as shown by Fig. 3.11b. The directional axes of the UDCN tank are labeled in Fig. 3.11a and 3.11b to correspond with the testing orientations, with the primary nylon fibers along the longitudinal axis and the secondary fibers along the transverse axis.

(A) LVDT Wiring Damaged by Squirrels

(B) LVDT Sensor Reinforced by Vinyl Tubing

FIGURE 3.10: LVDT Sensor Damage and Conduit

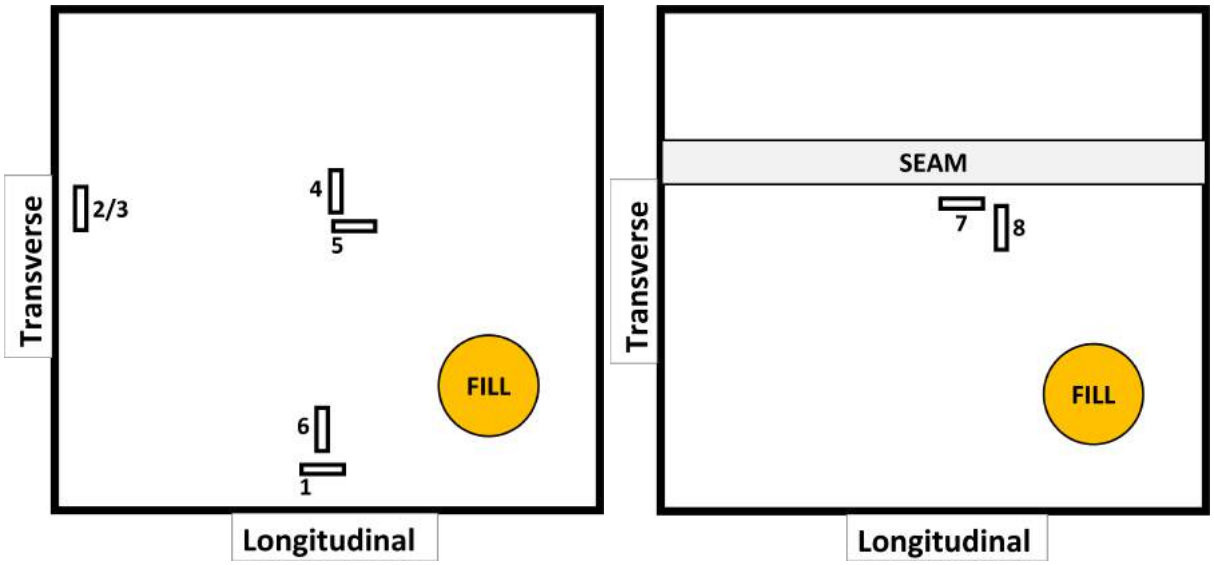

(A) LVDT placements on the top of the UDCN tank

(B) LVDT placements on the bottom of the UDCN tank

FIGURE 3.11: Schematic of UDCN bladder tank and LVDT sensor placements

3.3.2 Analysis and Implications of Results

The displacement data collected via the LVDT sensors was converted to strain using the initial displacement. As the strain rate during the PSH cycles was found to be smaller than the lowest strain rates seen monotonic testing, a stress model was developed using the UDCN uniaxial data at the lowest strain rate of 2.5 mm/min. The stresses calculated in this model using the strains from the PSH data were taken to be a good approximation of the actual stresses. These approximations can be verified through more rigorous testing. The calculated stresses and strains at the various locations are shown in Table 3.1. The values appear to be in the correct magnitude and display trends that are accurate to the system. The stresses in the longitudinal direction are always larger than those in the transverse direction, which is to be expected since the transverse direction has lower stresses than the longitudinal at the same strains. In addition, the stresses increase near the center of the tank, especially along the seam. The high stresses at the seam are expected since the seam itself is more rigid and resistant to strain, resulting in greater strains at the surrounding areas to compensate.

TABLE 3.1: PSH Loop-UDCN Tank Data

Location Orientation	Maximum Strain	Maximum Stress (MPa)	Average Strain	Average Stress (MPa)
1-Longitudinal	0.0099	**4.7591**	0.0054	**2.8263**
2/3-Transverse	0.0051	**0.5104**	0.0021	**0.2169**
4-Transverse	0.0194	**1.8895**	0.0071	**0.6974**
5-Longitudinal	0.0042	**2.2090**	0.0017	**0.8926**
6-Transverse	0.0200	**1.9510**	0.0089	**0.8620**
7-Longitudinal	0.0305	**9.3282**	0.0227	**7.7824**
8-Transverse	0.0514	**5.0219**	0.0352	**3.4897**

3.4 Flexible Tank Numerical Model

3.4.1 Curvature-based Derivation of Equations

A study by Osadolor et. al. created a numerical model to analyze the stresses seen by collapsible bioreactors [48]. This model was used as a basis for a model on collapsible fluid storage tanks. The original model was coded in MATLAB to calculate the stresses seen by membrane bladder tanks (in terms of Tension per unit length) based on curvature properties. Eqn. 3.1-3.3 are constituent equations for curvature-based analysis.

$$k = \frac{P_0 - y_- g\rho}{T} \tag{3.1}$$

$$y_- = \begin{cases} y, & y \leq 0 \\ 0, & y > 0 \end{cases} \tag{3.2}$$

$$\begin{cases} \frac{d^2x}{ds^2} = k\frac{dy}{ds} \\ \frac{d^2y}{ds^2} = -k\frac{dx}{ds} \end{cases} \tag{3.3}$$

where k = curvature, s = arc length, P_0 = static pressure above the liquid, $h = y_-$ liquid height, Hg = gas height above liquid, T = membrane stress force/tension per unit length, W = width of collapsible tank, and L = length of collapsible tank. Fig. 3.12 shows a schematic of a collapsible tank with reference points for the parameters.

Using the constituent curvature equations, first and second order differential equations were derived

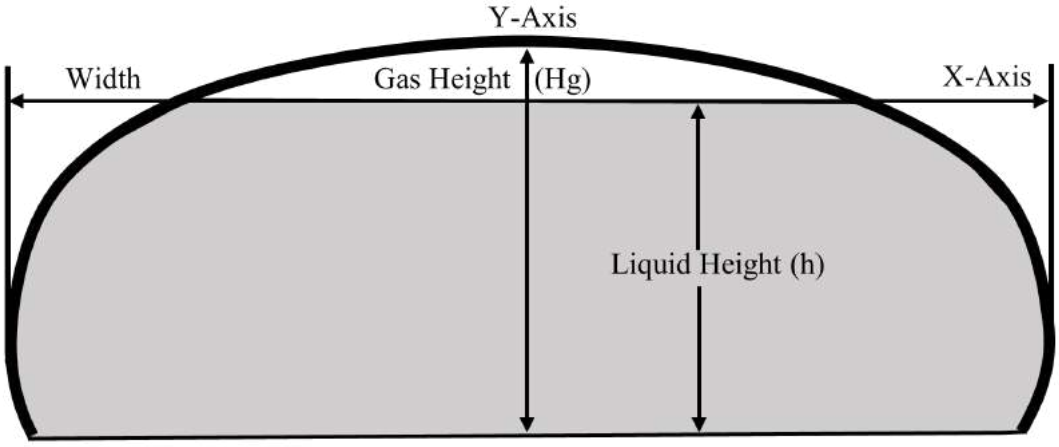

FIGURE 3.12: Collapsible tank schematic. The orgin is located on the surface on the water in the center of the tank.

as seen by Eqn. 3.4-3.8. These equations can be solved by iteration given initial values of $U_1(0) = 0$, $U2_(0) = Hg$, $U_3(0) = 1$, and $U_4(0) = 0$.

$$U_1(s) = x(s) \tag{3.4}$$

$$U_2(s) = y(s) \tag{3.5}$$

$$U_3(s) = \frac{dU_1}{ds} = \frac{dx}{ds} \tag{3.6}$$

$$U_4(s) = \frac{dU_2}{ds} = \frac{dy}{ds} \tag{3.7}$$

$$\begin{cases} \frac{dU_1}{ds} = U_3(s) \\ \frac{dU_2}{ds} = U_4(s) \\ \frac{dU_3}{ds} = \frac{P_0 - U_2 g\rho}{T} U_4(s) \\ \frac{dU_3}{ds} = -\frac{P_0 - U_2 g\rho}{T} U_3(s) \end{cases} \tag{3.8}$$

3.4.2 Flexible Tank Program

Using the derived differential equations, a program was initially created in MATLAB to calculate tension per unit length (T) based on the given input parameters. This T value is directly proportional to stress via the tank thickness. The user inputs the tank capacity, dimensions, and filling liquid before the program iterates to solve the static pressure above the liquid and tension along the membrane, and subsequently

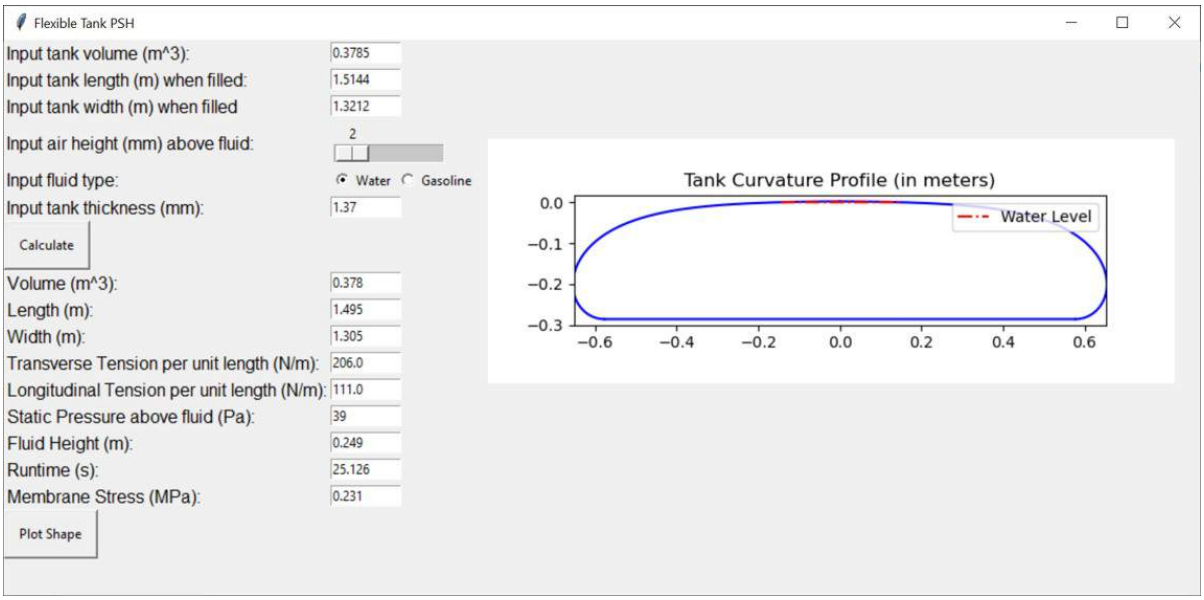

FIGURE 3.13: Python model GUI with parameters for 100-gal. UDCN tank

the membrane stress. Each iteration calculates the width and volume of the tank and compares the results to the input values. Based on the comparisons, the values of the tension and/or the static pressure are changed before the next iteration. This process is repeated until the width and volume are within 1% of the user input values.

Results were initially promising, but MATLAB was exceedingly slow in running the intensive program at higher tank volumes due to the large number of iterations. This prompted a conversion of the program to Python, which increased processing speeds by 800-2150%. The program was then divided into a main program with modules for volume, shape and width calculation to allow for faster processing and more efficient updates to the code. The program also contains a graphical user interface (GUI) created with the guizero library to provide a simple user interface with 2D and 3D models of the tank. The GUI is shown in Fig. 3.13.

After the calculations have finished, the user can choose to model the tank using the "Plot Shape" button. This outputs a cross-section of the tank from the side perpendicular to the width, as well as a 3D representation of the tank. The 3D model uses the ipyvolume library to revolve a curve based on the calculated parameters (volume, length and width). The model features an open bottom for inspection of the inside of the tank. An example of the 3D model is shown by Fig. 3.13, with the 2D cross-section

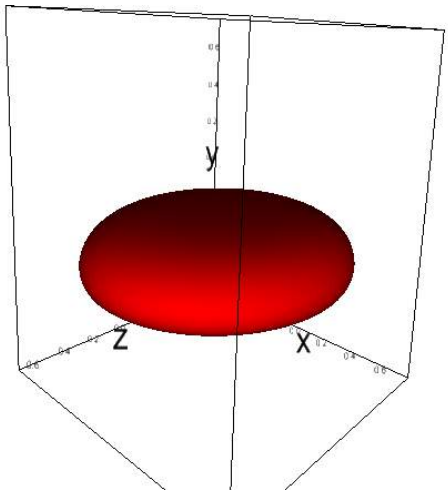

FIGURE 3.14: 3D ipyvolume representation of a flexible tank

shown in Fig. 3.14.

3.4.3 Results and Optimization

The initial MATLAB and Python programs sought to replicate the results of Osadolor et. al. in order to verify the implementation of the program. The replication was mostly successful, resulting in most of the calculated values lying within ±5% of the reported values. Satisfied with the results of the program, the Python code was updated to provide a simpler and more accurate implementation for PSH applications. This included the reduction of the number of input variables and a more direct approximation of the tank volume using an ellipsoid. In addition, a function was added to allow the tank to be filled with gasoline rather than water, resulting in different stresses. This function could be useful for modeling fuel-storage tanks that are often used in military applications.

The numerical model was initially optimized solely based on experimental data provided by Osadolor et. al., where the tank volumes ranged from 100-1000 m^3. The program is segmented into three iterative solvers, with each solver more precise than the previous. The program was optimized by calibrating the results of the solvers to the data provided by Osadolor et. al. This optimization proved to be relatively accurate and allowed for further calibration based on empirical data from the lab-scale PSH-loop. The program output was close to the lowest stress seen by the 100-gallon UDCN membrane tank, as seen in Table 3.2. The Python model calculates a stress close to the lowest average stress seen by the UDCN tank

TABLE 3.2: PSH Loop Data vs Python Model

Tank Classification	**Volume (m^3)**	**Length (m)**	**Width (m)**	**Stress (MPa)**
UDCN Membrane Tank	0.3785	1.5144	1.3212	**0.2169 (at location 2,3)**
Python Tank Model	0.378	1.495	1.305	**0.231**

during use. With further testing of the PSH loop the model can be further developed and calibrated for better accuracy. Note that the calculations were performed using the dimensions of the tank when filled, not the base dimensions of the membrane tank. In addition, a 2-mm air height was used for above the fluid within the tank. An example of the code from the Python model is shown in Appendix D

Chapter 4

Conclusions and Future Work

4.1 Conclusions

A comprehensive study of the properties of UDCN membranes is important for future developments in fluid-storage and PSH technologies. Monotonic testing of UDCN membranes found a strong correlation between fiber direction and the stress-strain behavior. UDCN membranes showed a similar strain energy along the directions of the nylon fibers (transverse and longitudinal directions), while the energy in other directions increased drastically. The nylon fibers help the material withstand higher stresses while the urethane coating allows the membranes to stretch more. Comparison with the properties of XR-5 membranes shows that UDCN membranes are more resistant to strains, though the strengths are similar between the materials. Monotonic testing verified that UDCN membranes are viscoelastic, allowing for further investigation using creep testing.

Results from UV irradiation testing are not fully verified due to the small sample size, but indicate a large degree of cross-linking in UV irradiated specimens. This behavior is seen in many polyurethanes, and SEM characterization also supports this theory. Hydrolysis testing shows that UDCN membranes degrade after prolonged exposure to water, though the membranes did not degrade further after additional weeks of water immersion.

Viscoelastic and hyperelastic modeling was performed on the UDCN membranes using the empirical data. Viscoelastic modeling used data from 5-hour creep testing at 21°C and 50°C to model creep

behavior using Nutting's law. The Miller-Norton law is also a good approximation but requires further study. Gent, Yeoh and Exponential-Logarithmic hyperelastic models had strong correlations with UDCN test data for most cases. Higher-order Mooney-Rivlin models were also fit to data that those models did not adhere to.

Experimental testing of UDCN membranes also included construction and operation of a lab-scale PSH loop involving a UDCN tank as the upper reservoir. Cycling the PSH loop showed that the stresses seen by the UDCN tank during use were very low in relation to the material strength. In addition, a Python program was developed to model the stress seen by the UDCN tank during use. The model was calibrated using data from the creep testing and was found to be a good approximation for the tank stresses.

In regards to using UDCN membrane tanks in developing PSH technologies, such as h-mcs-PSH systems, the results of this study indicate that UDCN membranes are durable for use in PSH systems. The stresses and strains seen by UDCN membrane tanks during use in PSH systems are minimal even when considering extreme scenarios. The UV and hydrolytic degradation of UDCN membranes is not significant enough to weaken UDCN membrane tanks below the threshold for PSH system usage. Long-term studies of UDCN membranes may prove useful for fully verifying their viability in PSH applications.

4.2 Future Work

While this study covered many aspects of UDCN membrane material testing and characterization, there are still many facets that are unexplored. As the focus of the study on UDCN membranes is for use in fluid-storage applications, priority should be given to further investigate the behavior of UDCN when subjected to prolonged UV and water exposure. UV testing should be performed on greater numbers UDCN membranes and cover time spans of up to 25 years equivalent UV irradiation. Accelerated hydrolysis testing should also be performed at increased temperatures (e.g. 50°C) and for longer time periods (e.g. 1-year). Creep testing at a wider array of temperatures would also be beneficial for temperature-based viscoelastic modeling of UDCN.

Future work with the UDCN membrane tank is also of importance. Testing of the constructed PSH loop should continue to observe the longevity of using the UDCN tank. In addition, fatigue testing on the membrane should be a priority to provide insight into the long-term use of UDCN membrane tanks under cyclic loading (i.e. filling and emptying). Fatigue testing is especially important for the use of UDCN membrane tanks in developing PSH technologies. Results from future PSH loop testing should also be used to further develop and refine the Python model so that a more accurate model may be produced.

Appendix A

XR-5 Hyperelastic Modeling

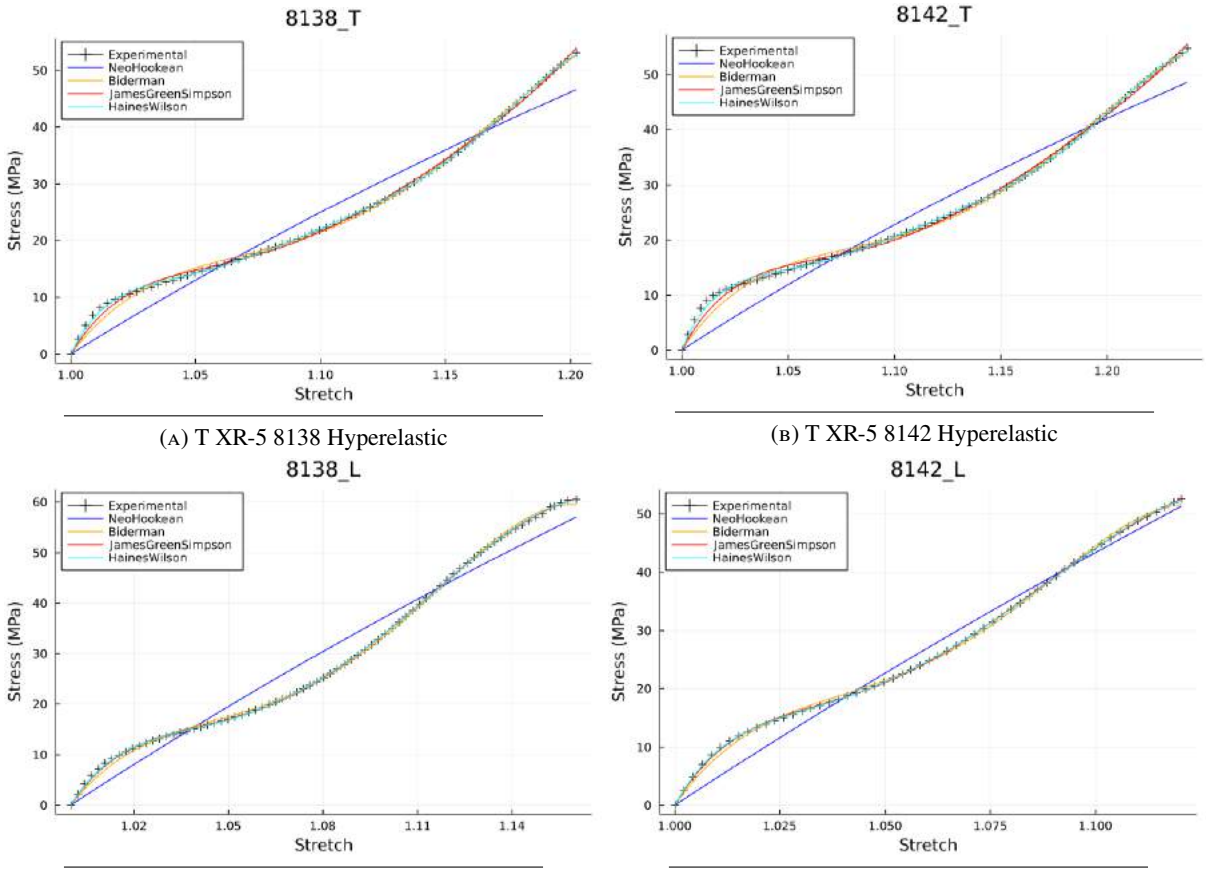

(A) T XR-5 8138 Hyperelastic

(B) T XR-5 8142 Hyperelastic

(C) L XR-5 8138 Hyperelastic

(D) L XR-5 8142 Hyperelastic

FIGURE A.1: Mooney-Rivlin hyperelastic models for XR-5 geomembrane specimens.

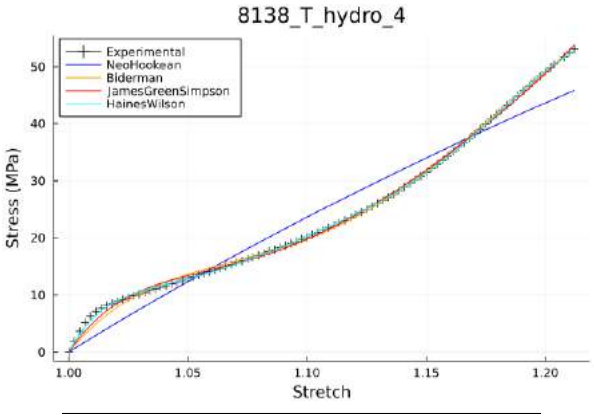

(A) Transverse 4-wk Hydrolysis

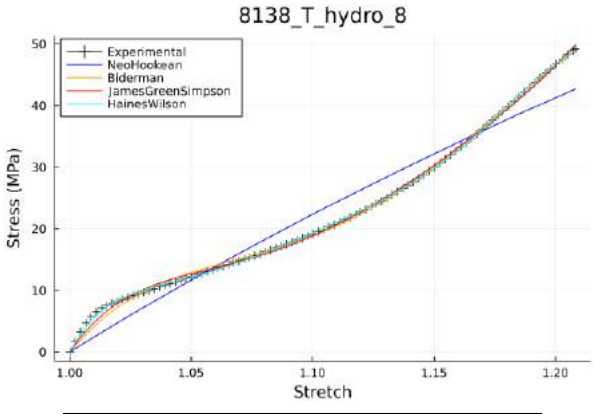

(B) Transverse 8-wk Hydrolysis

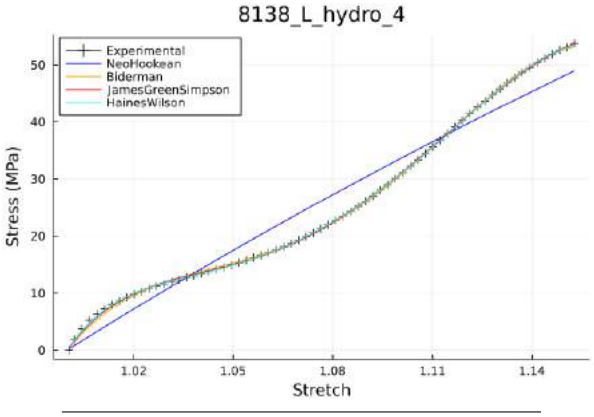

(C) Longitudinal 4-wk Hydrolysis

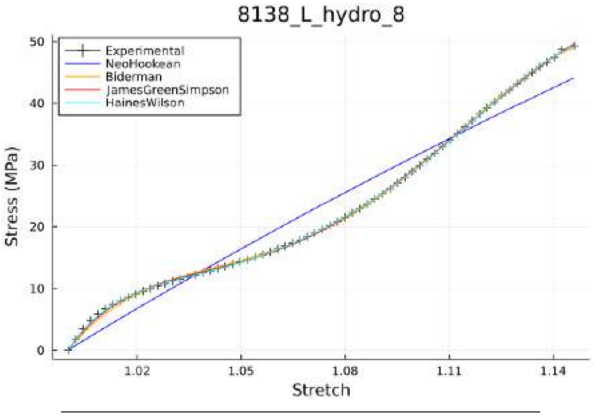

(D) Longitudinal 8-wk Hydrolysis

FIGURE A.2: XR-5 8138 Hydrolysis Hyperelastic Models

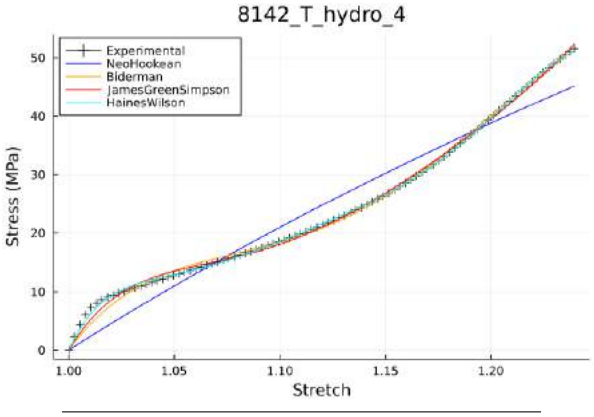

(A) Transverse 4-wk Hydrolysis

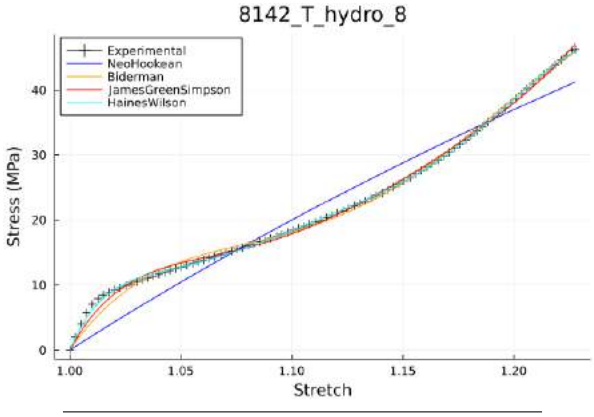

(B) Transverse 8-wk Hydrolysis

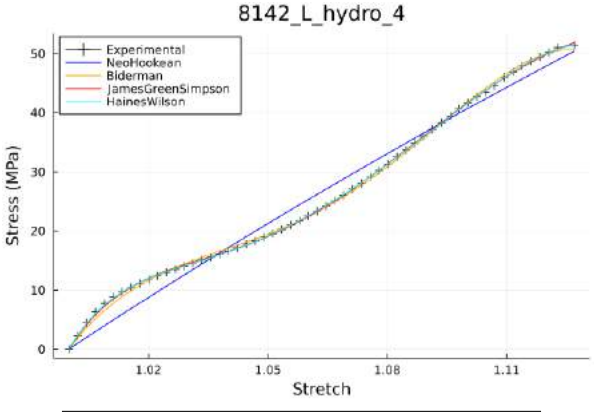

(C) Longitudinal 4-wk Hydrolysis

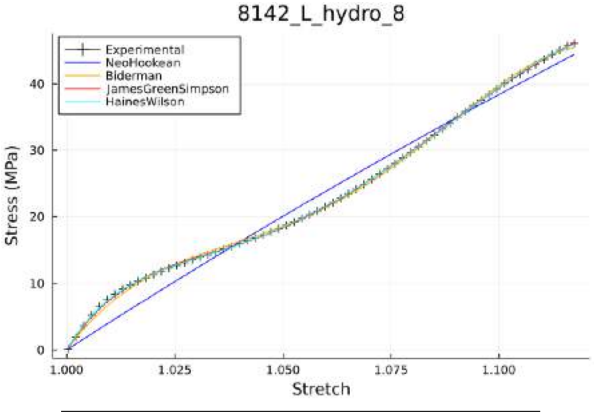

(D) Longitudinal 8-wk Hydrolysis

FIGURE A.3: XR-5 8142 Hydrolysis Hyperelastic Models

Appendix B

Hydrolysis Fracture Specimens

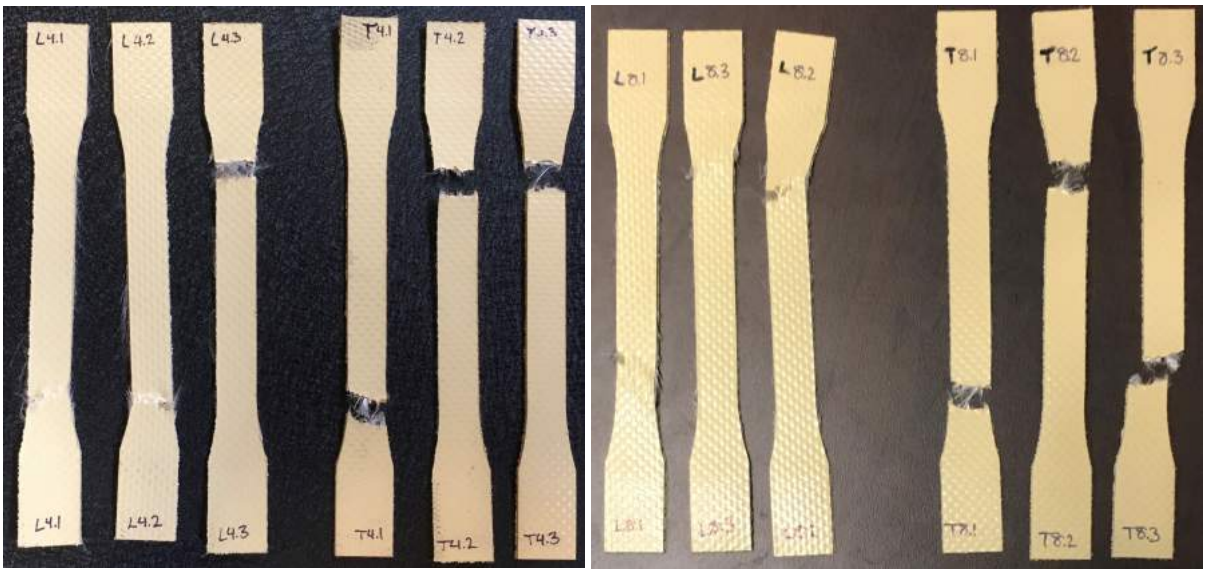

(A) 4-Week Hydrolysis (B) 8-Week Hydrolysis

FIGURE B.1: Transverse and longtudinal UDCN fracture specimens after hydrolysis

(A) 30°: 4-Week (left) and 8-week (right) water immersion

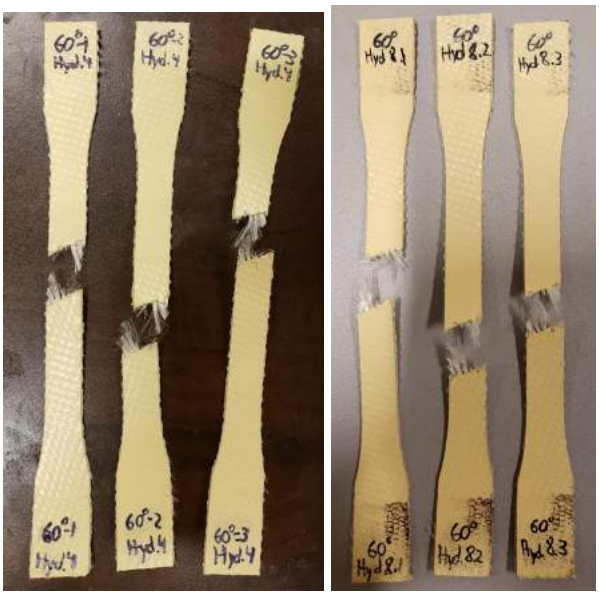

(B) 60°: 4-Week (left) and 8-week (right) water immersion

FIGURE B.2: Angled UDCN fracture specimens after water immersion

(A) Transverse 4-Week Hydrolysis

(B) Transverse 8-Week Hydrolysis

(C) Longitudinal 4-Week Hydrolysis

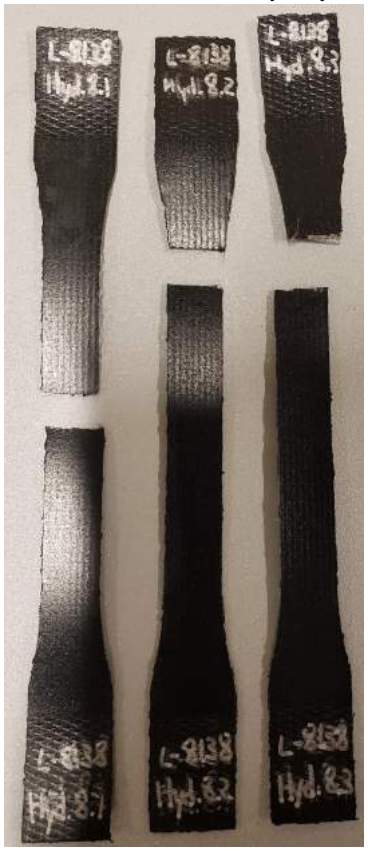

(D) Longitudinal 8-Week Hydrolysis

FIGURE B.3: XR-5 8138 fracture specimens after water immersion.

(A) Transverse 4-Week Hydrolysis

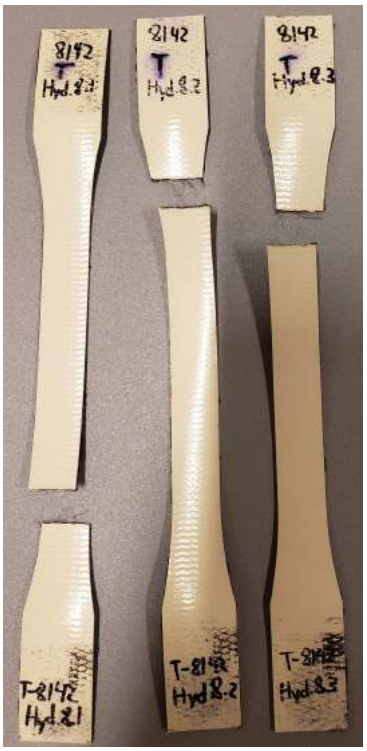

(B) Transverse 8-Week Hydrolysis

(C) Longitudinal 4-Week Hydrolysis

(D) Longitudinal 8-Week Hydrolysis

FIGURE B.4: XR-5 8142 fracture specimens after water immersion.

Appendix C

Creep Experimental Data and Modeling

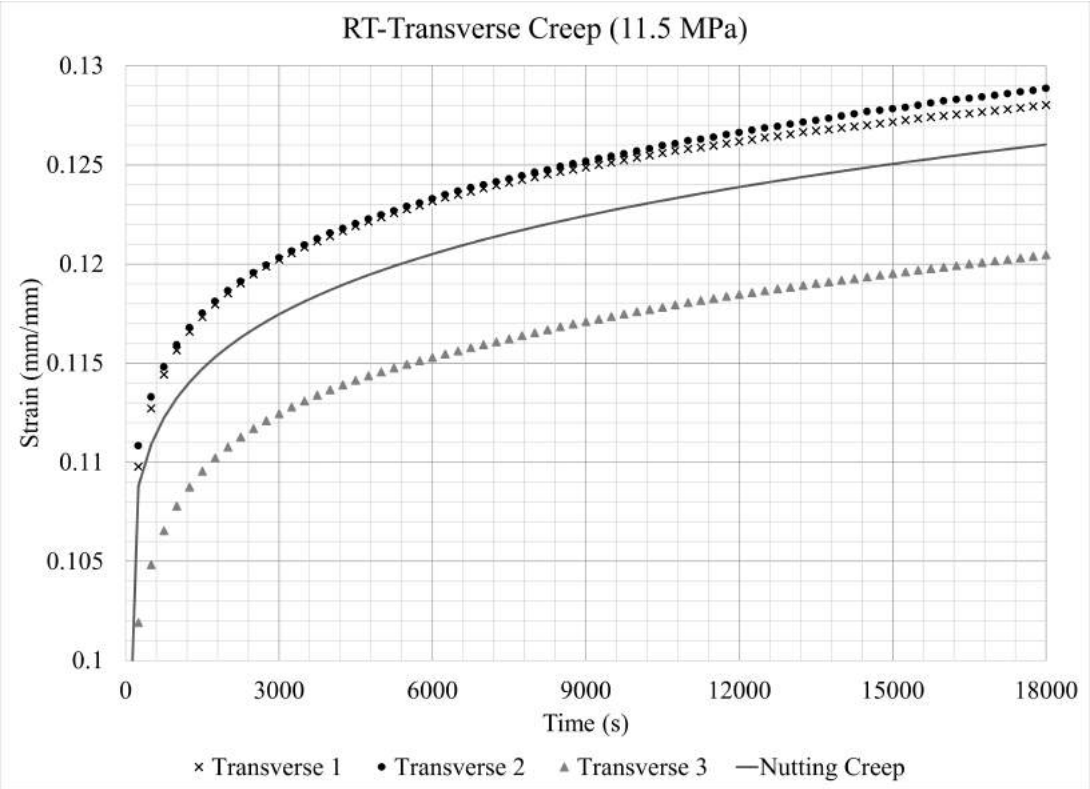

FIGURE C.1: 5-hour creep data for transverse UDCN specimens at 11.5 MPa and 21°C, including a Nutting model corresponding to the average data.

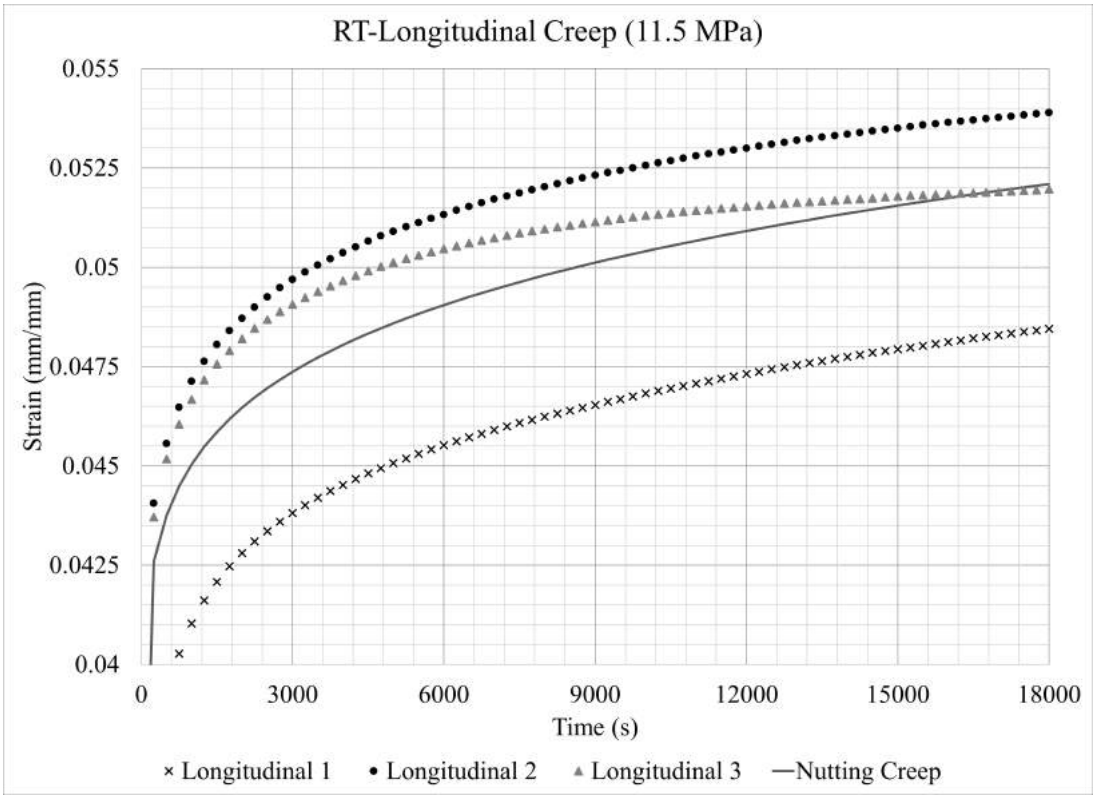

FIGURE C.2: 5-hour creep data for longitudinal UDCN specimens at 11.5 MPa and 21°C, including a Nutting model corresponding to the average data.

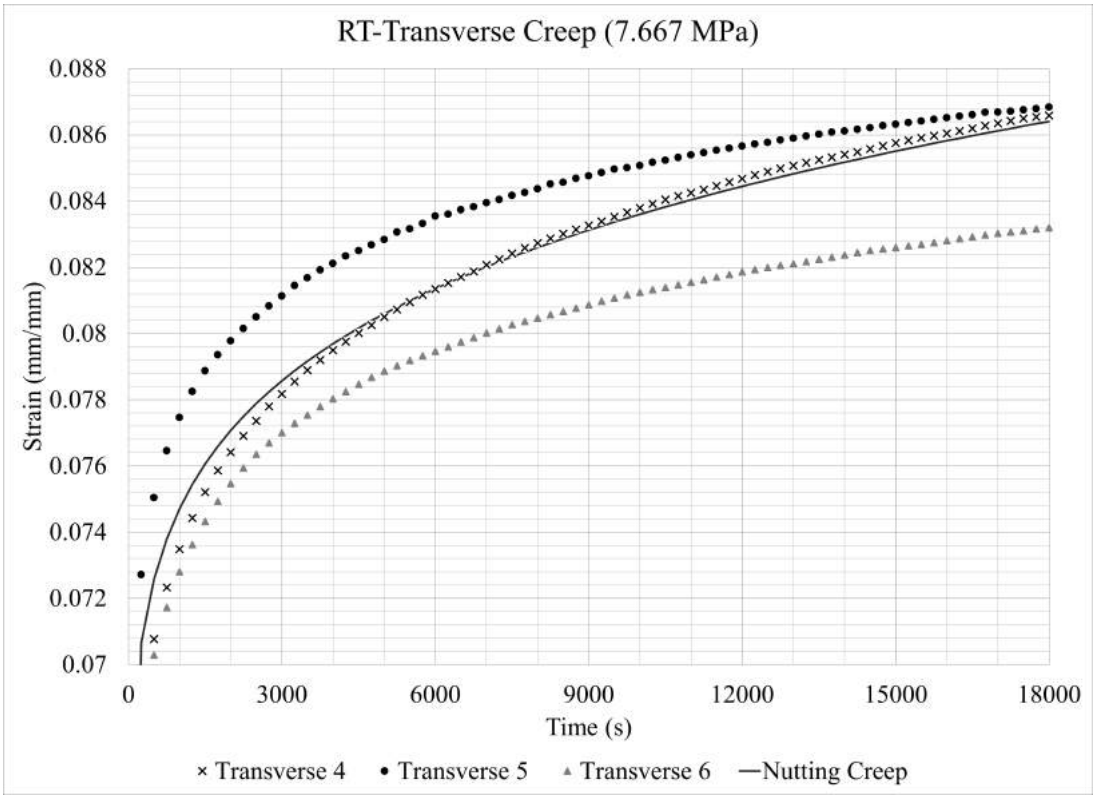

FIGURE C.3: 5-hour creep data for transverse UDCN specimens at 7.667 MPa and 21°C, including a Nutting model corresponding to the average data.

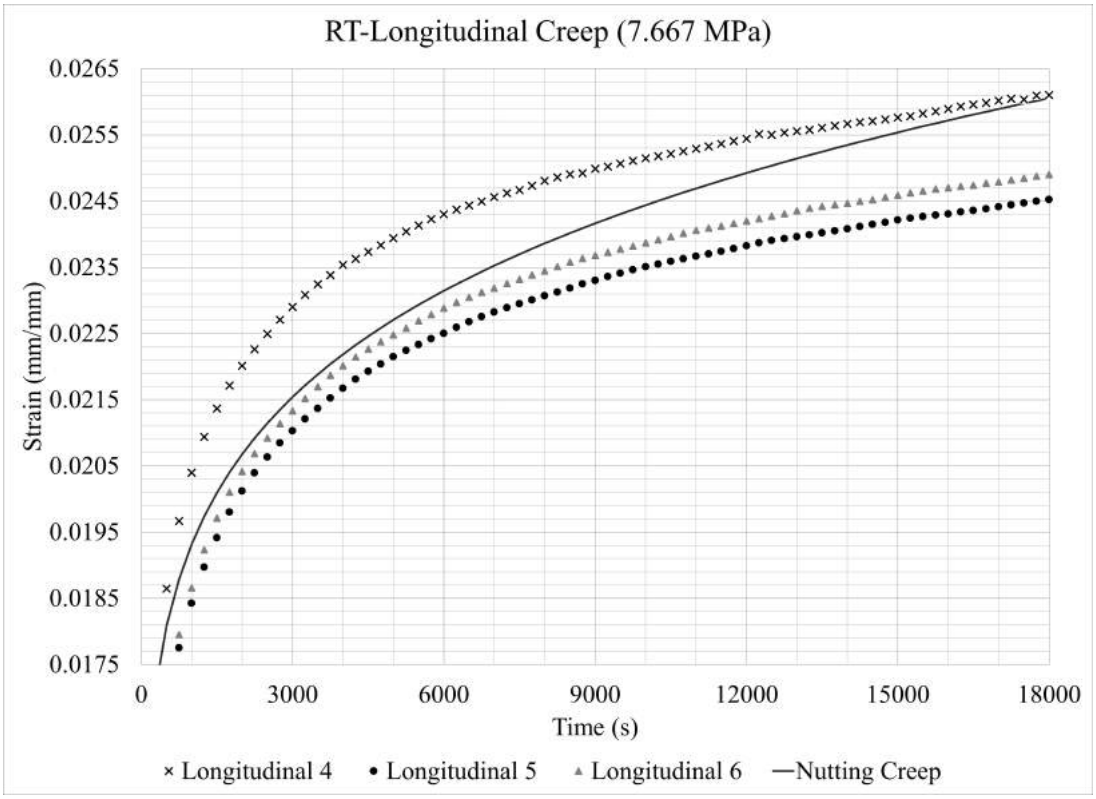

FIGURE C.4: 5-hour creep data for longitudinal UDCN specimens at 7.667 MPa and 21°C, including a Nutting model corresponding to the average data.

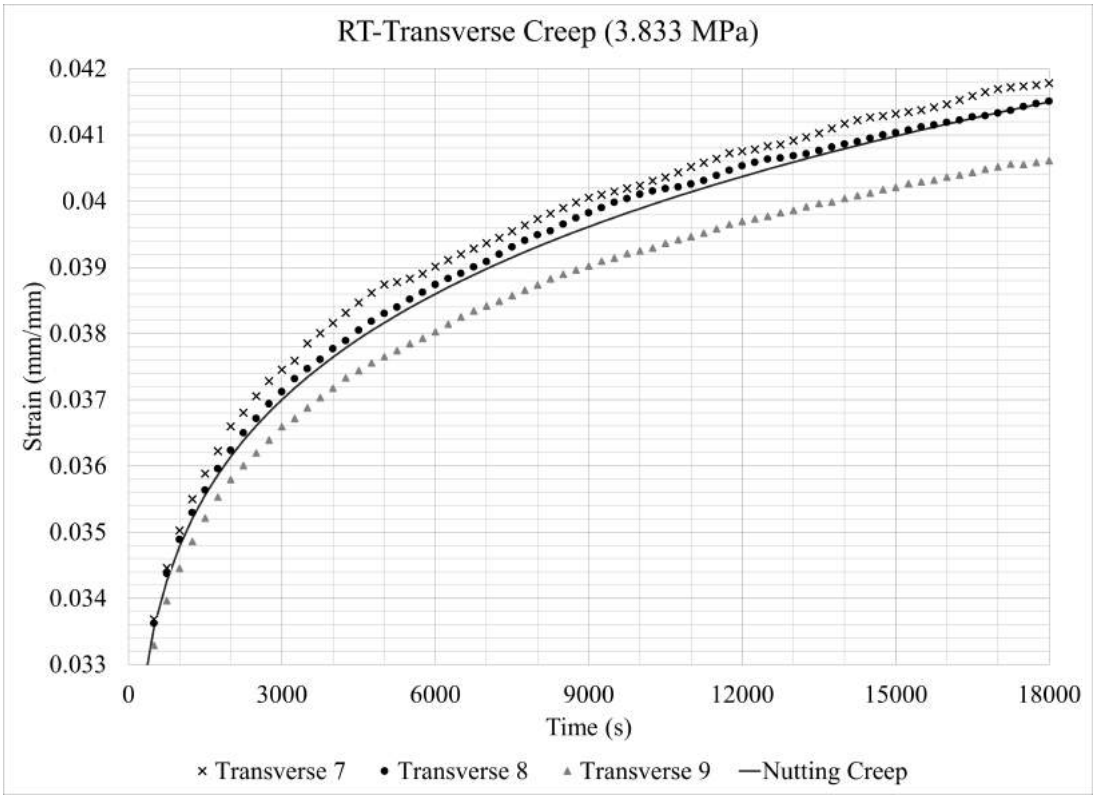

FIGURE C.5: 5-hour creep data for transverse UDCN specimens at 3.833 MPa and 21°C, including a Nutting model corresponding to the average data.

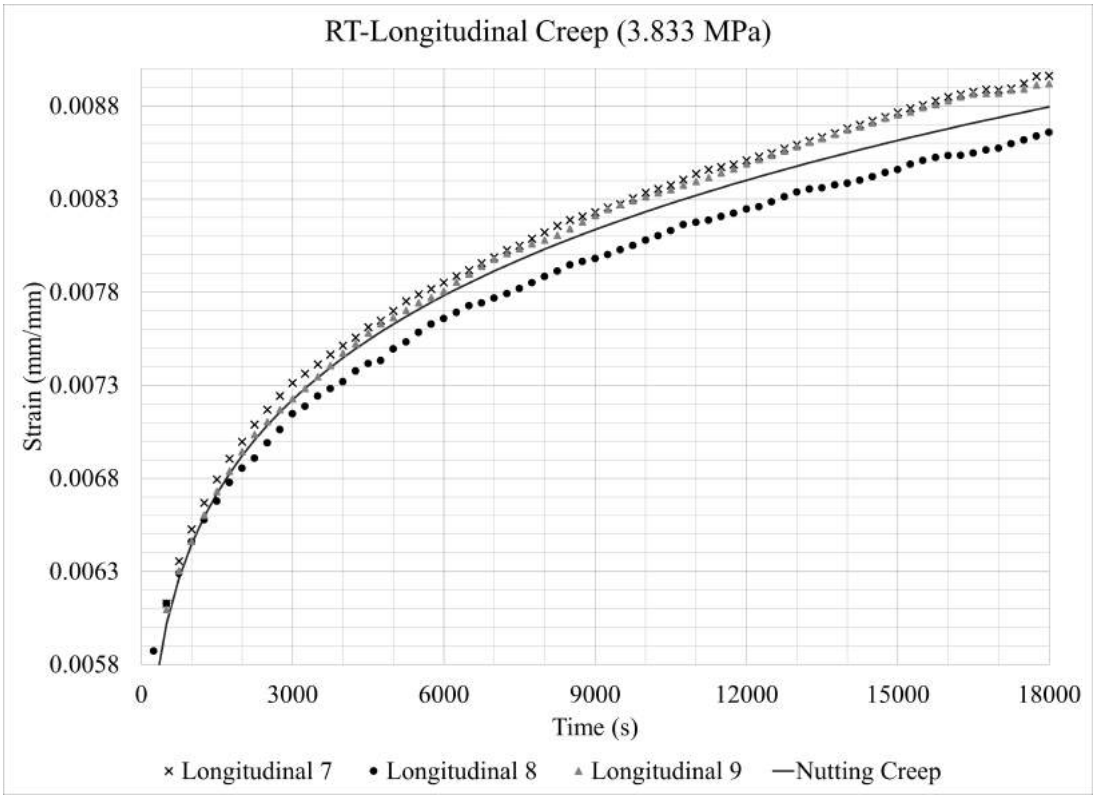

FIGURE C.6: 5-hour creep data for longitudinal UDCN specimens at 3.833 MPa and 21°C, including a Nutting model corresponding to the average data.

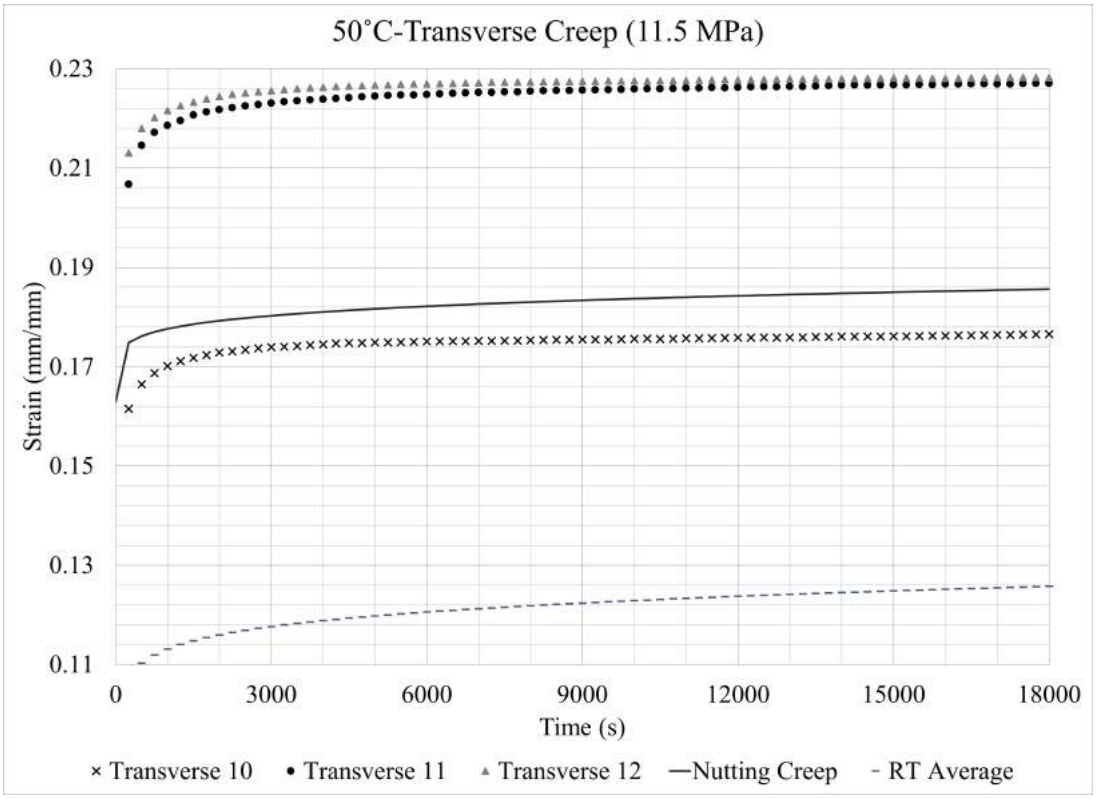

FIGURE C.7: 5-hour creep data for longitudinal UDCN specimens at 11.5 MPa and 50°C, including a Nutting model corresponding to the average data.

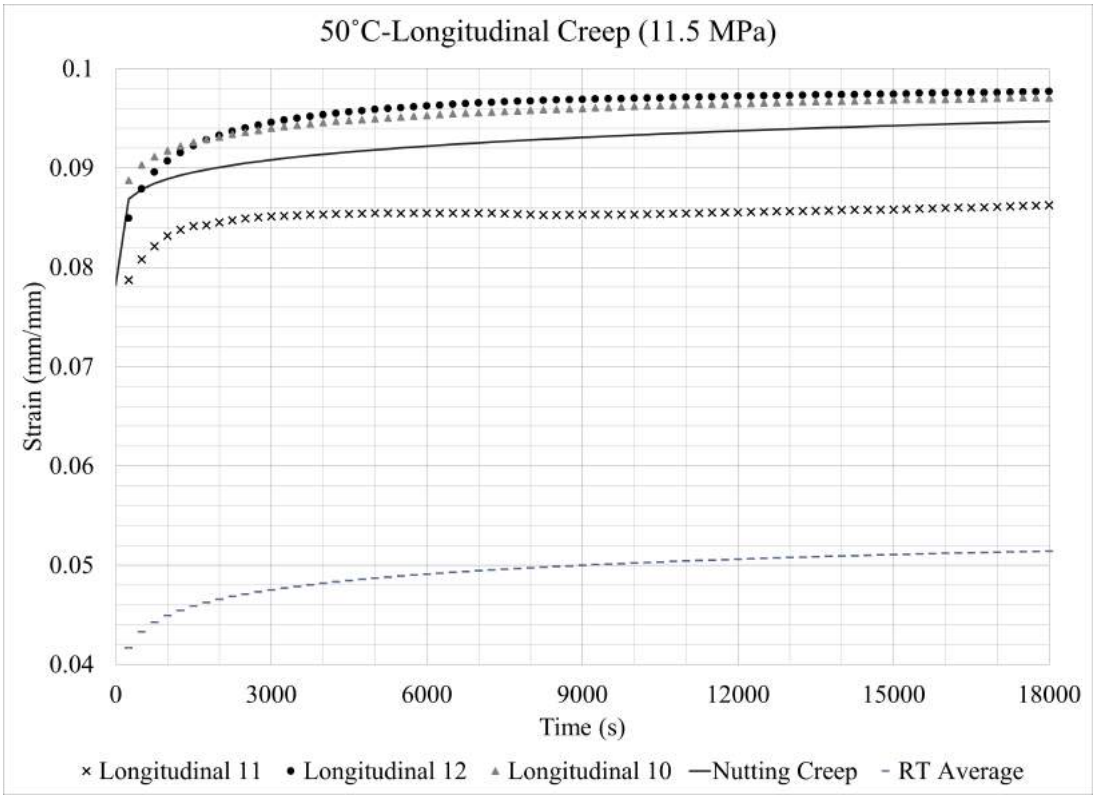

FIGURE C.8: 5-hour creep data for longitudinal UDCN specimens at 11.5 MPa and 50°C, including a Nutting model corresponding to the average data.

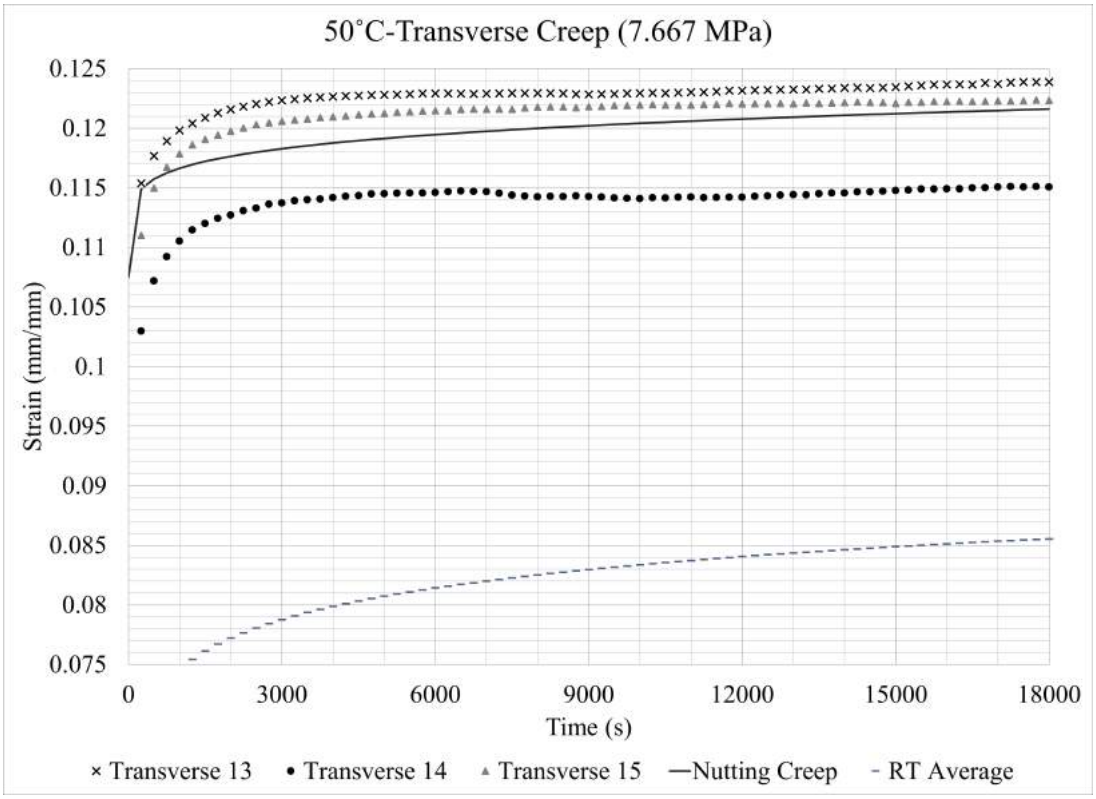

FIGURE C.9: 5-hour creep data for transverse UDCN specimens at 7.667 MPa and 50°C, including a Nutting model corresponding to the average data.

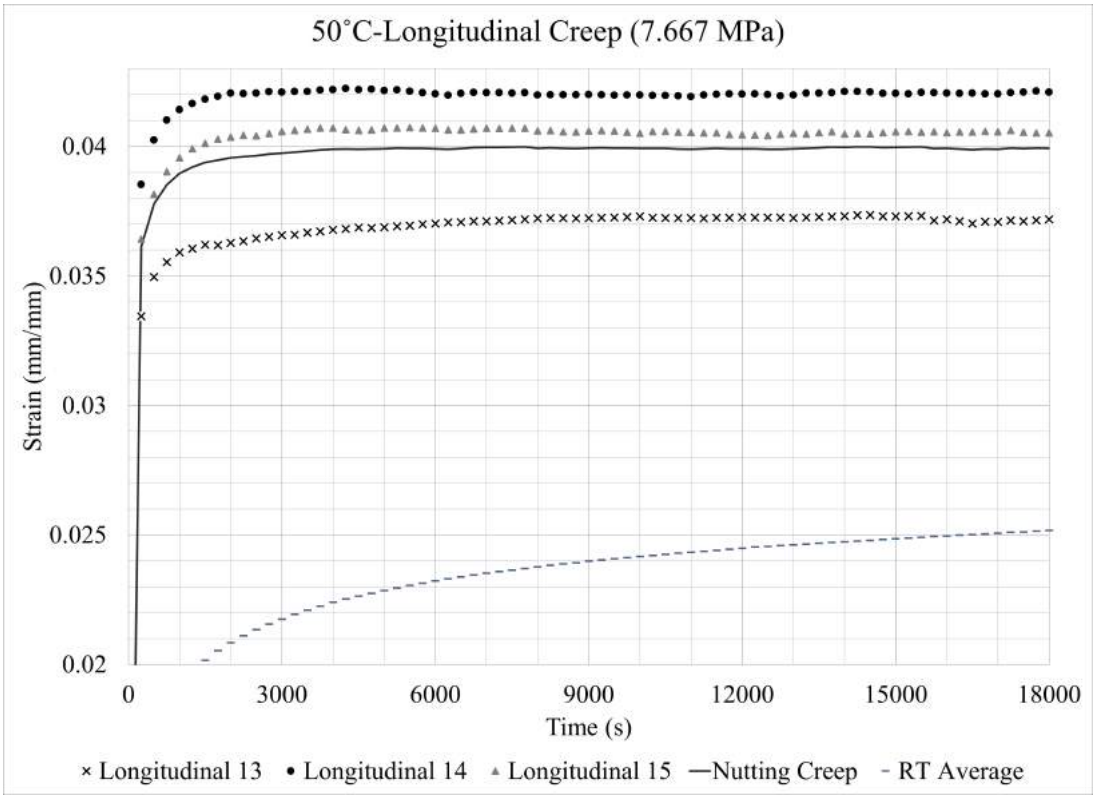

FIGURE C.10: 5-hour creep data for longitudinal UDCN specimens at 7.667 MPa and 50°C, including a Nutting model corresponding to the average data.

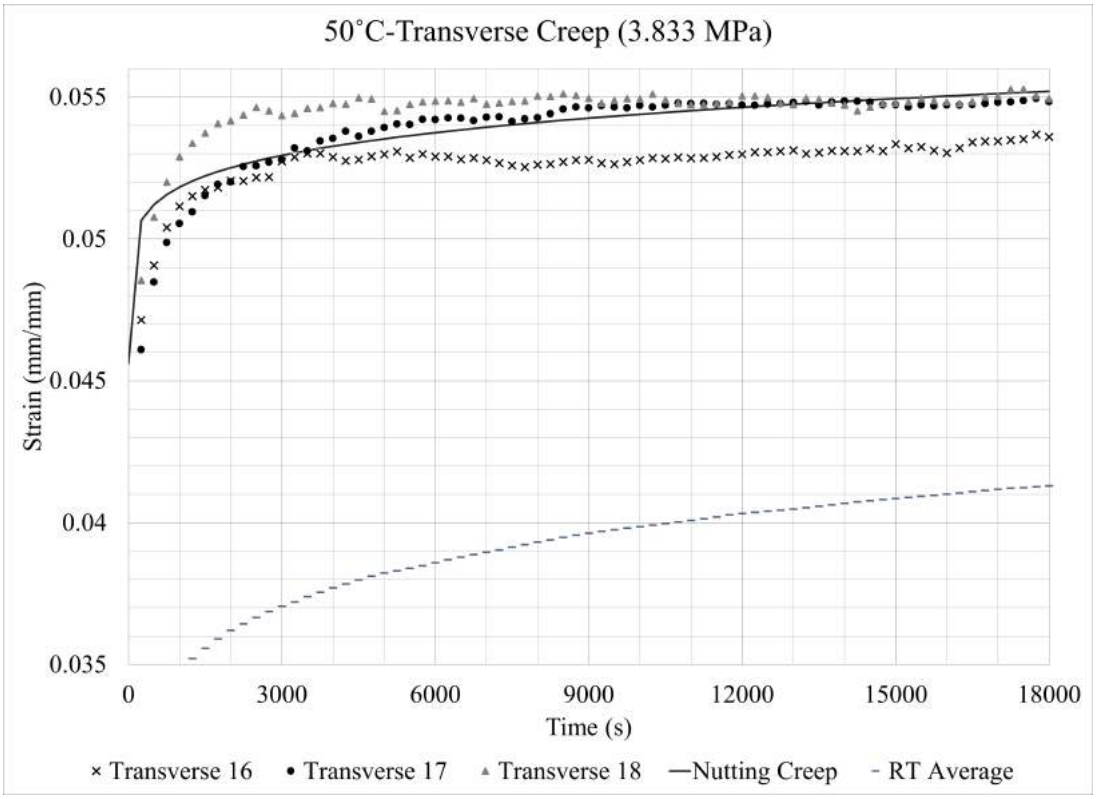

FIGURE C.11: 5-hour creep data for transverse UDCN specimens at 3.833 MPa and 50°C, including a Nutting model corresponding to the average data.

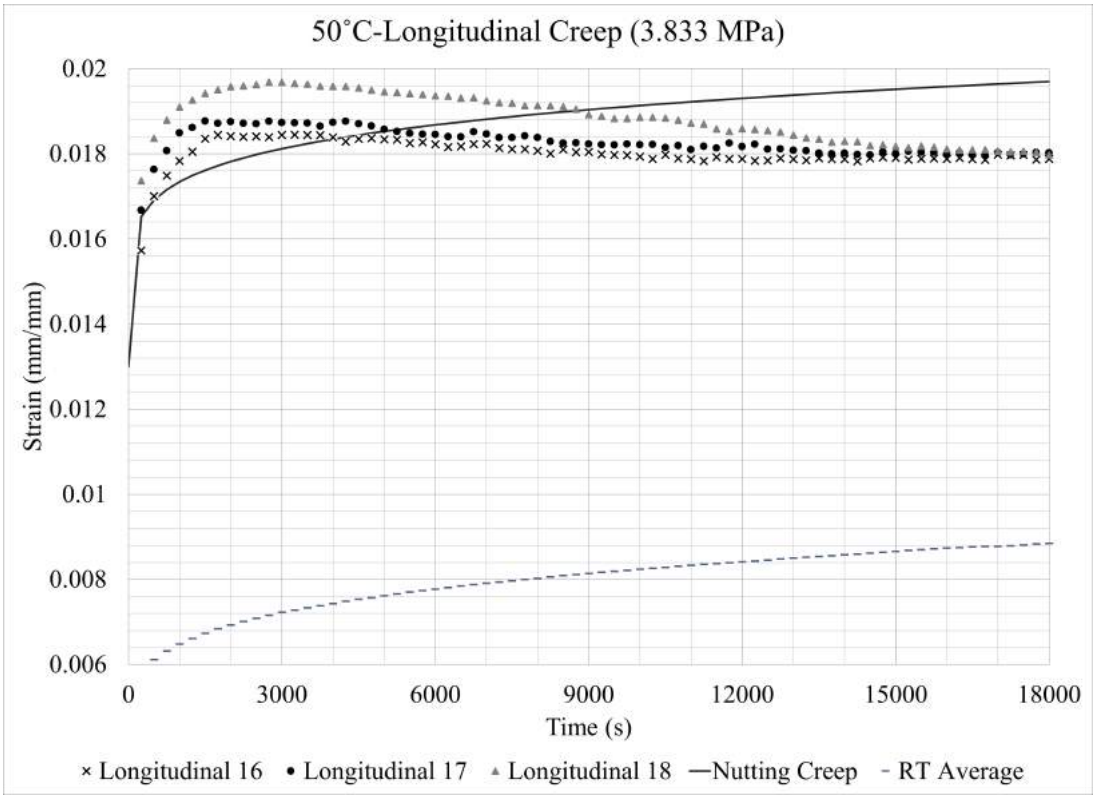

FIGURE C.12: 5-hour creep data for longitudinal UDCN specimens at 3.833 MPa and 50°C, including a Nutting model corresponding to the average data.

Appendix D

Flexible Tank Python Code

```
if D.value == 'Water':
    rho = 1000
elif D.value == 'Gasoline':
    rho = 711

g = 9.81
T = 100
P0 = 1

dt = 0.0001
s = np.arange(0,25,dt)
n = len(s)

for k in range(250):
    y = shape_calculation(rho,T,Hg,P0,g,n,s)
    Width = width_calculation(y)
    Volume,liquidheight = volume_calculation(Ldata,Width,y)
    if (Width-Wdata)/Wdata>0.01:
        P0=P0+0.5
    elif (Vdata-Volume)/Vdata>0.01:
        T=T+2
    elif (Volume-Vdata)/Vdata>0.01:
        P0=P0+0.5
    elif (Wdata-Width)/Wdata>0.01:
        T=T+2
    else:
        break

for k in range(250):
    T = T+0.5
    y = shape_calculation(rho,T,Hg,P0,g,n,s)
    Width = width_calculation(y)
    Volume,liquidheight = volume_calculation(Ldata,Width,y)
```

```
        while (Width-Wdata)/Wdata>0.01 or (Volume-Vdata)/Vdata>0.01:
            P0=P0+0.1
            y = shape_calculation(rho,T,Hg,P0,g,n,s)
            Width = width_calculation(y)
            Volume,liquidheight = volume_calculation(Ldata,Width,y)

        if (Vdata-Volume)/Vdata>0.01:
            break

        elif (Wdata-Width)/Wdata>0.01:
            break

    T_T = T-0.5
    P0_T = P0
    y = shape_calculation(rho,T_T,Hg,P0_T,g,n,s)
    Width = width_calculation(y)
    Volume,liquidheight = volume_calculation(Ldata,Width,y)
    H_T = liquidheight
    Vol_T= Volume
```

Bibliography

[1] J. M. Sloan, "Hydrolytic stability of polyurethane-coated fabrics used for collapsible fuel storage containers," ARMY RESEARCH LAB ABERDEEN PROVING GROUND MD WEAPONS AND MATERIALS RESEARCH . . . , Report, 2014.

[2] B. Hadjerioua, T. Eldredge, H. Medina, and S. DeNeale, "Hydrodynamic and structural response modeling of a prototype floating membrane reservoir system for pumped storage hydropower," *Journal of Hydraulic Engineering*, vol. 145, no. 9, p. 04019032, 2019. [Online]. Available: https://doi.org/10.1061/(ASCE)HY.1943-7900.0001625

[3] ASTM D638-14, "Standard test method for tensile properties of plastics," American Society for Testing and Materials, Standard.

[4] ASTM D751-06, "Standard test methods for coated fabrics," American Society for Testing and Materials, Standard.

[5] ASTM D2990-09, "Standard test methods for tensile, compressive, and flexural creep and creep-rupture of plastics," American Society for Testing and Materials, Standard.

[6] ASTM D3039, "Standard test method for tensile properties of polymer matrix composite materials," American Society for Testing and Materials, Standard.

[7] ISO 899-1, "Plastics – determination of creep behaviour," International Organization for Standardization, Standard.

[8] S. Corporation, "Xr geomembranes," 2022. [Online]. Available: https://www.xrgeomembranes.com/

[9] D. L. Faria, L. M. Júnior, A. A. Resende, D. E. Lopes, L. M. Mendes, M. A. Martins, J. M. Marconcini, and J. B. G. Junior, "Physical and mechanical properties of polyurethane thermoset matrices reinforced with green coconut fibres," *Journal of Composite Materials*, vol. 54, no. 30, pp. 4841–4852, 2020.

[10] C. Mattu, T. Wang, A. Siri, S. Sartori, and G. Ciardelli, "Ionic cross-linking of water-soluble polyurethane improves protein encapsulation and release," *Engineering in Life Sciences*, vol. 15, no. 4, pp. 448–455, 2015. [Online]. Available: https://doi.org/10.1002/elsc.201400188

[11] Q. Gao, M. Feng, E. Li, C. Liu, C. Shen, and X. Liu, "Mechanical, thermal, and rheological properties of ti3c2tx mxenethermoplastic polyurethane nanocomposites," *Macromolecular Materials and Engineering*, vol. 305, no. 10, p. 2000343, 2020. [Online]. Available: https://doi.org/10.1002/mame.202000343

[12] K. Petcharoen and A. Sirivat, "Electrostrictive properties of thermoplastic polyurethane elastomer: Effects of urethane type and soft–hard segment composition," *Current Applied Physics*, vol. 13, no. 6, pp. 1119–1127, 2013. [Online]. Available: https://www.sciencedirect.com/science/article/pii/S156717391300117X

[13] M. M. Ghobashy and Z. I. Abdeen, "Radiation crosslinking of polyurethanes: Characterization by ftir, tga, sem, xrd, and raman spectroscopy," *Journal of Polymers*, vol. 2016, p. 9802514, 2016. [Online]. Available: https://doi.org/10.1155/2016/9802514

[14] Y.-C. Chung, M. J. Song, H.-A. Kwon, and B. C. Chun, "Modification of polyurethane by the lateral cross-linking using a modified poly(vinyl alcohol) for the improvement of tensile strength and the control of water vapor permeation," *Fibers and Polymers*, vol. 16, no. 9, pp. 1819–1829, 2015. [Online]. Available: https://doi.org/10.1007/s12221-015-5410-y

[15] Y. E. Elmogahzy, *8 - Fibers*. Woodhead Publishing, 2020, pp. 191–222. [Online]. Available: https://www.sciencedirect.com/science/article/pii/B9780081024881000083

[16] R. Chattopadhyay, *1 - Introduction: types of technical textile yarn*. Woodhead Publishing, 2010, pp. 3–55. [Online]. Available: https://www.sciencedirect.com/science/article/pii/B9781845695491500011

[17] H. O. Feuer Jr and P. Touchet, "Failure mechanism of urethane-elastomer-coated-fabric collapsible fuel tanks," *Journal of Coated Fabrics*, vol. 20, no. 3, pp. 188–210, 1991.

[18] L. Tian, D. Wang, and Q. Wei, "Study on dynamic mechanical properties of a nylon-like polyester tire cord," *Journal of Engineered Fibers and Fabrics*, vol. 14, p. 1558925019868807, 2019.

[19] T. Hongu, G. O. Phillips, and M. Takigami, *3 - Superfibers*. Woodhead Publishing, 2005, pp. 65–98. [Online]. Available: https://www.sciencedirect.com/science/article/pii/B9781855736016500030

[20] F. Xie, T. Zhang, P. Bryant, V. Kurusingal, J. M. Colwell, and B. Laycock, "Degradation and stabilization of polyurethane elastomers," *Progress in Polymer Science*, vol. 90, pp. 211–268, 2019. [Online]. Available: https://www.sciencedirect.com/science/article/pii/S0079670018302995

[21] D. Rosu, L. Rosu, F. Mustata, and C.-D. Varganici, "Effect of uv radiation on some semi-interpenetrating polymer networks based on polyurethane and epoxy resin," *Polymer Degradation and Stability*, vol. 97, no. 8, pp. 1261–1269, 2012. [Online]. Available: https://www.sciencedirect.com/science/article/pii/S0141391012002091

[22] M. Moezzi and M. Ghane, "The effect of uv degradation on toughness of nylon 66/polyester woven fabrics," *The Journal of The Textile Institute*, vol. 104, no. 12, pp. 1277–1283, 2013. [Online]. Available: https://doi.org/10.1080/00405000.2013.796629

[23] R. Shamey and K. Sinha, "A review of degradation of nylon 6. 6 as a result of exposure to environmental conditions," *Review of Progress in Coloration and Related Topics*, vol. 33, no. 1, pp. 93–107, 2003. [Online]. Available: https://doi.org/10.1111/j.1478-4408.2003.tb00147.x

[24] G. A. Horsfall, "Factors influencing the daylight photodegradation of nylon 66, nylon 6, and polyester in commercial fabrics," *Textile Research Journal*, vol. 52, no. 3, pp. 197–205, 1982.

[25] N. R. E. Laboratory, "U.s. annual solar ghi," 2018.

[26] A. Ehrmann, "Non-toxic crosslinking of electrospun gelatin nanofibers for tissue engineering and biomedicine—a review," *Polymers*, vol. 13, no. 12, 2021.

[27] A. Ahmad, F. Jamshaid, M. Adrees, S. S. Iqbal, A. Sabir, T. Riaz, H. Zaheer, A. Islam, and T. Jamil, "Novel polyurethane/polyvinyl chloride-co-vinyl acetate crosslinked membrane for reverse osmosis (ro)," *Desalination*, vol. 420, pp. 136–144, 2017. [Online]. Available: https://www.sciencedirect.com/science/article/pii/S001191641730468X

[28] S. Sahoo, H. Kalita, S. Mohanty, and S. K. Nayak, "Degradation study of biobased polyester–polyurethane and its nanocomposite under natural soil burial, uv radiation and hydrolytic-salt water circumstances," *Journal of Polymers and the Environment*, vol. 26, no. 4, pp. 1528–1539, 2018. [Online]. Available: https://doi.org/10.1007/s10924-017-1058-6

[29] M. H. Mohamed, L. D. Wilson, and J. V. Headley, "Tuning the physicochemical properties of β-cyclodextrin based polyurethanes via cross-linking conditions," *Microporous and Mesoporous Materials*, vol. 214, pp. 23–31, 2015. [Online]. Available: https://www.sciencedirect.com/science/article/pii/S1387181115002413

[30] W. D. Davies, "Urethane coated textiles," *Journal of Coated Fabrics*, vol. 4, no. 4, pp. 205–222, 1975.

[31] C. S. Schollenberger and F. D. Stewart, "Thermoplastic polyurethane hydrolysis stability," *Die Angewandte Makromolekulare Chemie*, vol. 29, no. 1, pp. 413–430, 1973. [Online]. Available: https://doi.org/10.1002/apmc.1973.050290118

[32] H. Wang, D. G. Thompson, J. R. Schoonover, S. R. Aubuchon, and R. A. Palmer, "Dma-ftir creep-recovery study of a poly*esterurethane* elastomer with molecular-level viscoelastic modeling," *Macromolecules*, vol. 34, no. 20, pp. 7084–7090, 2001. [Online]. Available: https://doi.org/10.1021/ma001783b

[33] W.-R. Yu, M. S. Kim, and J. S. Lee, "Modeling of anisotropic creep behavior of coated textile membranes," *Fibers and Polymers*, vol. 7, no. 2, pp. 123–128, 2006. [Online]. Available: https://doi.org/10.1007/BF02908256

[34] A. Boubakri, N. Haddar, K. Elleuch, and Y. Bienvenu, "Influence of thermal aging on tensile and creep behavior of thermoplastic polyurethane," *Comptes Rendus Mécanique*, vol. 339, no. 10, pp. 666–673, 2011. [Online]. Available: https://www.sciencedirect.com/science/article/pii/S1631072111001264

[35] Y. cui, J. E. Campbell, M. burley, M. patel, K. hunt, and T. W. Clyne, "Effects of temperature and filler content on the creep behaviour of a polyurethane rubber," *Mechanics of Materials*, vol. 148, p. 103461, 2020. [Online]. Available: https://www.sciencedirect.com/science/article/pii/S0167663620301551

[36] A. Kasgoz, "Mechanical, tensile creep and viscoelastic properties of thermoplastic polyurethane/polycarbonate blends," *Fibers and Polymers*, vol. 22, no. 2, pp. 295–305, 2021. [Online]. Available: https://doi.org/10.1007/s12221-021-0113-z

[37] D. W. A. Rees, "Nutting creep in polymer composites," *Journal of Materials Processing Technology*, vol. 143-144, pp. 164–170, 2003. [Online]. Available: https://www.sciencedirect.com/science/article/pii/S0924013603003996

[38] J. Conway and P. Flagella, "High-temperature reactor materials research," 2022.

[39] W. N. Findley, J. S. Lai, and K. Onaran, Eds., *CHAPTER 2 - Historical Survey of Creep*. North-Holland, 1976, vol. 18, pp. 8–21. [Online]. Available: https://www.sciencedirect.com/science/article/pii/B9780720423693500059

[40] M. Burley, J. E. Campbell, J. Dean, and T. W. Clyne, "A methodology for obtaining primary and secondary creep characteristics from indentation experiments, using a recess," *International Journal of Mechanical Sciences*, vol. 176, p. 105577, 2020. [Online]. Available: https://www.sciencedirect.com/science/article/pii/S0020740319337804

[41] Y. Cui and T. W. Clyne, "Creep of particle and short fibre reinforced polyurethane rubber," *Mechanics of Time-Dependent Materials*, 2021. [Online]. Available: https://doi.org/10.1007/s11043-021-09524-x

[42] D. W. A. Rees, "Nutting creep in mono- and bi-layer polymers," *Plastics, Rubber and Composites*, vol. 31, no. 8, pp. 350–358, 2002. [Online]. Available: https://doi.org/10.1179/146580102225006477

[43] A. H. Slocum, M. Haji, and K. Kruger, "Innovative pumped storage hydropower configurations and uses," 2021.

[44] V. Koritarov, Q. Ploussard, J. Kwon, and P. Balducci, "A review of technology innovations for pumped storage hydropower," 2022.

[45] R. Shan, J. Reagan, S. Castellanos, S. Kurtz, and N. Kittner, "Evaluating emerging long-duration energy storage technologies," *Renewable and Sustainable Energy Reviews*, vol. 159, p. 112240, 2022. [Online]. Available: https://www.sciencedirect.com/science/article/pii/S1364032122001630

[46] C. Sasthav and G. Oladosu, "Environmental design of low-head run-of-river hydropower in the united states: A review of facility design models," *Renewable and Sustainable Energy Reviews*, vol. 160, p. 112312, 2022. [Online]. Available: https://www.sciencedirect.com/science/article/pii/S1364032122002271

[47] K. Mongird, V. V. Viswanathan, P. J. Balducci, M. J. E. Alam, V. Fotedar, V. S. Koritarov, and B. Hadjerioua, "Energy storage technology and cost characterization report," Pacific Northwest National Lab.(PNNL), Richland, WA (United States), Report, 2019.

[48] O. A. Osadolor, M. Lundin, P. R. Lennartsson, and M. J. Taherzadeh, "Membrane stress analysis of collapsible tanks and bioreactors," *Biochemical Engineering Journal*, vol. 114, pp. 62–69, 2016. [Online]. Available: http://www.sciencedirect.com/science/article/pii/S1369703X16301760